NTNU – Trondheim
Norwegian University of
Science and Technology

Dynamic Analysis of ROV Operation

Fredrik Rødne Jenssen

Marine Technology
Submission date: June 2015
Supervisor: Svein Sævik, IMT
Co-supervisor: Kjell Larsen, IMT

Norwegian University of Science and Technology
Department of Marine Technology

NTNU Trondheim
Norges teknisk-naturvitenskapelige universitet
Institutt for marin teknikk

MASTER THESIS SPRING 2015

for

Stud. tech. Fredrik Rødne Jenssen

Dynamic Analysis of ROV Operation

Dynamisk analyse av ROV operasjon

The background for this project is related to the ROV operations performed from the Snorre B semi-submersible platform where water entry limits the weather window for such operations. The ROV is launched through a separate deck opening by means of a winch and a cable running over a banana shaped sheave. Due to space limitations, the distance from the sheave to the winch is quite small leading to cable fatigue problems. The distance from the water entry point to the pontoon, further limits the weather window before clashing occurs. The main purpose of the master thesis work is to perform parameter studies with a numerical model in order to evaluate the ROV operation criteria, possibly also the amount of inherent conservatism in the current procedure. Previously, the basis for modelling the ROV launch operation has been established as part of the project work, such that the effect of different means for optimizing and improving the procedure can be investigated and documented prior to in-field testing. The project part included:

1. Familiarization with respect to the Snorre B ROV operation details including the basis for the operation criteria presently applied . This was obtained by the candidate having a summer job in Statoil, Stavanger.
2. Literature study, including relevant standards for lift operations, theoretical basis for computational tools like Sima (Simo/Riflex), familiarization with the Sima tool, hydrodynamic coefficients.
3. Establish a model that can be used to evaluate the lift operations and to be used as basis for comparisons/calibration with regard to field experience. This requires input data in terms of environmental and platform motion characteristics as well as geometry details.

The master thesis is to continue from the above including:

4. Establish strategies for re-modelling with respect to the effect of different measures that can be implemented to extend the weather window.
5. Perform sensitivity studies with respect to governing parameters to document the performance of the different methods and procedures with respect to statistic variability and using the current operation criteria as a reference.
6. Conclusions and recommendations for further work

All necessary input data is assumed to be provided by Statoil.

The work scope may prove to be larger than initially anticipated. Subject to approval from the supervisors, topics may be deleted from the list above or reduced in extent.

In the thesis the candidate shall present his personal contribution to the resolution of problems within the scope of the thesis work

Theories and conclusions should be based on mathematical derivations and/or logic reasoning identifying the various steps in the deduction.

The candidate should utilise the existing possibilities for obtaining relevant literature.

Thesis format
The thesis should be organised in a rational manner to give a clear exposition of results, assessments, and conclusions. The text should be brief and to the point, with a clear language. Telegraphic language should be avoided.

The thesis shall contain the following elements: A text defining the scope, preface, list of contents, summary, main body of thesis, conclusions with recommendations for further work, list of symbols and acronyms, references and (optional) appendices. All figures, tables and equations shall be numerated.

The supervisors may require that the candidate, in an early stage of the work, presents a written plan for the completion of the work.

The original contribution of the candidate and material taken from other sources shall be clearly defined. Work from other sources shall be properly referenced using an acknowledged referencing system.

The report shall be submitted in two copies:
- Signed by the candidate
- The text defining the scope included
- In bound volume(s)
- Drawings and/or computer prints which cannot be bound should be organised in a separate folder.

Ownership
NTNU has according to the present rules the ownership of the thesis. Any use of the thesis has to be approved by NTNU (or external partner when this applies). The department has the right to use the thesis as if the work was carried out by a NTNU employee, if nothing else has been agreed in advance.

Thesis supervisors:
Prof. Svein Sævik, NTNU
Prof. II Kjell Larsen, Statoil

Deadline: June 10, 2015

Trondheim, January , 2015

Svein Sævik

Preface

This report is the result of a Master thesis carried out during the spring semester of 2015 at the Department of Marine Technology, Norwegian University of Science and Technology (NTNU).

The background for the work is an initiative by Olav Bruset, Platform Manager at Snorre B, Statoil. During the spring semester of 2014, he organized a summer internship at Statoil in Stavanger for two students at the Marine Technology Department. The intention was to investigate ROV operations at Snorre B and identify limitations of the system. This work was continued by evaluating the launch and recovery operation in the Specialization Project course during the fall semester of 2014. Literature study and familiarization with the computer program SIMO were the main intention. In addition, a preliminary model of the ROV and the launch and recovery system was made.

In the master thesis work, the preliminary model has been modified and validated to give a better representation of the operation. Much time was used to obtain usable results from SIMO. Motion measurements of the ROV were conducted by borrowing an IMU from NTNU, which the ROV operators at Snorre B mounted onto the ROV and logged data from. Preparations for the measurements took longer time than planned and resulted in limited extent of results and references for verification. Also post processing the results proved to be more difficult than anticipated, partly due to uncertainties in the IMU orientation data. However, the measurements obtained have given an indication of the ROV wave zone behaviour and been used extensively in the discussion part of the report. In addition, the process has been very educational.

The work has been carried out under supervision of Svein Sævik and Kjell Larsen, who have provided much appreciated guidance and support. I would also like to thank Olav Bruset for initiating the work, organizing the summer internship and follow up the project. In addition, I want to thank Professor Martin Ludvigsen and Mauro Candeloro for lending out the IMU and Saipem for organizing and conducting the measurements at Snorre B.

Trondheim, June, 2015

Fredrik Rødne Jenssen

Sammendrag

Den fjernstyrte undervannsfarkosten (ROV) på den halvt nedsenkbare plattformen Snorre B er avgjørende for å utføre bore- og produksjonsaktiviteter. Dagens værkriterie for å sjøsette ROVen er satt til fire meter signifikant bølgehøyde. Dette fører til begrensninger for undervannsoperasjoner. Værkriteriet er basert på forenklede beregninger beskrevet i anbefalte metoder fra DNV. Disse er antatt å overvurdere kreftene på grunn av antagelser og usikkerheter.

I dette arbeidet har sjøsetting og opptak av ROVen blitt vurdert på bakgrunn av analyser i SIMO og bevegelsesmålinger utført på ROVen. I tillegg er de forenklede beregningene brukt som sammenlikningsgrunnlag. Hensikten har vært å identifisere kritiske faktorer for fastsettelsen av værkriteriet. Videre har tiltak for å redusere effekten av de kritiske faktorene blitt evaluert.

En foreløpig modell av ROVen og sjøsettingssystemet ble laget som en del av prosjektoppgaven i høstsemesteret 2014. Denne modellen har blitt endret og verifisert for å gi en bedre representasjon av operasjonen. Videre er modellen brukt til å forstå bakgrunnen for effekter som påvirker værkriteriet. Basert på resultatene, ble en modell av skiveopphenget montert på Snorre B inkludert ved hjelp av to metoder. Akselerasjons-, vinkelhastighet- og retningsmålinger ble utført ved å montere en Inertial Measurement Unit (IMU) på ROVen. Dette ble brukt for å vurdere den faktiske oppførselen av ROVen, og til en viss grad verifisere SIMO resultatene.

Basert på analysene i SIMO er impulslaster i løftekabelen (umbilical) funnet som den mest kritiske faktoren. Disse oppstår som følge av at drag-krefter på ROVen i bølgesonen gir slakk i løftekabelen. Opptak av ROVen og fare for kollisjon med plattformskroget er funnet å være av mindre betydning for værkriteriet. Også bevegelsesmålingene indikerer at slakk i kabelen kan ha oppstått. De horisontale ROV-akselerasjonene fra målingene i bølgesonen var i samme størrelsesorden som resultatene fra SIMO. Likevel fører mangel på posisjonsreferanser og usikkerheter til at det er vanskelig å verifisere bevegelsesmålingene.

På bakgrunn av impulsbelastningene i kabelen er et effektivt skiveoppheng for å redusere stivheten i systemet antatt å være det beste alternativet for å redusere dimensjonerende krefter i systemet. De to modellene av skiveopphenget i SIMO reduserte kabelstrekket under impulsbelastninger, men forkortet ikke perioden med slakk kabel. Imidlertid gjør forenklinger av systemet og usikkerheter rundt stivheten i opphenget det vanskelig å vurdere effekten av et slikt system. Forutsatt at målte impulsakselerasjonen er på grunn av slakk i kabelen, kan målingene indikerer begrenset påvirkning i stivheten med dagens skiveoppheng.

Summary

At the semi-submersible rig Snorre B, the work class remotely operated vehicle (WROV) is essential to perform drilling and production activities. Currently, the weather criterion for launching the ROV is set to four meters significant wave height. This leads to restrictions for subsea operations dependent on the ROV. The weather criterion is based on simplified calculations from DNV's Recommended Practice, which is suspected to overestimate the forces due to assumptions and uncertainties.

In this work, the launch and recovery operation has been evaluated based on time domain analysis in SIMO and motion measurements of the ROV. In addition, simplified calculations have been conducted for comparison. The intention has been to determine critical factors when setting the weather criterion for the operation. Further, measures to reduce the effect of the critical factors have been evaluated.

A preliminary model of the ROV and the launch and recover system was made in the project thesis work during the fall semester in 2014. This model has been modified and verified to give a better representation of the operation. Further, the model has been used to understand the background for effects influencing the weather criterion. Based on the results, a representation of the sheave suspension mounted at Snorre B was included by two methods. Accelerations, angular velocities and orientation measurements were done by mounting an inertial measurement unit on the ROV. This was used to evaluate the actual behaviour of the ROV, and to some extend verify the SIMO results.

Based on the SIMO analysis, large snap loads in the umbilical during launch is identified as a critical factor. This is a consequence of slack umbilical due to drag force from vertical water particle velocity. The recovery phase and pontoon impact risk are of less importance for the weather criterion. Occurrence of snap load in the umbilical is also indicated from the motion measurements. Horizontal accelerations in the wave zone were in the same magnitude as the results from SIMO. However, lack of position references and uncertainties in the measurements makes them difficult to verify.

Because of the snap loads, an effective sheave suspension system seems to be the best option to reduce the dimensioning forces. The two sheave suspension stiffness models in SIMO reduced the umbilical tension during snap loads, but did not reduce the duration of slack umbilical. However, simplifications of the system and uncertainties in input parameters makes it difficult to evaluate the effect. Assuming measured impulse acceleration is due to a snap load, the measurements can indicate limited effect of the current sheave suspension system.

Contents

List of Figures

List of Tables

Nomenclature

Abbreviations

AHRS	Attitude and heading reference system
DAF	Dynamic amplification factor
DNV	Det Norske Veritas
DPS	Degrees per second
IMU	Inertial measurement unit
JONSWAP	Joint North Sea Wave Observation Project
LARS	Launch and recovery system
OROV	Observation class remotely operated vehicle
OS	Offshore standard
ROV	Remotely operated vehicle
RP	Recommended practice
SIMO	Simulation of marine operations
SWL	Safe working load
TMS	Tether management system
WROV	Work class remotely operated vehicle
XKF	Xsens Kalman Filter

Roman symbols

Symbol	**Description**
A	Effective umbilical area
A_{33}	Added mass in heave
A_{33}^{∞}	High-frequency limit added mass in heave
a_{ct}	Crane tip acceleration
$\boldsymbol{A}^{G}$	Inertial reference frame accelerations

$\boldsymbol{A}^L$	Local reference frame accelerations
A_m	Total added mass
$\boldsymbol{A}^{MP}$	Accelerations at point of measurement
A_p	Projected area
A_s	Slamming area
$\boldsymbol{A}^{SP}$	Accelerations at specified point
$\tilde{A}_w$	Water line area
a_w	Water particle acceleration
B_1	Linear damping
b_1	Linear damping coefficient
B_2	Quadratic damping
b_2	Quadratic damping coefficient
C	Snap velocity correction factor
C_a	Added mass coefficient
C_D	Drag coefficient
C_s	Slamming coefficient
D	Characteristic length
d	Depth of penetration
E	Modulus of elasticity
F_B	Buoyancy force
F_D	Drag force
F_{hyd}	Hydrodynamic force
F_{line}	Lifting line force
F_M	Mass force
F_{slam}	Slamming impact force
F_{snap}	Snap force
F_{static}	Static force
$F_{w,slender}$	Wave force on slender element
F_{total}	Total force
F_ρ	Varying buoyancy force
g	Acceleration of gravity
H	Wave height
H_s	Significant wave height
h	Submergence relative to water surface
I	Mass moment of inertia
K	System stiffness

k	Wave number
KC	Keulegan-Carpenter number
K_0	Connection flexibility
L	Length of lifting line
$\boldsymbol{L}_{IB}$	Rotation matrix
M	Mass of lifted object
m	Mass per unit length
Re	Reynolds number
$\boldsymbol{r}^{MP}$	Distance from measurement point to specified point
S_J	JONSWAP wave spectrum
T	Tension
T_p	Wave spectrum peak period
T_z	Zero-up-crossing period
T_0	Natural period
V	Volume of displaced water
v_c	Winch speed
v_{ct}	Crane tip velocity
v_{ff}	Free fall velocity
v_r	Relative velocity
v_s	Slamming velocity
v_{snap}	Snap velocity
v_w	Water particle velocity
V_0	Total submerged volume
X_n	Amplitude of oscillation
z_{ct}	Motion of crane tip

Greek symbols

Symbol	**Description**
β	Wave direction
δV	Change in volume displacement
δ_j	JONSWAP period parameter
γ	JONSWAP peakedness parameter
ϕ	Roll about x-axis
Φ_0	Velocity potential
Φ_ζ	Wave component phase angle

η_{ct}	Vertical crane tip motion amplitude
$\ddot{\eta}_3$	Vertical acceleration of object
$\boldsymbol{\Lambda}$	Angular acceleration
λ	Wave length
θ	Pitch about y-axis
ψ	Yaw about z-axis
ρ	Density of salt water
σ	JONSWAP width parameter
ω	Wave angular frequency
$\boldsymbol{\omega}$	Angular velocity
ω_p	JONSWAP angular peak period
ζ_a	Wave amplitude

Chapter 1

Introduction

1.1 Background

At the semi-submersible rig Snorre B, the work class remotely operated vehicle (WROV) is essential to perform drilling and production activities. Examples are operation of valves, observation during drilling and template intervention. Because of this, the weather criterion for the ROV should not be lower than criteria for the production and drilling activities.

Currently, the weather criterion for launching the WROV is based on simplified calculations from DNV's Recommended Practice (Det Norske Veritas, 2014b). The limit for lunch and recovery is set at four meters significant wave height, which leads to restrictions for other subsea operations dependent on the ROV. Due to assumptions and uncertainties in these calculations, the resulting forces may be overestimated. Better methods for determining the dimensioning effects for the launching system can reduce the safety factors in the calculations. Thus, operation of the system in larger waves may be allowed. This requires a better understanding of how the dimensioning forces occurs during launch and recovery of the ROV.

1.2 Objectives

The objectives for the work is to present the background for the current weather criterion and investigate limiting parameters. A preliminary model of the system for numerical analysis in SIMO has been made previously for this purpose. In addition, acceleration measurements on

the real operation will be used to investigate the real behaviour of the ROV during launch and recovery. This will also contribute in the validation of the SIMO model.

Based on time domain simulations, forces acting on the ROV system during the lifting operation through the splash zone can be evaluated more accurate. This model can be used to investigate the current weather criterion and critical effects for increasing the weather window. Further, the effect of modifications on the lifting system can be evaluated.

The main objectives of the project can be summarized as:

1. Describe the ROV launch and recovery phases and the lifting system at Snorre B with focus on limiting factors for the weather criterion.
2. Present the most important force contributions acting during launch and recovery of the ROV based on the simplified calculation method from Det Norske Veritas (2014b), numerical analysis in SIMO and full scale motion measurements.
3. Identify important parameters in procedures and the ROV launch and recovery system to extend the weather window, and investigate the effect of changing these by using time domain analysis in SIMO.

1.3 Literature review

The problem of determining forces on structures in waves has been discussed thoroughly in the literature. Most of the theory used in this work was developed during the 20th century, and the linear wave representation is based on theories introduced in the 1800s. The method for calculating the wave forces are based on the Morison equation, which was introduced in Morison et al. (1950). This formulation proposes that the forces acting on a section of a pile due to wave motion can be divided into drag and inertia forces, represented by the use of drag and inertia coefficients. It requires that the body is small compared to the wave length resulting in an uniform incident flow in the vicinity of the body (Sarpkaya and Isaacson, 1981).

To use the Morison equation on subsea modules, the force coefficients are found from empirical data based on the parameters characterizing the flow. During the 1980s, Marintek conducted a research program concerning marine operations. As a part of this, a series of model tests were performed to determine hydrodynamic coefficients for different subsea structures and modules in both steady and oscillatory flow. The tests are described in Øritsland and Lehn (1987) and a summary of the coefficients are presented in Øritsland (1989). An

alternative way of presenting the drag term from the Morison equation was used to provide a linear and quadratic damping term. This description was found to give the most convenient representation both for a partly and fully submerged body (Øritsland and Lehn, 1987). The results are presented with corresponding Reynolds (Re) number and Keulegan-Carpenter (KC) number, where the KC number represents the amplitude of the fluid motion relative to the body size and the Re number represents the ratio between the inertial and viscous forces. However, three-dimensional complex structures makes it difficult to determine the force coefficients due to factors such as interaction effects. Uncertainties due to input parameters makes it necessary to properly verify results from time domain simulation programs.

At the University of Victoria, Canada, motions of a deep sea remotely operated vehicle system were logged and used to develop a continuous one-dimensional model of the system behaviour. In their case, operation depths of more than 1000 meters were the concern, unlike this work where the wave zone is the main focus. However, the tether length during deep sea operations gave resonance with the vessel motion leading to slack tether and snap loads. The motion measurements are described in Driscoll et al. (2000b), while the model development is presented in Driscoll et al. (2000a). Further, the model was used to develop and optimize a passive heave compensator to reduce the risk of slack tether and decrease the tension variation, as described in Driscoll et al. (2000c) and Driscoll et al. respectively. By tuning the stiffness and damping, slack umbilical were avoided even in extreme wave conditions.

1.4 Structure of the report

In Chapter 2, the remotely operated vehicle (ROV) and launch and recovery system (LARS) are presented together with the different launch and recovery phases. The basic theory related to the operation is presented in Chapter 3. Also the theory behind the simplified analysis and time domain simulation software SIMO is referred to. Further, strategies for the full scale tests, SIMO modelling and input values used in the calculations are discussed in Chapter 4.

In Chapter 5, the results are presented and discussed. This includes sensitivity analysis, parameter variation and comparison between the different methods. The conclusion and suggestions for further work are presented in Chapter 6.

Chapter 2

Problem description

The dimensioning factors during launch and recovery of the ROV will be influenced by many aspects. This includes the semi-submersible platform, launch and recovery system and the properties of the ROV system. Also the procedure used during launch and recovery of the ROV is important. In this section, both the equipment and the phases during the launch and recovery are presented.

2.1 Equipment

The semi-submersible platform Snorre B is equipped with two ROVs, one work class ROV and one observation class ROV. An A-frame is used to launch the observation class ROV from the platform side, while the work class ROV is launched through a deck opening. Unlike the work class ROV, the observation class ROV does not have manipulators and payload capacity. This is why many of the subsea tasks conducted at Snorre B requires use of the work class ROV. Thus, only the launch and recovery of the work class ROV is analysed.

2.1.1 Snorre B

Snorre B is an integrated production, drilling and quarters semi-submersible unit located at the Tampen area in the Norwegian North Sea. The hull is symmetrical about both the roll and pitch axis, and consists of four columns connected by four pontoons. Figure 2.1 illustrates the top-side of the platform. A SIMO model of Snorre B has been provided by Statoil.

Figure 2.1: Snorre B, view from north-west. Photo by Harald Pettersen, Statoil.

2.1.2 ROV system

The main components of the work class ROV system is a tether management system (TMS), the ROV and a tool skid. A steel armoured umbilical connected to the TMS is used to lift the system. In addition, the umbilical transfers power and signal between the surface and the TMS. During launch and recovery, the TMS is connected to the top of the ROV. This TMS arrangement is called a top-hat, as opposed to a garage where the TMS surrounds the ROV. At the operational depth, the ROV is disconnected from the top-hat. Power and signal are transferred between the TMS and the ROV by a smaller cable called tether. The tool skid is fixed to the underside of the ROV. In Figure 2.2, the ROV and the tool skid is placed on the deck hatches. The lower part of the TMS is seen on top of the ROV.

Normally, the ROV and tool skid is designed to have neutral weight submerged. This is done to preserve the manoeuvrability during operations. On the contrary, the weight of the submerged TMS will give a downward acting force. This leads to a low centre of buoyancy compared to the centre of gravity when the ROV and TMS are connected. If the centre of gravity is located above the centre of buoyancy, loss of tension in the umbilical will lead to a rotational motion of the submerged ROV system.

Figure 2.2: The WROV system as seen from behind.

Snorre B is equipped with an old work class ROV. This has made it difficult to obtain precise properties of the system. Most of the properties are found in the calculations done as basis for the current weather criterion (JMC Engineering, 2006a) and the load test document for the launch and recovery system (Saipem LTD, 2012). In Table 2.1, a summary of the data is presented.

Table 2.1: Properties of the ROV system.

Length ROV [m]	3.2
Width ROV [m]	1.5
Mass ROV [kg]	3000
Mass TMS [kg]	2300
Mass tool skid [kg]	1100

2.1.3 Launch and recovery system

The work class ROV is launched through a deck opening using a winch. From the winch, the umbilical is passed through a spooling device and over a sheave to the bullet at the top-hat. The sheave is placed approximately 18.5 meters north and 6.5 meters west relative to the centre of the platform. The clearance between the sheave and deck hatches is 5 meters, while the distance from the deck opening to the water surface is approximately 22 meters. A photo of the sheave system is shown in Figure 2.4.

A hydraulic winch with maximum speed of 0.8 m/s is used for the lifting operation. The safe working load (SWL) for the launch and recovery system is 9000 kg at 4 meters significant wave height (COSALT Offshore Norge AS, 2012). In Table 2.2, a summary of the properties are presented.

Table 2.2: Properties of the launch and recovery system.

Max winch speed [m/s]	0.8
Umbilical effective stiffness (EA) [kN]	38 985
Umbilical diameter [mm]	42

Due to a small deck opening, guidewires are used to reduce the ROV motions through the deck opening. This is done by connecting two guide wires to a guide frame (cursor) which is connected to the TMS. A hydraulic system in the guide frame can be used to rotate the ROV system. This is normally done before the ROV is lifted through the deck opening during recovery.

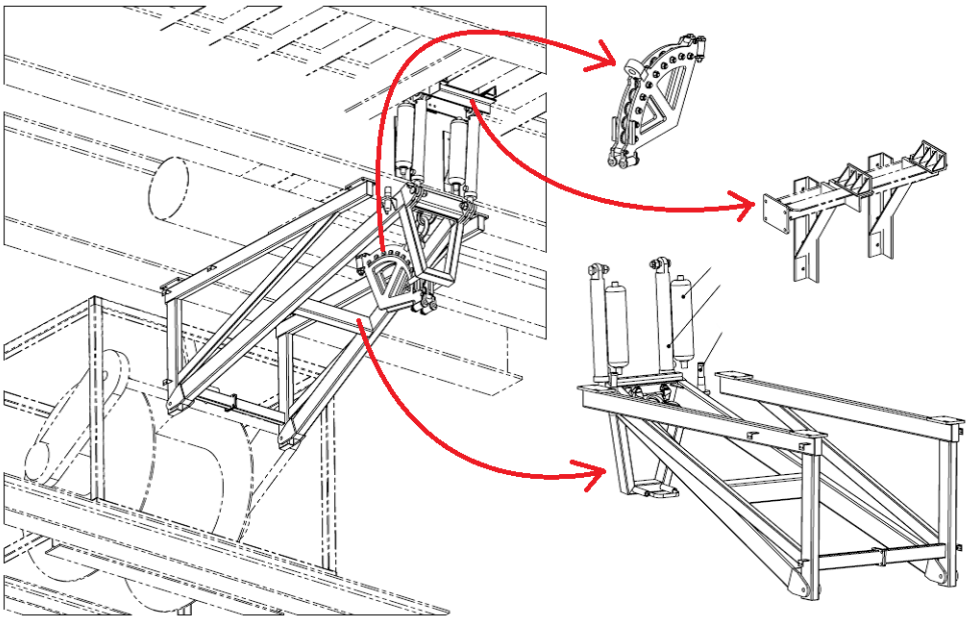

Figure 2.3: Drawing of the sheave suspension in front of the winch (JMC Engineering, 2006b).

The sheave is supported by a frame connected to a suspension system. All the data about the suspension system are taken from JMC Engineering (2006b), where structural analysis and dynamic behaviour analysis are presented. The system is illustrated in Figure 2.3. It consists of two passive pneumatic hydraulic cylinders preloaded by two gas accumulators. The cylinders are fastened to the girder supporting the main deck. In addition, two shock absorbers are used to reduce impact forces from the sheave frame due to sudden slack umbilical. The suspension

is preloaded with 87.4 kN, corresponding to the weight of the ROV system including the guide frame. Further, the stiffness is linearised and based on the assumption of an adiabatic process due to fast response of the system (JMC Engineering, 2006b). This gives a suspension stiffness of 196 kN/m. Both stiffness and damping properties of the system is based on assumptions. This must be considered if the sheave suspension is used to further change the weather criterion.

2.2 Phases during launch and recovery

To better understand the launch and recovery system and procedure, the operation will be divided into different phases based on forces acting on the ROV and the physical behaviour. In addition, this will be used to identify the most critical phase for determining the weather criterion.

2.2.1 Lift off

The lift off phase covers lifting the ROV system off deck, moving the hatches covering the deck opening and lowering the ROV system through the deck opening. As mentioned in the equipment presentation, a guidewire system has been installed to lead the ROV system through the deck opening. In addition to restrict motions of the ROV, the cursor will relieve the umbilical tension while rotating the ROV before it is lifted through the deck opening during retrieval.

The cursor is lifted by the same umbilical as the ROV system. This will introduce an extra mass of 2600 kg. However, the dynamic amplification is low compared to other phases because of limited platform motion in the relevant weather conditions. Therefore, this phase is not considered critical in terms of the umbilical tension and weather criterion.

Increasing the mass of the lifted object will introduce more wear in the umbilical. This is especially relevant because of large concentrated loads over the sheave and at the spooling arrangement into the winch. The concentrated loads due to bending of the umbilical will be present independent of the guide frame. However, in case of modifications to the launching system, the design and need for a guiding system through the deck opening has to be considered. The current system gives a low clearance between the sheave and cursor, as shown in Figure 2.4. This will restrict modifications of the sheave to reduce the concentrated loads on the umbilical.

Figure 2.4: The blue cursor frame on top of the TMS illustrating clearance to the sheave.

2.2.2 Lifting below deck

In this phase, the lifting between the deck opening and water surface is covered. After the ROV system is lowered through the deck opening, the cursor frame will be disconnected and act as a pivot point for the pendulum motion. This is illustrated in Figure 2.5.

The distance from the mean water level to the deck opening is approximately 22 meters. This distance combined with limited damping makes the operation vulnerable for pendulum motion. Both platform motions and wind forces can excite the motion. This will depend on the natural period of the pendulum motion in air. A simplified assumption of the pendulum period is $T_0 = 2\pi\sqrt{\frac{L}{g}}$, where L is length of hoisting line and g is acceleration of gravity. With a umbilical length between 5 and 20 meters, the natural period increases from 4.5 to 9.0 seconds. However, since the natural period depends on length of the hoisting line, it is unlikely to coincide with the period of the excitation force over a long period. Assuming that the clearance to the columns is sufficient, the most critical effect from horizontal motion will be during the water impact. The water surface impact will be discussed for the next phase.

Also the vertical natural period is checked to determine the characteristic behaviour in the vertical direction. This is done by $T_0 = 2\pi\sqrt{\frac{M}{K}}$, where M is the mass term and K is the stiffness

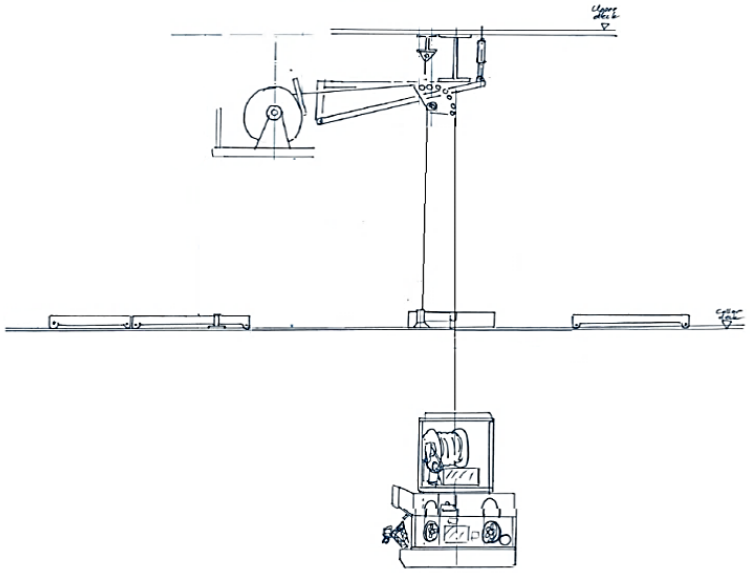

Figure 2.5: Drawing of the ROV below the deck opening. Adapted from Bruset (2014)

term in the equation of motion. Assuming only umbilical stiffness contribution with a length of 20 meters, $K = \frac{EA}{L} = 1950\ kN/m$. This gives $T_0 = 0.34\ s$. Compared to the first order wave force periods, this indicates a stiffness dominated system with a quasi-static behaviour. Including the sheave suspension system reduces the stiffness to 178 kN/m. The natural period is increased to 1.2 seconds, which also gives a low frequency ratio.

2.2.3 Lifting through the wave zone

This phase covers the impact with the water surface and the transit through the wave zone. Normally, the winch speed is reduced before the water impact to reduce the slamming force. Once the ROV has penetrated the water, it is desirable to transit the wave force area as quickly as possible. The intention is to reduce the time of wave force interaction.

Loss of tension in the umbilical is a condition that might occur in this phase. If the combined slamming impact force, buoyancy force and vertical wave forces is larger than the weight of the ROV system, tension in the umbilical is lost. The result will be a snap load in the umbilical as the tension is restored. In addition to limit the weather criterion due to the safe working load of the lifting cable, snap loads can reduce the life of the umbilical due to damage on the structural armour and internal conductors (Driscoll et al., 2000c).

For simplified calculations, it is common to divide this phase into several stages and determine if snap loads will occur for each phase. However, the wave zone represents a complicated

environment which makes it difficult to consider assumptions around the forces without detailed analysis. Based on the description of the other phases, the wave zone is assumed to be the dimensioning phase for the weather criterion. A more detailed theoretical description of the wave zone lifting is presented in Chapter 3.

2.2.4 Operating below the wave zone

The ROV is further lowered to the operating depth of 350 meters. Even if the wave forces decreases exponentially, the platform motion will still influence the dynamic behaviour. As the umbilical gets longer, the vertical stiffness is reduced and weight of the system increases. Combined, this may lead to larger weight of the system and resonance with the sheave vertical motion.

As previously, the vertical natural period is taken as $T_0 = 2\pi\sqrt{\frac{M+A_{33}}{K}}$. A_{33} is the vertical added mass and will increase the natural period found in air. Assuming an umbilical length of 350 meters and $A_{33} = M$, including the sheave stiffness gives a natural period of 2.7 seconds. This is regarded as outside the resonance domain for the first order wave forces. In addition, it is a conservative estimate. However, the natural period have to be checked if further reduction of the sheave stiffness is carried out.

Chapter 3

Theory of the analysis

As previously discussed, lifting through the wave zone is regarded as the most critical phase during launch and recovery of the ROV. In addition, the forces on the lifted object are difficult to predict. Oscillating flow because of waves, water impact effects and varying degree of submergence due to sheave motion and incoming waves are examples of factors influencing the total force.

In this section, the basic theory relevant to lifting through the wave zone is presented. It is important to understand assumptions and limitations in the calculations when evaluating the results. In addition, the calculation methods and limitations of DNV's simplified method and the time domain simulations in SIMO are discussed.

3.1 Wave zone analysis

3.1.1 Environment

The environment will include wind, waves and current. However, it is assumed that first order wave forces will dominate the object behaviour and platform motions in the wave zone. As the focus will be on forces and effects during the wave zone lifting, only waves are included in the environment modelling.

In this case, the waves are based on linear wave potential theory. This means that the undisturbed incoming wave field can be expressed in terms of the velocity potential Φ_0 (SIMO Project Team, 2013). Derivation of the velocity potential for a regular wave at infinite water depth can be found in Faltinsen (1990). Water particle velocity and acceleration can be found

from the velocity potential. In linear theory, it is assumed that the velocity potential and fluid velocity are constant between the mean free surface level and the actual free surface level. This is illustrated by Figure 2.2 in Faltinsen (1990).

For deep water waves we have (SIMO Project Team, 2013):

$$\Phi_0 = \frac{\zeta_a g}{\omega} e^{kz} cos(\omega t - kxcos\beta - kysin\beta + \Phi_\zeta) \tag{3.1}$$

where ζ_a is the wave amplitude, g is the acceleration of gravity, $k = \frac{\omega^2}{g}$ is the wave number, β is the direction of wave propagation and Φ_ζ is the wave component phase angle.

The dimensions of the ROV in horizontal plane is assumed small compared to the wave length. This assumption can be evaluated in relation to the wave breaking limit. The limit is set from the maximum wave steepness, and gives $\lambda = 7H$ for deep water waves (Det Norske Veritas, 2014b). H is the wave height and λ is the wave length.

A real sea state will be irregular and have random height, length, shape and speed of propagation (Det Norske Veritas, 2014b). This can be represented by a wave spectrum. A wave spectrum represents the energy distribution of the sea state. The main parameters for most wave spectra are significant wave height H_S and spectral peak period T_p. In this case, the JONSWAP spectrum is used to simulate wind sea. It describes wind sea conditions for the most severe sea states, and is assumed to be a reasonable model for $3.6 < T_p/\sqrt{H_s} < 5$ (Det Norske Veritas, 2014b).

The JONSWAP spectrum is defined by a non-dimensional peak shape parameter, γ, a spectral width parameter, σ, as the following relation:

$$S_J(\omega) = \frac{5}{32\pi} H_s^2 \; T_p (\frac{\omega_p}{\omega})^5 e^{-\frac{5}{4}(\frac{\omega p}{\omega})^4} (1 - 0{,}287 \; ln\gamma) \gamma^{exp(-\frac{(\frac{\omega}{\omega p}-1)^2}{2\sigma^2})} \tag{3.2}$$

$$\sigma = \begin{cases} 0{,}07 & \omega \leq \omega_p \\ 0{,}09 & \omega_p < \omega \end{cases} \text{ where } \omega_p = \frac{2\pi}{T_p}$$

The relationship between the spectrum peak period, T_p, and the zero-up-crossing wave period, T_z, is $T_z = T_p \; (0.6673 + 0.05037 \; \gamma - 0.006230\gamma^2 + 0.0003341\gamma^3)$ (Det Norske Veritas, 2014b). Usage of the JONSWAP spectrum in SIMO is described in Section 4.2.4.

3.1.2 Motions and forces in the wave zone

The equation of vertical motion is derived from the second law of motion, mass multiplied by the acceleration equals the sum of external forces, $Ma = \sum F_{ext}$. For a small object compared to the wave length, the external forces will mainly consist of buoyancy, inertia, wave excitation, slamming, and drag forces during launch (Det Norske Veritas, 2014b). Based on the description in Det Norske Veritas (2014b), the different hydrodynamic forces will be presented in this section, before the resulting equation of motion is expressed.

Buoyancy

The buoyancy force equals the weight of displaced water, and the centre of buoyancy equals the centre of the volume displacement. Leaking air that was trapped in the submerged object may cause a decreasing buoyancy force after the object is completely submerged. This must be considered based on perforation of the object when the dimensioning forces are determined. The time dependant buoyancy force is expressed by:

$$F_B(t) = \rho g V(t) \tag{3.3}$$

where ρ is the mass density of water, g is the acceleration of gravity and $V(t)$ is the displaced volume of water.

The static weight can then be expressed by:

$$F_{static} = M \cdot g - F_B(t) \tag{3.4}$$

where M is the structural mass.

Inertia

The inertia force due to motion of the object is given by the mass of the object, M, and added mass in vertical direction due to vertical acceleration, A_{33}, multiplied with the vertical acceleration of the object, $\ddot{\eta}_3$:

$$F_I = -(M + A_{33})\ddot{\eta}_3 \tag{3.5}$$

Wave excitation

Assuming a small object compared to the wave length, the wave excitation force can be found by:

$$F_{w,i} = (\rho V + A_{ii}) \cdot a_{w,i} + F_{D,i} \tag{3.6}$$

where the first term represents the inertia force due to water particle acceleration, a_w, and $F_{D,i}$ is the viscous drag force due to the relative velocity on the object in direction i. In the inertia term, A_{ii} is the added mass term in direction i due to motion in the same direction and V is the submerged volume of the object. This is for a fully submerged object. If the object is partly submerged, a hydrostatic force due to the wave elevation is added (Det Norske Veritas, 2014b).

Viscous drag

The viscous drag force in oscillating flow can be found from the drag term in the Morison equation:

$$F_D = \frac{1}{2}\rho C_D A_p |v_r| v_r \tag{3.7}$$

where C_D is drag coefficient in oscillatory flow, A_p is projected area normal to the flow direction and v_r is relative velocity. Depending on the relative velocity between the object and fluid, the viscous drag force can act as either damping or excitation of the system (Det Norske Veritas, 2014b).

Model tests have shown that the drag coefficient in oscillatory flow is dependent on the Keulegan-Carpenter (KC) number in addition to the Reynold's number (Øritsland and Lehn, 1987). Decay test have also shown that a linear term may contribute significantly to the damping in oscillatory flow. Further, Øritsland and Lehn (1987) states that by expressing the viscous drag with a linear and quadratic term, the KC dependency is reduced. This gives the following expression:

$$F_D = B_1 v_r + B_2 v_r |v_r| \tag{3.8}$$

where B_1 and B_2 is the linear and quadratic damping term respectively. This expression is further discussed in Section 3.1.3.

Slamming

The slamming force can be expressed as the rate of change of fluid momentum (Faltinsen, 1990):

$$F_{slam}(t) = \frac{d}{dt}(A_{33}^{\infty} v_s) = \frac{dA_{33}^{\infty}}{dh} v_s^2 \tag{3.9}$$

where A_{33}^{∞} is the high frequency added mass in heave, v_s is the slamming impact velocity and h is the submergence relative to the water surface.

Equation of vertical motion and line force

If these forces are combined, the equation of vertical motion for a lowered object is obtained (Det Norske Veritas, 2014b):

$$(M+A_{33})\ddot{\eta}_3 = B_{33}^1(v_3-\dot{\eta}_3)+B_{33}^2(v_w-\dot{\eta}_3)|(v_w-\dot{\eta}_3)|+(\rho V+A_{33})a_w+\frac{dA_{33}^{\infty}}{dh}(\dot{\zeta}-\dot{\eta}_3)^2+\rho g V(t)-Mg+F_{line}(t) \tag{3.10}$$

where $\eta(t)$ is vertical object motion, v_w is the water particle vertical velocity, v_c is the winch speed and $F_{line}(t)$ is force in the hoisting line.

The time dependant force in the hoisting line can found by using the cable stiffness, $F_{line}(t) = Mg - \rho g V(t) + K(z_{ct} - \eta)$. Then K is the cable stiffness multiplied by the difference in crane tip motion, z_{ct}, and motion of the lifted object, η. If the winch speed is constant and the crane tip motions are neglected, the lifting line force can be expressed as (Det Norske Veritas, 2014b).

$$F_{line}(t) = Mg-\rho g V(t)-(\rho V+A_{33})a_w-\frac{dA_{33}^{\infty}}{dh}(\dot{\zeta}-v_c)^2-B_1(v_w-v_c)-B_2(v_w-v_c)|(v_w-v_c)| \tag{3.11}$$

3.1.3 Hydrodynamic properties

A difficult part of the analysis in the wave zone is to determine hydrodynamic properties. Free surface interaction and oscillating flow combined with a complex structure will introduce complicating effects. In this case, drag and added mass forces are calculated using dimensionless coefficients.

As mentioned in Section 3.1.2, the drag force can be split into linear and quadratic damping terms. The physical representation of the linear and quadratic terms can be skin friction and form drag respectively (Det Norske Veritas, 2014b). According to Øritsland and Lehn (1987),

this will make it possible to use constant damping coefficients in oscillating flow. This assumption is only valid for a limited domain of the Keulegan–Carpenter number. $KC < 10$ is mentioned as a valid domain based on results from model tests. It is defined as $KC = 2\pi \cdot \frac{X_n}{D}$, where X_n is the amplitude of oscillation and D is the characteristic length. Due to a complex structure and uncertain motion, both X_n and D are difficult to determine. However, Øritsland and Lehn (1987) states that the range is assumed to be valid for most conditions related to the lifting operations that is covered, which is similar to this case.

The linear damping coefficient b_1 and quadratic damping coefficient b_2 are defined as (Øritsland and Lehn, 1987):

$$b_1 = B_1 \cdot \frac{3\pi^2\sqrt{D/2g}}{2\rho A_p D} \tag{3.12}$$

$$b_2 = \frac{B_2}{0.5\rho A_p} \tag{3.13}$$

where B_1 and B_2 are the linear and quadratic damping terms respectively, D is the characteristic body length and A_p is the projected area in the velocity direction.

The added mass coefficient is defined as (Øritsland, 1989):

$$C_a = \frac{A_m}{\rho V_0} \tag{3.14}$$

where A_m is total added mass and V_0 is total submerged volume. As shown in Figure 6-11 in Det Norske Veritas (2014a), the added mass depends strongly on submergence relative to the free surface. In addition, the slamming impact force is defined as the added mass variation with depth. Because of a high slamming impact velocity compared to the water particle velocity is assumed, the vertical added mass is taken as its high frequency limit (Det Norske Veritas, 2014a).

The coefficients used in the SIMO model are discussed in Section 4.2.3. Further, sensitivity analysis have been conducted to check validity and importance. The results are presented in Chapter 5.

3.2 Simplified analysis method

The simplified analysis described in Det Norske Veritas (2014b) will for many cases provide a good estimate of the forces involved in a lifting operation. The current weather criterion for

ROV launch and recovery at Snorre B is based on this method (JMC Engineering, 2006a). A fundamental property of the method is that it should overestimate the forces. This provides safety margins, but may lead to a unnecessary strict weather criterion. In addition, the results will depend on the method and assumptions used to determine the input parameters.

3.2.1 Main assumptions

In Det Norske Veritas (2014b), three main assumptions are listed for the method:

- Small object in the horizontal plane compared to the wave length.
- The vertical motion of the object follows the vertical motion of the crane tip.
- The dominating loads on the object are caused by the vertical relative motion between object and water so that other modes of motion can be disregarded.

A small body can be based on the relation $5 \cdot D < \lambda$, where D is the horizontal extent of the object and λ is the wave length (Det Norske Veritas, 2014b). This should hold for critical wave heights with the length of the ROV equal to 3.2 meter compared to the wave breaking limit $7 \cdot H < \lambda$ for deep water.

The vertical motion of the object equal to the crane tip motion requires no amplification due to vertical resonance. In the wave zone, the following requirement is set by DNV for resonance not to occur (Det Norske Veritas, 2014b):

$$T_p > 1.6 T_0 \tag{3.15}$$

where T_p is the peak wave period, $T_0 = 2\pi\sqrt{\frac{M+A_{33}+\theta mL}{K}}$ is resonance period of the hoisting system, M is mass of the object in air, A_{33} is heave added mass of object, K is stiffness of the hoisting system, m is mass per unit length of lifting line, L is length of lifting line and θ is an adjustment factor. Based on the natural periods found in Section 2.2, this assumption is valid.

The last assumption is questionable for wave heights in the region of the weather criterion. Large waves may introduce other significant force contributions.

To further simplify the calculations, wave kinematics independent of the wave period can be used. This will introduce the requirement $T_Z \geq 10.6\sqrt{\frac{H_S}{g}}$, where T_Z is the zero-up-crossing period and H_S is the significant wave height. According to Det Norske Veritas (2014b), this wave period domain will be valid for most sea state conditions.

3.2.2 Force calculations

In the simplified method the different force contributions are calculated separately, put together and then compared to the accept criteria. The hydrodynamic forces are varying buoyancy, F_ρ, hydrodynamic mass, F_M, slamming impact, F_{slam}, and hydrodynamic drag, F_D. Each of the force components will vary in time. This makes it difficult to determine the time instant with the largest total hydrodynamic force. The simplified method introduce the following relation:

$$F_{hyd} = \sqrt{(F_D + F_{slam})^2 + (F_M - F_\rho)^2} \tag{3.16}$$

The total hydrodynamic force F_{hyd} is added to the static force F_{static} to find the tension in the lifting cable.

$$F_{static} = Mg - \rho g V \tag{3.17}$$

where M is structural mass and V is volume displacement.

The vertical water particle velocity and acceleration are found from the velocity potential Φ_0, $v_w = \frac{\delta \Phi_0}{\delta t}$ and $a_w = \frac{\delta^2 \Phi_0}{\delta t^2}$. Wave kinematic equations independent of the wave period then gives:

$$v_w = 0.30\sqrt{\pi g H_S} e^{-\frac{0.35d}{H_s}} \tag{3.18}$$

$$a_w = 0.10\pi g e^{-\frac{0.35d}{H_s}} \tag{3.19}$$

where v_w is the vertical water particle velocity, a_w is the vertical water particle acceleration and d is the distance from water plane to centre of gravity of submerged part of the object. These equations are based on maximum wave height H_{max} for a 30 minutes long operation, where it is assumed a wave amplitude of $\zeta_a = 0.9 H_s$.

Mass force

The characteristic mass force consists of the combined inertia force due to crane tip acceleration and water particle acceleration. The object can be divided into items, i. Based on this, the force contributions can be calculated separately and be included dependant on the launch phase.

$$F_{Mi} = \sqrt{[(M_i + A_{33i})a_{ct}]^2 + [(\rho V_i + A_{33i})a_w]^2} \tag{3.20}$$

where M_i is mass of object item in air, A_{33i} is heave added mass of object item, V_i is volume of displaced water of object item relative to still water level and a_{ct} is the crane tip acceleration.

Slamming impact force

When the object penetrates the water surface, a slamming impact force will occur. This is taken as:

$$F_{slam} = 0.5\rho C_s A_s v_s^2 \tag{3.21}$$

where C_s is the slamming coefficient, A_s is horizontal plane area of object subjected to slamming force and $v_s = v_c + \sqrt{v_{ct}^2 + v_w^2}$, where v_c is the winch speed.

Drag force

The characteristic drag force on an item is defined:

$$F_{Di} = 0.5\rho C_D A_{pi} v_r^2 \tag{3.22}$$

where C_D is drag coefficient in oscillatory flow of submerged part of the item, A_{pi} is projected vertical area of submerged part and the relative velocity is defined as $v_r = v_c + \sqrt{v_{ct}^2 + v_w^2}$, where v_c is the winch speed.

Varying buoyancy force

Waves will introduce a varying buoyancy force:

$$F_\rho = \rho\, \delta V\, g \tag{3.23}$$

where $\delta V = \widetilde{A}_w \sqrt{\zeta_a^2 + \eta_{ct}^2}$ is the change in volume of displaced water from still water surface to instantaneous water surface, $\widetilde{A}_w$ is the mean object area in the instantaneous water surface and η_{ct} characteristic single amplitude vertical motion of the crane tip.

Snap force

In case of slack umbilical, a snap force will occur. The expression can be derived from conservation of energy assuming kinetic energy is transformed into potential spring energy, and is taken as:

$$F_{snap} = v_{snap} \sqrt{K(M + A_{33})} \tag{3.24}$$

K is stiffness of the hoisting system, M is mass of the object in air and A_{33} is heave added mass of the object. The snap velocity is $v_{snap} = v_{ff} + Cv_r$ where v_{ff} is free fall velocity, v_r is relative vertical velocity as defined for the drag force and C is a correction factor given as $C = 0$ for $v_{ff} > 0.7v_r$, $C = cos[\pi(\frac{v_{ff}}{v_r} - 0.2)]$ for $0.2v_r < v_{ff} < 0.7v_r$ and $C = 1$ for $v_{ff} < 0.2v_r$.

The free fall velocity is calculated from the drag force:

$$v_{ff} = \sqrt{\frac{2F_{static}}{\rho A_p C_D}} \tag{3.25}$$

where A_p is projected area of submerged part of the object in vertical direction and C_D is the drag coefficient of submerged part of the object in vertical direction. The static force is given as $F_{static} = Mg - \rho Vg$, where V is the volume of submerged part of the object and M will include entrapped water in the object.

3.2.3 Accept criteria

The capacity checks of the lifted structure and lifting equipment will depend on occurrence of slack in the lifting cable. Det Norske Veritas (2014b) recommends a slack criterion of $F_{hyd} \leq 0.9 \cdot F_{static-min}$. Should slack occur, a snap force will be present as tension in the umbilical is restored. This lead to a large amplification factor and should be avoided. Two accept criteria are mentioned for the simplified method in Det Norske Veritas (2014b), with and without snap loads. The characteristic force without snap load is taken as:

$$F_{total} = F_{static} + F_{hyd} \tag{3.26}$$

and with snap load:

$$F_{total} = F_{static} + F_{snap} \tag{3.27}$$

where F_{hyd} is Equation 3.16 and F_{snap} is Equation 3.24. Lifting standards, e.g. DNV-OS-H205, applies dynamic amplification factors (DAF) for capacity checks. For offshore lifting, Det Norske Veritas (2014b) gives the following equation: $DAF_{conv} = \frac{F_{total}}{Mg}$, where M is the mass of object in air and F_{total} is the largest force during the lifting operation.

3.3 SIMO time domain analysis

Simulation of Marine Operations (SIMO) is a computer program where time domain simulation is applied to solve equations of motion. This section is based on (SIMO Project Team, 2013), and will give a brief overview of the most important parts relevant to the model used in this analysis. For further information, the SIMO theory manual (SIMO Project Team, 2013) should be consulted.

SIMA has been used as the graphical interface of SIMO to make the model, run analysis, visualize the simulations and post-process the results.

3.3.1 Coordinate systems

To model the system and interpret the results, it is necessary to obtain an overview of the coordinate systems. SIMO uses multiple right-handed cartesian coordinate systems where counter clockwise rotations are positive. As a reference, a global earth fixed coordinate system is used. That is positioned with the xy-plane in the calm water surface and an upward pointing z-axis. Local body fixed coordinate systems are used for bodies and will follow the local body motion. The local system is used to provide coordinates for body elements. In addition, a body related coordinate system which only follows the horizontal motion of floating bodies exist.

3.3.2 Environment

The ocean environment can be simulated by wind, waves and current in SIMO. Only waves are simulated in this project.

Linear wave potential theory is used to simulate waves, as described in section 3.1.1. Both regular waves and irregular random waves can be modelled. A number of different wave spectra enables simulation of wind sea, swell sea or a combination. In addition, a user specified numerically defined wave spectrum can be applied.

3.3.3 Force models

Body types

The type of body used will determine which force and motion models that are used in the simulation. In SIMO Project Team (2013), four different body types are presented.

- Type 1: Large volume body with 6 degrees of freedom where the total motion is simulated in time domain.
- Type 2: Large volume body with 6 degrees of freedom where the motions are separated into frequency domain and time domain.
- Type 3: Small volume body with 3 degrees of freedom (translations) where the forces are determined by position dependent hydrodynamic coefficients.
- Type 4: Same as type 1, but with fixed or prescribed body position.

If the main body is simulated as body type 1, distributed element force can be used. There are two ways of modelling distributed element force, either long slender elements or concentrated fixed elements. By using distributed elements, small body theory is used to calculate the forces. The forces are then transferred to the main body.

In theory, slender elements may be used to model all properties of the body. The only requirement for the main body is structural mass. However, this may be set to zero for the main body and defined in the distributed elements. By defining structural mass in the distributed elements, mass moment of inertia will be calculated based on the element locations.

Three coordinate systems are used in the body modelling, a global system, a body fixed system and a local coordinate system for the distributed elements. They are all orthogonal and right handed (SIMO Project Team, 2013). The hydrodynamic coefficients of slender elements are defined in the local element coordinate system.

Slender elements

The hydrodynamic forces on the slender element are based on the Morison equation. In addition, buoyancy forces F_ρ and slamming forces F_{slam} are modelled.

Both the gravity $F = -mg\ ds$ and buoyancy force $F_\rho = \rho V g dS$ acts in the global z-direction.

The wave forces are represented by:

$$F_{w,slender} = (\rho V + \rho V C_a)\ a_w + B_2 v_r |v_r| + B_1 v_r \tag{3.28}$$

V is submerged volume per unit length, a_w is water particle acceleration components in local strip coordinate system and v_r is the relative velocity. Based on the theory presented previously, the first term represents the Froude-Krylov and diffraction force, the second term is the Morison equation drag term and the third term is linear drag (SIMO Project Team, 2013).

The slamming force is expressed as:

$$F_{slam} = -\frac{\delta A_m}{\delta h} \cdot \frac{\delta h}{\delta t} v_r \tag{3.29}$$

where h is the distance between instantaneous surface elevation and strip origin in global z-direction (SIMO Project Team, 2013).

Coupling elements

To model the lifting cable, a simple wire coupling can be used. It is modelled as a linear spring, $\Delta L = \frac{T}{K}$. In this case, T is the umbilical tension, K is the effective axial stiffness and ΔL is the umbilical elongation. The possibility to include crane boom stiffness contribution, K_0, is added to the stiffness input as:

$$\frac{1}{K} = \frac{L}{EA} + \frac{1}{K_0} \tag{3.30}$$

The umbilical properties are given as the unstretched length, L, modulus of elasticity, E, and effective cross section area, A.

In addition, a tensioner may be given for the simple wire coupling (SIMO Project Team, 2013). This will simulate a passive pneumatic hydraulic cylinder. The supplied pressure will hold a mean tension in the cylinder. The input parameters consist of pretension, maximum rate of change in pretension, stiffness at the specified pretension and stroke length.

Solution methods

The calculation of water particle motion and forces due to waves are done using cosine series. That implies summation of the harmonic components in time domain. Pre-generated harmonic components by Fast Fourier transform will be a faster calculation method. However, that method will not take into account prescribed change in position using a winch. If the initial position of the ROV is in air, wave forces at the surface will be applied when the body is submerged regardless of the depth.

For the motion calculations, three integration methods can be used, Modified Euler, 3rd order Runge Kutta or Newmark predictor-corrector method (SIMO Project Team, 2013). The results in this report have been calculated using Runge Kutta.

Chapter 4

Procedure

In this chapter, calculation methods and input for the simplified method and the time domain analysis are discussed. Further, the set-up and procedure for the acceleration measurements are described.

4.1 DNV Simplified method

As mentioned previously, the current weather criterion is based on the simplified calculation method from DNV-RP-H103 (Det Norske Veritas, 2014b). The procedure is to determine the most critical phase and find the largest tension in the lifting cable. In Section 3.2, the background for the method is given.

4.1.1 Calculation method

The method of calculation will be dependant on the load case analysed. This will determine which hydrodynamic forces that are influencing the system. Thus, the results will be affected by the chosen load case, and the assumptions made for which forces that contributes. The assumptions are based on the calculations for the current weather criterion. Based on that, a better understanding of the background for the current wave height limit can be obtained.

The calculations can be divided into stages. In the first part, the hydrodynamic forces are calculated and compared to the static weight of the object. If the hydrodynamic forces exceeds the static force by a certain factor, slack umbilical leading to a snap load will occur. The next

part will then be to calculate the snap force in the umbilical. After this, the last part will be to determine the largest tension in the umbilical. That is done by summing the static and dynamic forces, where the dynamic force will be the largest of the hydrodynamic or snap force.

4.1.2 Input data

For simplicity, the calculations are done independent of the wave period. This means that significant wave height H_s is the only weather parameter in the calculations. In Table 4.1, the environment and motions of the LARS are given. These values are based on JMC Engineering (2006a), where v_{ct} is velocity of the sheave, a_{ct} is acceleration of the sheave and v_c is assumed hoisting velocity during water impact.

Table 4.1: Wave height and sheave motion.

$H_s[m]$	$v_{ct}[m/s]$	$a_{ct}[m/s^2]$	$v_c[m/s]$
4	0.5	0.46	0.17

Also the properties of the umbilical are based on JMC Engineering (2006a). The length is set to $30m$, which will be the approximate length during the water surface impact. Table 4.2 presents the properties.

Table 4.2: Properties of the umbilical.

$EA[N]$	$L[m]$	$K[N/m]$
$39 \cdot 10^6$	30	$1.3 \cdot 10^6$

The hydrodynamic properties are chosen specifically for the load case analysed. In this analysis, that corresponds to right after the water surface impact. The vertical projected area A_p is taken as the full horizontal plane area of the ROV, the volume displacement V is 0.5 m^3 and d is assumed to be small.

Table 4.3: ROV properties at the chosen load case.

$M[kg]$	$V[m^3]$	$A_p[m^2]$	$d[m]$
6400	0.5	4.8	0.2

The hydrodynamic forces are calculated based on force coefficients. Det Norske Veritas (2014b) provides recommendations for the values. These may in some cases be unnecessary

conservative due to limited information about the system. The slamming coefficient C_s should not be lower than 5 for structures other than smooth circular cylinders and the drag coefficient C_D should be higher than 2.5 in oscillatory flow unless model tests or CFD analysis has been conducted. The chosen coefficients are presented in Table 4.4.

Table 4.4: Hydrodynamic coefficients.

$C_D[-]$	$C_a[-]$	$C_s[-]$
2.5	0.8	5

4.1.3 Calculations

The calculations are based on the formulas presented in Section 3.2. In Table 4.5, water particle velocity v_w and acceleration a_w, static weight F_{stat},vertical added mass A_{33} and the relative velocity v_r are given. The slamming velocity v_{slam} is taken as the relative velocity.

Table 4.5: Static force, vertical added mass and calculated velocities and accelerations.

$F_{Stat}[kN]$	$A_{33}[kg]$	$v_w[m/s]$	$a_w[m/s^2]$	$v_r[m/s]$	$v_{slam}[m/s]$
56.775	410	3.27	3.03	3.48	3.48

The hydrodynamic forces and total force are presented in Chapter 5.

4.2 SIMO Modelling

Where determining a conservative weather criteria is the main objective of the simplified method, the intension of time domain analysis is to model the physical behavior during launch and recovery correctly. In this section, the modelling methods and simulation procedures in SIMO are presented.

4.2.1 Platform motions

Two methods have been tested to model the platform motions, a full body type 1 model and a simple body type 2 model using motion transfer functions as input. Statoil has provided a SIMO model of Snorre B to simulate the motions in the sheave point. This also included the motion transfer functions.

In order to use the motion transfer functions, the platform had to be modelled as body type 2. However, this lead to large transient motions of the ROV during the simulated operation. These motions were not damped out properly while the ROV was in air. The full body type 1 model did not cause the same problems. Thus, it was decided to use the body type 1 model. Instead, the motion transfer functions were used to validate the resulting platform motions.

The origin of the platform local coordinate system is placed at the calm water surface in the middle of the platform. At the simulation start-up, this corresponds to the global coordinate system.

4.2.2 Launch and recovery system

The model of the launch and recovery system represents the connection between the ROV and the platform. For the dynamic properties, correct motion of the sheave and stiffness in the lifting system are most important.

A body point connected to the platform is placed at the approximate winch position. SIMO enables winch simulation at a body point, where hoisting speed, acceleration and operation time can be given for several intervals. Guide points are fixed to the platform body to simulate the sheave and cursor. This will provide the correct cable length from the winch, which will influence the cable stiffness. In addition, the pendulum pivot point in the deck opening is simulated by the lowest guide point representing the cursor. The body point positions relative to the platform body coordinate system are given in table 4.6.

Table 4.6: Position of LARS components relative to the body coordinate system of Snorre B.

Coordinate	x	y	z
Winch [m]	6.5	15	26.5
Sheave [m]	6.5	18.5	27
Cursor [m]	6.5	18.5	22

The umbilical is modelled as a simple wire coupling between the winch and a body point fixed to the ROV system body. Initial length, connection flexibility, material damping and line stiffness are given as properties. The stiffness in the umbilical, elasticity modulus multiplied by cross section area, is assumed the same as used for the simplified calculations (JMC Engineering, 2006a). Based on the coupling force description in the theory manual (SIMO Project Team, 2013), material damping is chosen as 2 % of the stiffness. As the cable stiffness is assumed to provide the majority of the system stiffness, the connection flexibility is set negligibly low. The input values are presented in table 4.7

Table 4.7: Simple wire coupling input.

Initial length [m]	Connection flex. [m/N]	Stiffness (Ea) [N]	Material damping [Ns]
10	10^{-10}	$39 \cdot 10^6$	$780 \cdot 10^3$

The sheave suspension will influence the stiffness and damping in the system. Not including it in SIMO will introduce a simplification compared to the real system. On the other hand, this will make it easier to troubleshoot the model, conduct sensitivity analysis and evaluate the results from the simplified calculations.

To check how the sheave suspension affects the results, it has been modelled in two ways. The first is to insert the suspension stiffness , $1/K_0 = 1/196000\ m/N$, as the connection flexibility in the simple wire coupling input. An alternative way is to use the tensioner described in Section 3.3.3. Based on the assumptions in JMC Engineering (2006b), the input parameters are chosen as presented in Table 4.8.

Table 4.8: Tensioner input.

Pretension [N]	Max. rate of change in pretension [N/s]	Stiffness [N/m]	Stroke length [m]
87 400	$8.6 \cdot 10^5$	196 000	0.7

4.2.3 ROV system

The ROV system is modelled as a body type 1 assigned with structural mass and mass moment of inertia. To model the buoyancy and hydrodynamic forces, slender elements have been attached to the main body. The model is visualized in Figure 4.1. The black sphere represents centre of gravity for the ROV system.

Main body

To be able to build the model using slender elements, the main body has to be type 1 (SIMO Project Team, 2013). The only input requirement for this body is structural mass, which can be set to zero. In this case, structural mass, centre of gravity and mass moment of inertia is defined for the main body. By doing this instead of defining structural mass for the slender elements, a better control over the mass properties is obtained.

Information about the mass moment of inertia has not been obtained. Thus, it is assumed that the mass of the ROV and tool skid is homogeneous distributed in a cuboid. By doing this, the

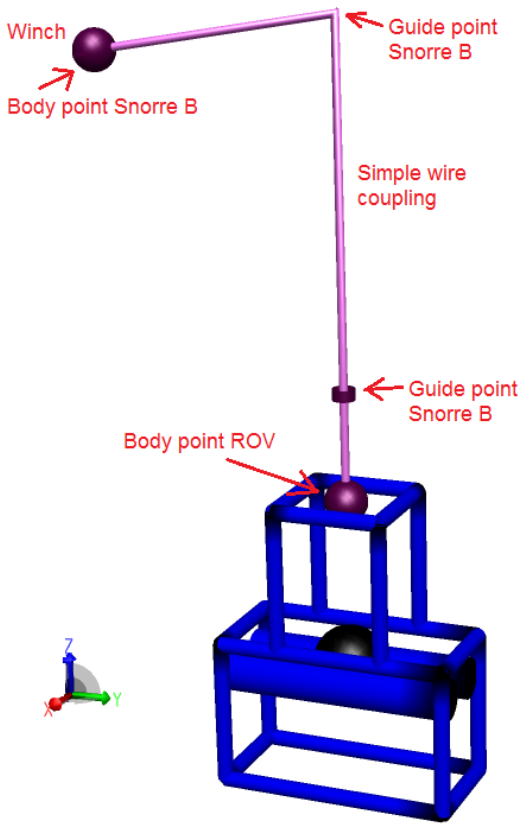

Figure 4.1: Visualization of the ROV and LARS model.

mass moment of inertia can be found from $I = \frac{1}{12}M(a^2 + b^2)$, where M is total mass and a and b are lengths out from the rotation axis (Irgens, 1999). The input values are found in Table 4.9.

Table 4.9: Mass properties of the ROV system.

Mass $[kg]$	I_{xx} $[kg \cdot m^2]$	I_{yy} $[kg \cdot m^2]$	I_{zz} $[kg \cdot m^2]$
6400	6000	3000	6000

Slender elements

Slender elements are used to simulate buoyancy and hydrodynamic properties. This is done by distributing the elements to match the geometry of the ROV system. Volume, linear and quadric drag coefficients and added mass coefficient is then defined for each element. Both the distribution and the sum of the properties should match the real object. Depth dependent volume and force coefficients are defined for the elements with length in the horizontal plane.

In Figure 4.1, the distribution of the slender elements are presented. The ROV system consists of the ROV, TMS and tool skid, as shown in Figure 2.2. This is modelled by rectangular frames placed low, mid and high in the horizontal plane. Vertical corner elements are used to simulate the forces between the horizontal planes. All these slender elements are defined with buoyancy, drag coefficients and added mass coefficients. In addition, two slender elements are placed high in the ROV frame. Only buoyancy is modelled for these. The intention is to make an element distribution that models the real hydrodynamic properties by using as few elements as possible.

Hydrodynamic properties

The method to determine hydrodynamic properties can introduce a significant error source. In this case, the hydrodynamic properties are based on model test data from Øritsland (1989). Several different structures are tested to determine force coefficients.

Two types of structures has been chosen from Øritsland (1989), a buoyant type body to represent the ROV with tool skid and a working tool body to represent the TMS. Total linear and quadratic drag force and added mass are calculated for the ROV and the TMS in x, y and z direction. Then the hydrodynamic coefficients of the slender elements in SIMO are adapted to provide the total calculated properties. In Table 4.10, the results of the calculations from Øritsland (1989) is presented. The SIMO slender elements input is adapted to match the calculated values, and is presented in Appendix C. The local coordinate system of the ROV is the same as shown in Figure 4.4.

Table 4.10: Hydrodynamic properties of the ROV system.

	TMS			ROV			Total		
	x	y	z	x	y	z	x	y	z
$M_a[kg]$	769	513	769	2306	1538	2306	3075	2050	3075
$B_1[Ns/m]$	169	169	127	462	282	451	631	451	578
$B_2[Ns^2/m^2]$	1538	1538	1153	4369	3075	4920	5907	4613	6073

For each structure that was model tested, a solidity ratio describing projected area, a fullness factor describing volume and the weight in air related to the submerged weight are given. These parameters are compared to the ROV and TMS. Based on this, the most similar modelled structure is chosen. The drag and added mass coefficients for oscillating flow have been determined by decay tests in low frequency, wave frequency and high frequency. Results from the wave frequency test is used for the linear and quadratic drag coefficient.
Keulegan–Carpenter number $KC < 6$ and Reynold number $Rn < 4.35 \cdot 10^4$ are assumed

(Øritsland and Lehn, 1987). Added mass coefficient is taken from the high frequency decay test. This is to model the slamming force due to high speed water entry, which depends on the change in added mass relative to submergence (Det Norske Veritas, 2014a). The formulas used to calculate the total force is given in Section 3.1.3.

The input values for the slender elements and properties of the model are given in Appendix C. In addition to the hydrodynamic properties, the total displacement is found to be 4215 kg and centre of buoyancy is 1.61 m higher than the lowest slender element frame, $z = 0.11$ m in the ROV body fixed coordinate system.

To model the varying forces when the ROV system is partly submerged, depth dependant coefficients are defined in SIMO. For the buoyancy and drag, they are assumed to vary linearly with the submergence. The added mass depth dependency is based on Figure 6-11 in DNV-RP-C205 (Det Norske Veritas, 2014a). In Table 4.11, the depth dependency is presented for the relative vertical position based on the element radius, R.

Table 4.11: Depth dependency of the horizontal slender element properties.

Vert. pos $z/R[-]$	$C_V[-]$	$C_{B_1}[-]$	$C_{B_2}[-]$	$C_{M_a}[-]$
1	0	0	0	0
0	0.5	0.5	0.5	0.5
-1	1	1	1	0.65
-3	1	1	1	1

4.2.4 Sea state representation

The waves are modelled as a two parameter JONSWAP spectrum with significant wave height, H_s, and peak period, T_p, as input. The peakedness parameter is taken as $\gamma = \exp[3.484\ (1 - 0.1975\ \delta_J\ T_p^4/H_s^2)]$ and $\delta_J = 0.036 - 0.0056\ T_p/\sqrt{H_s}$ (SIMO Project Team, 2013). This is valid for $3.6\ \sqrt{H_s} < T_p < 5\ \sqrt{H_s}$. Outside this domain the peakedness parameter is $\gamma = 1.0$ for $T_p \geq 5\ \sqrt{H_s}$ and $\gamma = 5.0$ for $T_p \leq 3.6\sqrt{H_s}$. Based on this, the zero-up-crossing wave period can be calculated from the relationship in Section 3.1.1.

According to Det Norske Veritas (2014b), a lower limit for the zero-up-crossing period should be $T_z = 8.9 \cdot \sqrt{H_s/g}$, which gives $T_z = 5.7$ s in $H_s = 4$ m and $T_z = 6.4$ s in $H_s = 5$ m. In addition, a maximum period of $T_z = 13$ s is mentioned. However, only wave periods up to $T_z = 10.7$ s are used. The wave periods run in the SIMO analysis are presented in Table 4.12.

Table 4.12: Zero-up-crossing period for the JONSWAP spectrum.

$H_s = 4\ m$			$H_s = 5\ m$		
$T_p\ [s]$	γ	$T_z\ [s]$	$T_p\ [s]$	γ	$T_z\ [s]$
7	5.0	5.6	8	5.0	6.4
8	3.0	6.2	9	2.9	6.9
9	1.6	6.6	10	1.6	7.3
10	1.0	7.1	11	1.1	7.9
11	1.0	7.8	12	1.0	8.5
12	1.0	8.5	13	1.0	9.3
13	1.0	9.3	14	1.0	10.0
14	1.0	10.0	15	1.0	10.7

4.2.5 Verification of SIMO model

To ensure that the variables are used correctly in the SIMO model, several tests have been conducted. The intention is to prevent errors like wrong input units and misunderstanding the coordinate systems. In addition, the numerical solver properties have been checked to provide stable simulations and correct results.

Model properties

To ensure correct input of the model parameters, simulations without waves has been run. The umbilical tension will indicate mass and buoyancy of the ROV, effects from the winch dynamics and depth dependent hydrodynamic coefficient.

In Figure 4.2, the tension during a launch in still water is presented. This graph illustrates the mass in air, buoyancy variation during water penetration, winch acceleration, hydrodynamic drag force and how the tension variations are damped. Before the winch is started, the tension corresponds to the mass of 6400 kg. The winch acceleration gives a lower tension corresponding to a reduction in gravitational acceleration. When the ROV penetrates the water surface, buoyancy and slamming impact force reduces the tension. Deceleration of the winch increases the tension after 190 seconds, before the tension is stabilized at 21.4 kN. This corresponds to the buoyancy force of 41.4 kN.

The drag coefficient will influence the tension when the ROV is submerged due to the winch speed. In this run, a velocity of 0.8 m/s leads to a vertical drag force of 3.4 kN. Using a projected area of 4.8 m^2 in Formula 3.7 gives a quadratic drag coefficient of 2.16. This is based on the assumption that the quadratic drag force is the only contribution. The input for the drag

coefficient is intended to model drag force in oscillating flow, which is larger than the steady flow coefficient without surface interaction (Øritsland and Lehn, 1987). Thus, this force is probably too high in a simulation without waves. However, it is in the same region as the drag coefficient proposed for the simplified method in Det Norske Veritas (2014b).

Depth dependant coefficients are confirmed during the water penetration. The tension reduction occur over a time span due to buoyancy, drag and slamming. Individual contributions from drag and buoyancy are difficult to distinguish. However, the slamming impact contribution is dependent on change in added mass. Thus, a small increase in tension is observed after each element with vertical added mass coefficient becomes fully submerged. The time between the first impact and the first tension rise is approximately 0.3 seconds. By calculating the time it takes to apply 65 % of the added mass coefficient with 0.8 m/s winch speed, 0.26 seconds is obtained. The last 35 % is added over the next 0.26 seconds. This confirms that the tension increase is due to reduction in the slamming impact force.

Sensitivity analysis and further discussion on the hydrodynamic properties are presented in Chapter 5.

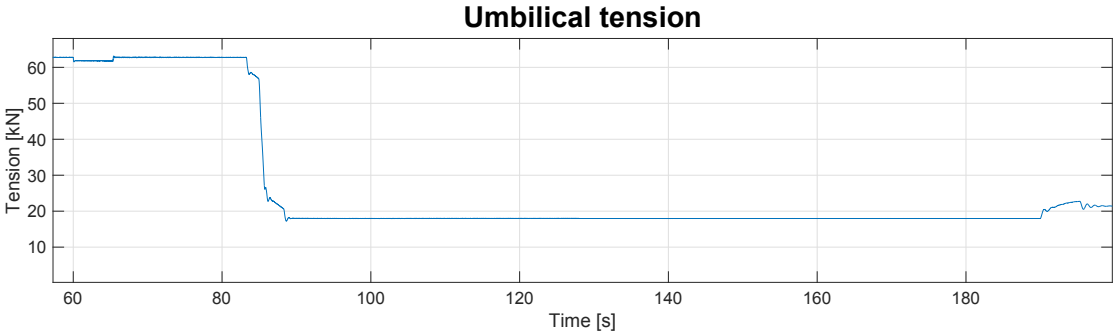

Figure 4.2: Time domain analysis without waves.

The full body type 1 Snorre B model provided by Statoil has been used to simulate the platform motions in SIMO. This model also includes first order motion transfer functions that can be used to model the platform motions as body type 2. Instead of doing that, the transfer functions have been used to check the motions obtained from the body type 1 model in regular waves. The results indicates similar motions. However, a certain time is required to stabilize the motions. It is assumed that the same results are valid for irregular waves. Because of this, the winch is started at 160 seconds in simulations with irregular waves to make sure that the platform motions are stabilized.

Numerical solving properties

The numerical properties and procedures will also influence the results. In this case, time series are generated by summation of harmonic components in time domain. This will ensure that the slender elements are subjected to wave kinematics corresponding to the actual position, as mentioned previously. Thus, this method is the only applicable for lifting operation simulations with vertical position change in the wave zone. Further, a sufficiently low time step must be used in the numerical integration.

The time step is checked by ensuring that tension peaks during snap loads are captured. A simulation with irregular waves where three subsequent snap loads occur was checked. This was done by reducing the time step until the maximum tension stabilized for the three spikes. Since 0.005 and 0.001 seconds gave the same results, a time step of 0.005 seconds was used for further analyses. In addition to the integration time step, also the storage interval was checked. After the tension spikes had stabilized, the storage interval was increased until the peaks changed. A integration time step of 0.005 seconds combined with a storage interval of 0.01 seconds is concluded to be sufficient.

4.3 Motion measurements

To investigate the actual behaviour of the ROV system during launch and recovery, an inertial measurement unit (IMU) was fitted to the ROV. In addition to look at the physical behaviour, the results can to some extent be used to validate analytical results. This will represent a simple and low cost full scale test of the ROV motions.

4.3.1 Equipment and installation

The IMU consists of an accelerometer, gyroscope and magnetometer, which together works as a three-dimensional compass and provides accelerations and rotation rates that can be transformed into an inertial reference system. Both the IMU and the camera house used as protection were borrowed from NTNU. The IMU was of type Xsens MTi-28 with device ID 01301955, and sensor specifications are summarized in Table 4.13. More information about the IMU can be found in Xsens Technologies B.V. (2010).

Before the equipment was sent to the platform, the camera house had to be modified. Better internal IMU fastening was mounted and the opening mechanism was replaced. In addition,

Table 4.13: IMU sensor specifications.

MTi-28A53G35	Acceleration	Rate of turn	Magnetic field
Units	m/s^2	deg/s	$mGauss$
Scale [units]	50	300	+/- 750
Bandwidth [Hz]	30	40	10
A/D Resolution [bits]	16	16	16
Dimentions	3	3	3

the connector on the camera house was replaced at the platform by the ROV operators, who also conducted the measurements. The connector change was done to ensue compatibility with the RS-232 communication and power supply through the ROV.

Several aspects had to be considered when mounting the IMU to the ROV. This includes connection options on the ROV and limiting the noise in the measured data. Acceleration and angular velocity will be affected by vibrations and magnetic disturbance will induce magnetic deviation on the 3D compass. Based on this, the IMU was mounted to the frame in front of the buoyancy element, as shown in Figure 4.3.

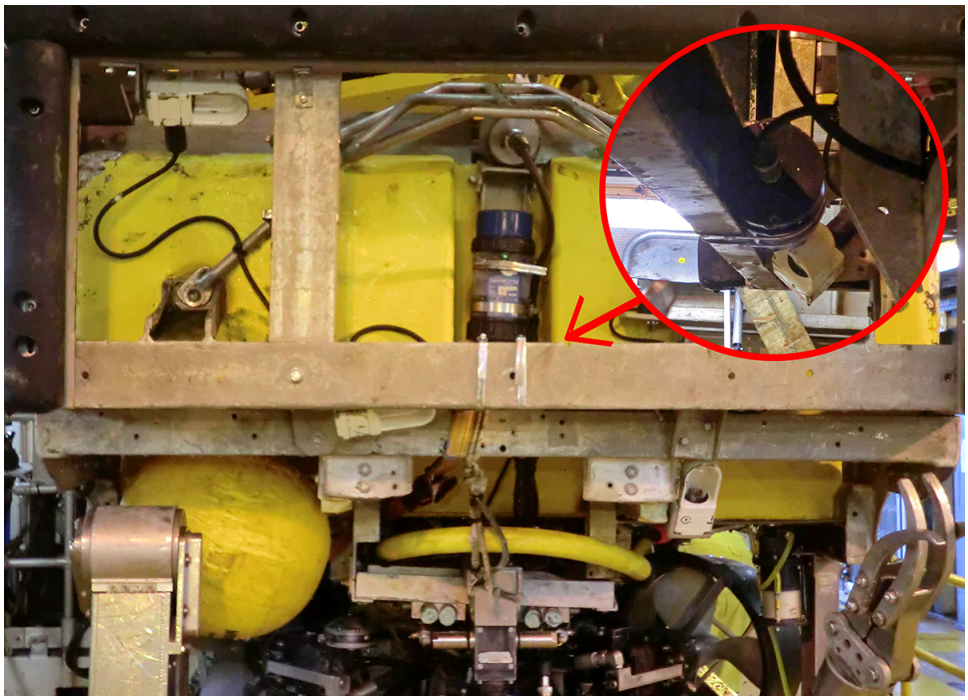

Figure 4.3: Position of IMU as seen in front of the ROV. Photos received form the ROV operators.

The location of the IMU provides distance to thrusters and electric motors. However, it also gives a distance to the centre of rotation for the ROV system. This is important to consider when comparing accelerations from the IMU with the results from the time domain

simulations. The IMU is positioned 1.67 m in front of the tether termination on the ROV and 1.70 m over the bottom of the tool skid. In SIMO, the ROV local coordinate system is placed in the middle of the horizontal slender elements frame, and 1.5 m over the lowest frame. As indicated by Figure 4.4, the horizontal distance in y-direction will have greatest influence on the difference between measurements and simulations.

4.3.2 Test procedure

The IMU manufacturers software, MT Manager, was used to change the IMU settings and log sensor data. By starting the record mode, accelerations, angular velocities and orientation are stored in a binary log file. This file can be opened in MT Manager to export the data to an ASCII file.

During launch, the record mode was started before the ROV was lifted from deck and ended when the ROV was situated below the wave zone. The same time span was covered during recovery. Based on recommendations from Xsens Technologies B.V. (2010), the IMU was powered up a while before the recording was started to stabilize the build in filters.

Wave data has been obtained from the weather monitoring system used at Snorre B, MIROS. It not possible to export time series of the wave data. Thus, the weather information has only been used to get an indication of environment at the operation time. Plots of wave height and wave periods were retrieved from Larsen (2015).

4.3.3 Post processing measurements

After extracting the data from the binary log files, Matlab was used to post process the results. This is divided into three parts:

- Transforming the accelerations into an inertial reference system.
- Further calculations to evaluate the measurements.
- Presentation of the results.

The accelerations are obtained by measuring force per unit mass. This means that the gravitational acceleration will be part of the measurements. Further, the direction of the accelerations will be given in the local IMU body fixed coordinate system. By transforming the measurements into an inertial reference frame, the global accelerations are obtained. Thus, the gravitational acceleration will only be part of the vertical acceleration. This also gives the

opportunity to compare measured accelerations with global accelerations retrieved from the SIMO analysis. Figure 4.4 illustrates the origin and coordinate system of the ROV in SIMO and the IMU in an inertial reference frame.

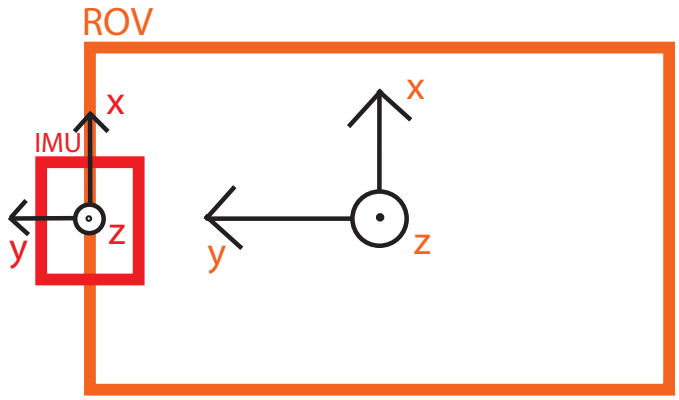

Figure 4.4: Origin of the coordinate systems from the IMU and the ROV as modelled in SIMO

The accelerations in the inertial reference frame, $\boldsymbol{A}^G = [A_x^G \; A_y^G \; A_z^G]^T$, are calculated by multiplying the local reference frame accelerations, $\boldsymbol{A}^L = [A_x^L \; A_y^L \; A_z^L]^T$ by a rotation matrix, $\boldsymbol{L}_{IB}$ (Driscoll et al., 2000b).

$$\boldsymbol{A}^G = \boldsymbol{L}_{IB}\boldsymbol{A}^L \tag{4.1}$$

$$\boldsymbol{L}_{IB} = \begin{bmatrix} \cos\psi\cdot\cos\theta & \cos\psi\cdot\sin\theta\cdot\sin\phi - \sin\psi\cdot\cos\phi & \cos\psi\cdot\sin\theta\cdot\cos\phi + \sin\psi\cdot\sin\phi \\ \sin\psi\cdot\cos\theta & \sin\psi\cdot\sin\theta\cdot\sin\phi + \cos\psi\cdot\cos\phi & \sin\psi\cdot\sin\theta\cdot\cos\phi - \cos\psi\cdot\sin\phi \\ -\sin\theta & \cos\theta\cdot\sin\phi & \cos\phi\cdot\cos\theta \end{bmatrix} \tag{4.2}$$

The orientation angles are defined such that ϕ is roll about x, θ is pitch about y and ψ is yaw about z, and obtained by using an attitude and heading reference system filter (AHRS). A build in Kalman filter, XKF-3, can be used to obtain the orientation output from the IMU (Xsens Technologies B.V., 2010). However, the transformed accelerations indicate a significant drift off in the horizontal plane. Thus, two open source AHRS filters were tested. One is developed by Sebastian Madgwick, while the other is Madgwick's implementation of Mayhony's AHRS algorithm. The Matlab code for the filter developed by Madgewick was obtained from x-IO Technologies (2012), while the implementation of Mayhony's filter was taken from Madgwick (2013).

Sebastian Madgwick's filter combines integration of angular velocities from the gyroscope, gravitational acceleration from the accelerometer and magnetic field measured by the magnetometer to obtain the orientation. By doing this, drift off due to integration of angular velocity and error due to magnetic deviation is corrected. The procedure is further described in Madgwick et al. (5550). The other filter was based on Robert Mahony's work, but did not involve data from the magnetometer. Assuming both the platform and the ROV equipment influences the magnetic field measurement differently over time, excluding the magnetometer data might give more accurate results. In addition, the magnetometer measurements is most important to provide a reference for the yaw orientation, which is of less importance in this work.

Positioning the IMU in front of the ROV pitch axis will introduce transient accelerations as the ROV rotates. To remove these, an attempt to transform the acceleration measurements to the centre of the ROV was made. Formula 4.3 was used to transform the accelerations in the point of measurement, $\boldsymbol{A^{MP}}$, to the accelerations at a specific point, $\boldsymbol{A^{SP}}$, where the specified point is given by a vector $\boldsymbol{r}^{MP}$ (Driscoll et al., 2000b).

$$\boldsymbol{A}^{SP} = \boldsymbol{A}^{MP} - \boldsymbol{L}_{IB} \cdot (\boldsymbol{\Lambda} \times \boldsymbol{r}^{MP} + \boldsymbol{\omega} \times (\boldsymbol{\omega} \times \boldsymbol{r}^{MP})) \tag{4.3}$$

The transformation requires the angular velocity, $\boldsymbol{\omega}$, and angular acceleration, $\boldsymbol{\Lambda}$. However, the measurements of angular velocity includes noise in the same frequency range as measured spikes at in the wave zone. Unfiltered angular velocities gave vertical accelerations up to 60 m/s^2, while filtered measurements gave unrealistic change around the acceleration spikes. Thus, the position compensated accelerations are considered unreliable and have not been included.

An attempt to obtain velocity and position by integrating the acceleration measurements was also made. To avoid drift off due to noise, the time series was high pass filtered. However, the filter will introduce uncertainties and remove position change due to the winch speed. This makes it difficult to obtain reliable results. Instead, integrating the wave zone accelerations over a limited time span is used to get an idea of the velocity change over a period in time.

4.3.4 Uncertainties and validation of measurements

The uncertainties in the measurements mainly consists of sensor measurement error, post processing error and interpretation error due to lack of other references.

Measurements from the sensors in the IMU have predictable noise and error, as documented in the test and calibration certificate found in Appendix D. However, external factors and post processing may introduce significant error sources. In this test, calculating the orientation used to transpose the acceleration measurements into an inertial reference frame will introduce an error source.

To check the results when transforming the accelerations into the inertial reference system, the two open source AHRS filters and the built in Kalman filter has been compared. As mentioned, the Euler angles from the IMU gives steady non zero horizontal acceleration, which indicates that the gravitational component has not been removed. Both of the open source AHRS filters uses an error correction factor to account for measurement uncertainties like sensor noise, calibration errors and sensor axis non orthogonality as mentioned in Madgwick et al. (5550). The factor has been chosen such that the steady horizontal accelerations are removed. This implies that the mean horizontal acceleration is close to zero in the time series. Further, the filter giving acceleration trends most similar to the acceleration obtained from the build in Kalman filter was used. In this case, that was the algorithm based on Mayhony's work. The results were compared to the angular velocities and accelerations for the local body fixed coordinate system as a reference.

Further verification of the transformed accelerations is difficult due to lack of other references for the ROV motion. This is also the case when the results are interpreted. Examples are the time of the first water impact, background for acceleration spikes and the degree of submergence of the ROV system. However, the combined results from the accelerometer and gyroscope compared to the knowledge about the launch and recovery procedure will reduce the risk of misinterpretation. This makes it possible to discuss theories about the behaviour of the ROV in the wave zone based on the motion measurements.

Chapter 5

Results and discussion

The results from simplified calculations, motion measurements and time domain analysis are presented in this chapter. In addition, comparison of the results and discussions around the consequences of the findings are carried out.

5.1 Simplified method

DNV recommends to divide the water penetration into four load cases between the first water impact and fully submerged (Det Norske Veritas, 2014b). However, to distinguish between the cases will be more difficult with a small volume object in large waves. In this case, each of the hydrodynamic force coefficients are calculated and checked by the snap load criterion given in Det Norske Veritas (2014b), $F_{hyd} < 0.9 \cdot F_{static}$. The hydrodynamic load components are given in Table 5.1.

Table 5.1: Static and hydrodynamic loads from simplified calculations.

$F_{stat}[kN]$	$F_{slam}[kN]$	$F_M[kN]$	$F_D[kN]$
56.8	149.1	4.2	74.5

The total hydrodynamic force is found from Formula 3.16. Not all of the force contributions are in phase and will contribute at the same time. However, both the slamming impact force and viscous drag force will individually lead to slack umbilical in the used load case according to the snap load criterion. Based on this, it can be concluded that snap load will occur for the respective load case.

In case of snap load occurrence, a more accurate calculation of the lifting operation is recommended by Det Norske Veritas (2014b). However, a simplified method to determine the snap load is provided. The results are presented in Table 5.2.

Table 5.2: Snap load calculation.

$v_{ff}[m/s]$	$C[-]$	$v_{snap}[m/s]$	$F_{snap}[kN]$	$F_{snap}+F_{static}[kN]$
3.07	0	3.07	288.3	346.0

The capacity check should be based on the largest total force, as mentioned in Section 3.2.3. In the simplified method, this is either $F_{total} = F_{stat} + F_{snap}$ or $F_{total} = F_{stat} + F_{hyd}$. To calculate the total hydrodynamic load, it is assumed that the slamming impact force do not have full effect at the same time as the hydrodynamic drag, mass and varying buoyancy force. Thus, the largest total force will be due to the snap load:

$$DAF_{snap} = \frac{F_{snap} + F_{static}}{M \cdot g} = \frac{346.0}{62.8} = 5.51\ [-] \tag{5.1}$$

The dynamic amplification factor of 5.51 is governed by the static weight, the free fall velocity when the umbilical tension is restored, the mass and the cable stiffness. Since the velocity is multiplied by the square root of the product of stiffness and mass, uncertainty in free fall velocity has the largest potential for error in the force.

The result obtained in JMC Engineering (2006a) concludes with $DAF_{snap} = 6.5$, which is even higher. This is mainly due to calculating the dynamic amplification factor by $DAF = \frac{F_{static}+F_{snap}}{F_{static}}$, using $C_D = 2.0$ and a structural mass of $M = 7000\ kg$ in their calculations. It should be noted that the current launch and recovery system is not dimensioned for a dynamic amplification factor of 6.5. By doing analysis of the sheave suspension arrangement, the DAF has been reduced to 3.0 (JMC Engineering, 2006b).

Based on the simplified calculations, the slamming force is the single largest contribution for snap loads to occur. The drag force is about half in size, but still large enough to cause slack umbilical. Motion measurements and SIMO analysis will be used to further investigate the validity of this.

5.2 Motion measurements

During the motion measurement test, six launches and two recoveries were logged in total. In Table 5.3, the loggings are presented with wave data taken from the MIROS system at Snorre B. Due to the short time period available and downtime on the ROV system, only this limited amount loggings were performed. Thus, generalisations from the results must be carefully handled. However, both launch and recovery of the ROV have been covered in four meter significant wave height. This gives the opportunity to evaluate examples of behaviour in weather conditions used around the current weather criterion. Plots of the most interesting period from each logging are found in Appendix A.

Table 5.3: Received log files with corresponding wave condition.

Local time	Phase	H_s [m]	T_z [s]	Sampling [Hz]	Length [s]
2015-04-02 19h58	Launch	3.7	7.9	100	270.7
2015-04-04 14h19	Launch	1.5	8.3	100	230.7
2015-04-05 03h47	Launch	1.7	8.3	100	7969.8
2015-04-09 22h36	Launch	3.0	6.9	100	4744.4
2015-04-12 20h32	Recovery	4.0	7.5	200	421.9
2015-04-13 01h47	Launch	3.5	7.1	200	360.4
2015-04-14 00h15	Recovery	3.0	6.5	200	591.4
2015-04-14 02h50	Launch	4.0	7.0	200	213.9

The launch phases discussed in Section 2.2 are recognised from the IMU data. Before lift-off from deck, vertical accelerations varying with the wave period are observed. This corresponds to the motion of the platform. Accelerations with a higher frequency dominates the measurements after lift-off and until the guide frame lands on the platform deck. The impact between the guide frame and deck gives large vertical acceleration spikes. After disconnecting the guide frame, a steady yaw velocity is observed. In addition, the gyroscope indicates local pitch and roll oscillations combined with a pendulum motion with lower frequency. The first water impact is identified by larger horizontal accelerations and angular velocity changes with lower frequency than in air.

The data have been evaluated based on accelerations, orientation and rotation rates only. This is sufficient information to identify phases as lift off from deck and the first water impact. On the other side, details concerning effects in the wave zone are easily misunderstood. Especially acceleration spikes are difficult to assess. The fact that accelerations and orientation are obtained through filters and transformations must also be kept in mind. This is discussed in Section 4.3.4. Position and coordinate system of the IMU are presented in Section 4.3.3.

5.2.1 Above the water surface

The most relevant measurement phase is the lowering from the deck and through the wave zone. Spikes in the vertical acceleration identifies the landing of the guide frame on the deck. For both recoveries and two of the launches, these represents the highest vertical accelerations in the time series. However, the duration is less than 0.1 seconds, which indicates that the acceleration spikes do not influence the tension in the umbilical much.

After disconnecting the ROV from the guide frame, a steady angular velocity in yaw is observed for most measurements. In addition, oscillations with an amplitude below 0.1 degrees per second and a period between one and two seconds are present for all three angular velocities. Because of the short period and low amplitude, this is assumed to represent local pitch, roll and yaw motion of the ROV.

The two recovery measurements indicates pendulum motion in addition to local rotations of the ROV. This is based on angular velocities with a period decreasing from around seven seconds toward zero as the umbilical length is reduced. Reduction of the period as the cable length, L, is reduced coincides with the simplified pendulum natural period formula $T = 2\pi\sqrt{L/g}$. The angular velocity amplitudes increases as the period decreases. Also oscillations that are damped out short after the ROV is assumed to be out of the water are shown. That can be local pitch and roll motions due to exit forces from the water. The recovery measurements are found in Figure A.5 and A.7.

5.2.2 Wave zone

The first water impact during launch is identified by a distinctive change from the pattern described above the water surface. Larger horizontal accelerations and higher angular velocities with longer period of oscillation are observed. This phase is shown in Figure 5.1, taken from the launch 14th of April at 02:50.

It is difficult to estimate the position of the ROV related to the water surface. The ROV might get hit by a wave top followed by a period without water contact. In addition, the winch speed is unknown, and will vary for each measurement logging. When the accelerations stabilize with longer periods and the high frequency oscillations in the angular velocities disappears, the ROV is assumed to be fully submerged. Assuming maximum wave height of $1.8 \cdot H_s = 1.8 \cdot 4\ m = 7.2\ m$ and winch speed of 0.4 m/s, 18 seconds transit time from wave top to wave trough is obtained. Thus, the ROV may exit the water several seconds after the first water

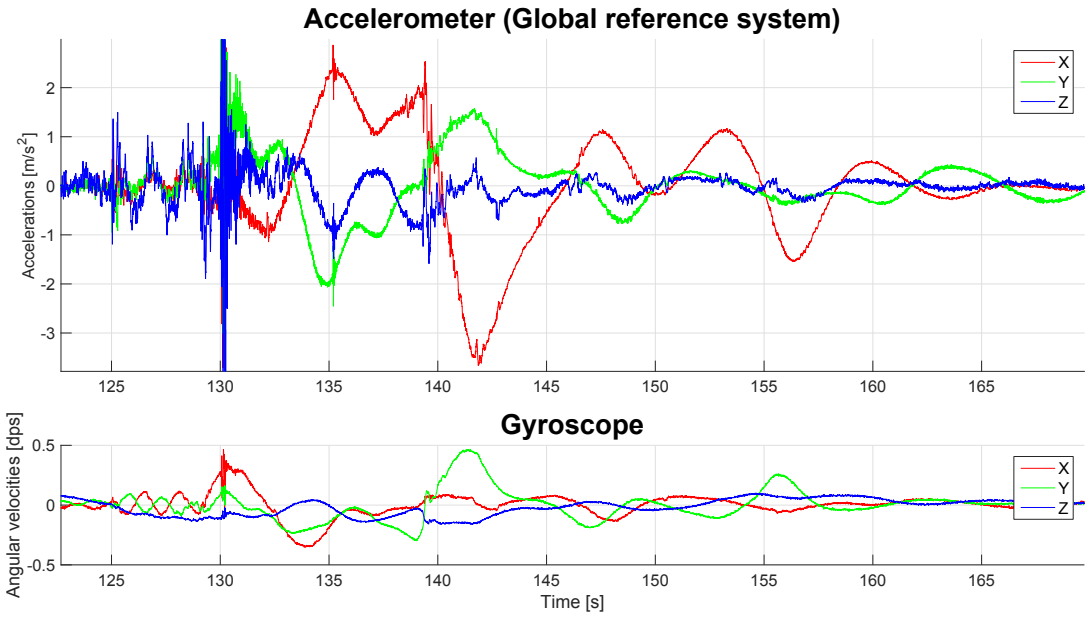

Figure 5.1: Wave zone accelerations during launch 2015-04-14 at 02:50

impact. This is a possible explanation for the variations in the period of the horizontal acceleration between 125 and 145 seconds in Figure 5.1. The motions stabilize from around 145 seconds.

Also an increase in vertical acceleration is measured in this phase. Considering that the IMU is mounted in the forward part of the ROV, the gyroscope data indicates that the cause is pitch motion causing local acceleration at the front of the ROV. Roll motion does not have the same effect since the position is along the mid axis of the length direction. An example is shown by the angular velocity peak at 142 seconds, which does not seem to influence the vertical acceleration much.

5.2.3 Acceleration spikes

Large vertical positive acceleration measurements with a duration shorter than 0.5 seconds are observed in the wave zone during launch. This does not necessarily translate into large tension increase in the umbilical. In this section, possible causes of the spikes and the consequences are discussed.

Table 5.4 shows the largest accelerations measured in the wave zone during launch. In addition, an approximate time duration of the impulse is included. This shows that most measurements have vertical acceleration spikes of duration less than 0.05 seconds. Based on

the short duration, it is uncertain if these spikes indicate large vertical acceleration of the whole ROV system or only local accelerations of the camera house or fastening beam. The fact that the camera house is covered by the fastening beam in front, the buoyancy element in the back, but is unprotected from the bottom, supports that the camera house suffers from direct water impact from below.

Table 5.4: Maximum positive acceleration in wave zone with approximate duration.

Logging	Acceleration $[m/s^2]$	Duration $[s]$
2015-04-02 19:58	8.3	0.04
2015-04-04 14:19	4.0	0.05
2015-04-05 03:47	2.9	0.04
2015-04-09 22:36	2.5	0.06
2015-04-13 01:47	9.7	0.22
2015-04-14 02:50	13.3	0.01

However, the acceleration spike shown in Figure 5.2 stands out from the others. Between 126.0 and 127.575 seconds the acceleration is negative without sudden changes. After this, a short negative acceleration spike combined with a positive pitch velocity spike appears. This happens before the large vertical acceleration measurement of 9.7 m/s^2 with a duration of 0.22 seconds is observed. Four similar oscillations over 1.05 seconds with amplitudes between 1.15 and 1.35 m/s^2 follow after the spike, giving a mean period of 0.26 seconds.

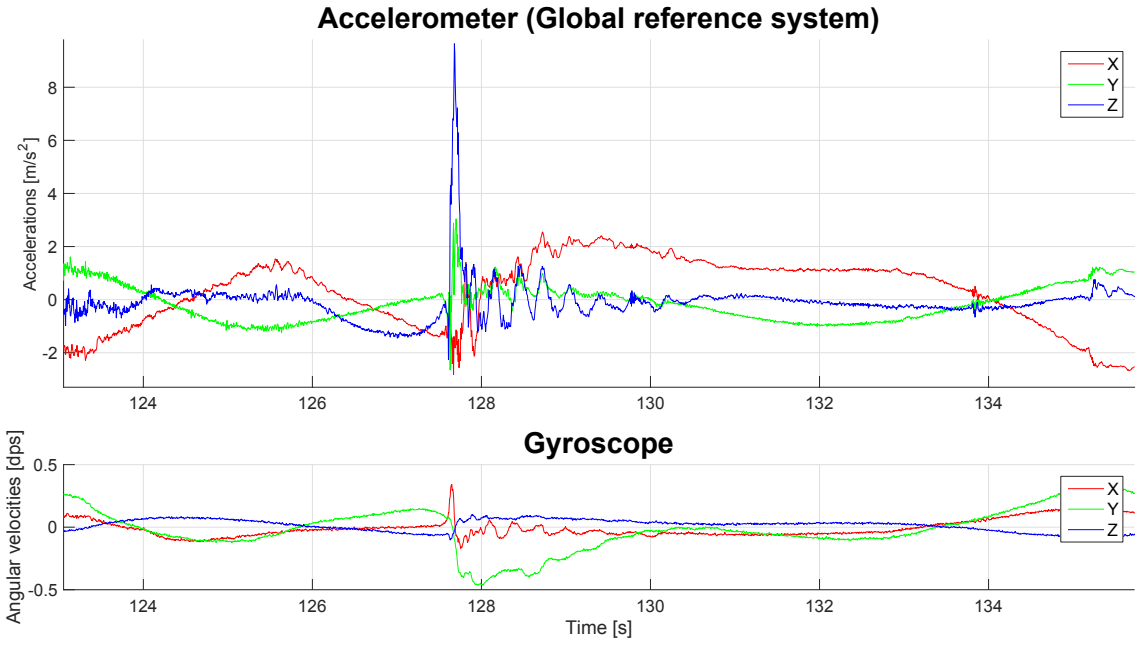

Figure 5.2: Acceleration spike during launch 2015-04-13 at 01:47

By calculating the area over the unfiltered signal, the negative acceleration gives a vertical velocity change of 1.47 m/s before the spike. Doing the same for the spike indicates a positive vertical velocity change of 0.83 m/s. One theory is that the negative acceleration occurs with a slack umbilical when the ROV is partly or fully submerged. When the umbilical tension is restored, a pitch correction is caused together with the positive acceleration spike. The following oscillations indicates low damping, which can be caused by the ROV being fully or partially out of the water.

A simple estimate of the natural period assuming the cable as the main stiffness contribution, EA/L, indicates $T_0 = 2\,\pi\sqrt{\frac{(M+A_{33})}{K}} = 0.36\ s$. The cable input EA is taken from the SIMO input and the length is assumed 20 meters. Since the system is assumed to be out of the water, vertical added mass term is not taken into account. Thus, the mass term is taken as $M = 6400\ kg$. If the ROV is fully or partially submerged, added mass will increase the natural period. The calculated natural period is 38 % longer than the measured period. Including the effect of the snap load damper will lower the stiffness. Thus, the natural period will become longer. If the acceleration spike and oscillations are due to a snap load, this indicates that the current sheave damper system has limited effect on the stiffness during snap loads.

After the wave zone transit, the winch is stopped to change operating place from outside on deck to the control container. This is shown in Figure 5.3 to illustrate a controlled velocity change of the ROV. The area corresponds to a velocity change of 0.88 m/s, which is higher than the maximum winch speed of $0.8 m/s$. Probable causes are positive heave acceleration of the platform or measurement post processing inaccuracies.

Also in this case, vertical acceleration oscillation is observed. However, the period is longer and decreasing amplitude indicates higher damping. Three oscillations are observed during 3.95 seconds, giving an approximate period of 1.32 seconds. Using a cable length of 120 meters based on full winch speed after the acceleration spike, the natural period is found to be 1.07 seconds neglecting the sheave suspension stiffness. Vertical added mass of 3000 kg is included in this case. Higher measured period coincides with lower stiffness due to the sheave damper system. In JMC Engineering (2006b) the stiffness of the suspension is assumed to be 196.0 kN/m, leading to a 37.6 % reduction with a combined stiffness of 122.2 kN/m. The natural period calculation then gives 1.74 seconds. This is 32 % longer than the measured period, which is between the two calculated periods. Uncertainties in cable length and stiffness, the suspension stiffness and added mass will influence the result.

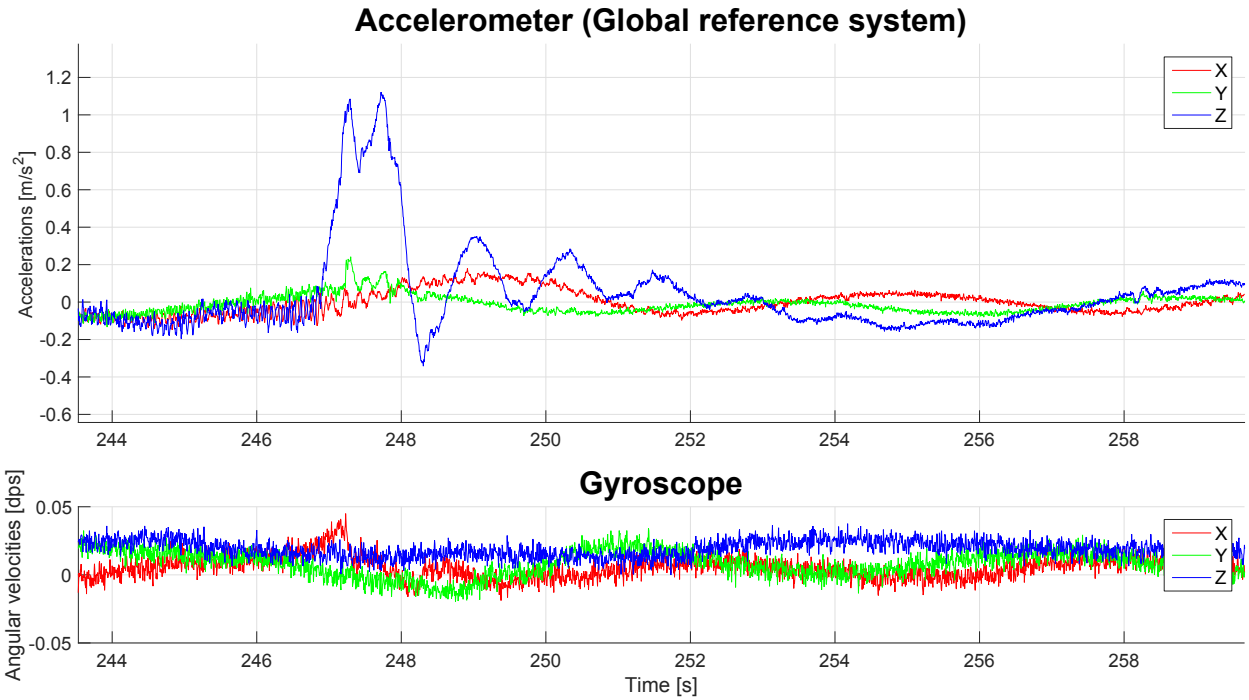

Figure 5.3: Winch stop below wave zone during launch 2015-04-13 at 01:47.

5.3 Time domain analysis

In this section, results from the SIMO model are presented and discussed. Sensitivities when changing input parameters are first checked to determine relationships and dependencies between the input and results. Further, the model is used to obtain better understanding of critical factors for the ROV motion and umbilical tension.

5.3.1 Sensitivity analysis

Sensitivity analysis have been conducted to illustrate how the different properties of the model influences the results. This will give a better understanding of the model behaviour and how inaccurate input can influence the results. Examples are the ratio between drag and inertia forces and relationship changes with different coefficients.

Hydrodynamic coefficients

Ten launches with winch speed 0.8 m/s were run with different wave seed using a two parameter JONSWAP wave spectrum with $T_p = 8\ s$ and $H_s = 4\ m$. All ten runs were checked with different coefficients, but only the run with highest umbilical tension is presented here. For the critical run with the initial input parameters, zero tension occurred twice with following snap loads.

Added mass will influence the inertia forces and the slamming impact force. In Figure 5.4, umbilical tension for three runs with the same environment, but changing added mass coefficient, are shown. The slamming impact force on the lowest frame of slender elements is evident before the buoyancy element gets submerged. Increasing the added mass coefficient by 50 % has limited impact on the tension during the slamming phase. On the other side, removing the added mass will reduce the tension by 5 - 10 kN. For SIMO's slamming model, this corresponds to removing the slamming contribution. The largest change in tension occurs during the re-tensioning after the first period of slack umbilical. Fifty percent higher added mass increases the tension from 44 kN to 51 kN, while eliminating it causes a snap load of only 24 kN.

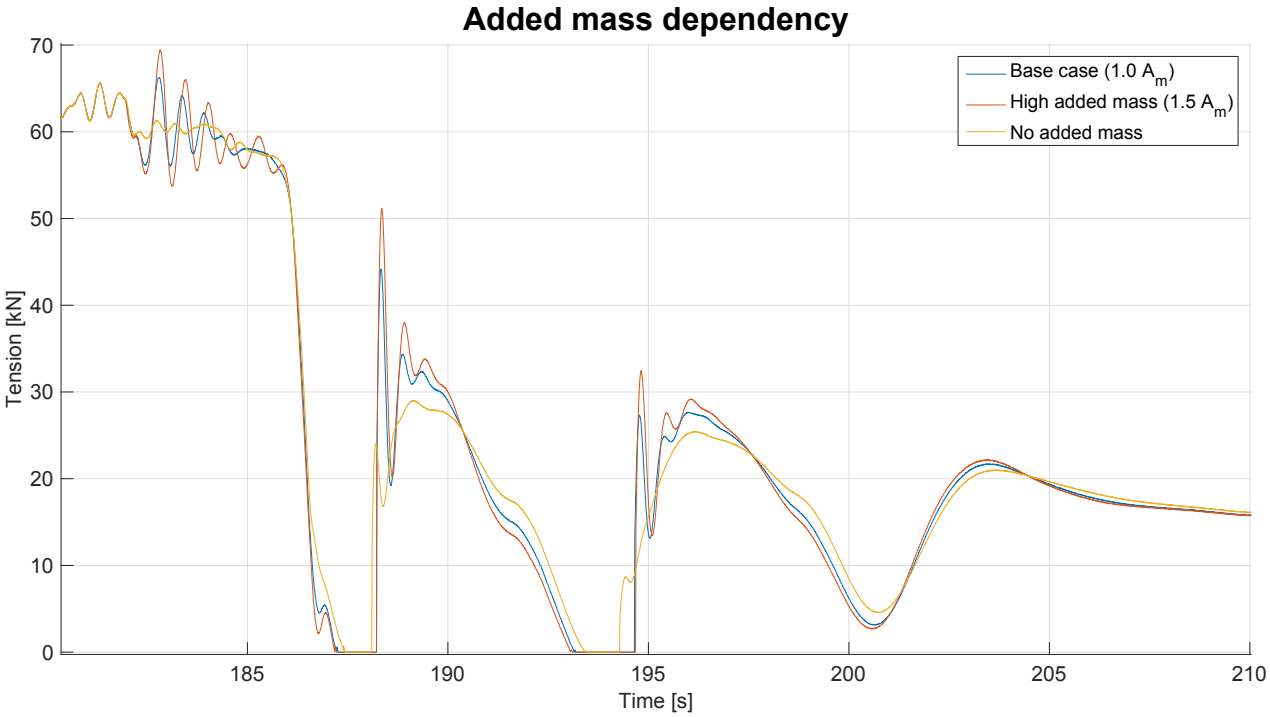

Figure 5.4: Sensitivity analysis of added mass coefficient on umbilical tension.

In Figure 5.5, tension variation due to change in quadratic drag coefficient is presented. Fifty percent increase in the quadratic drag coefficient gave an additional period of no umbilical tension leading to a snap load. In addition, the first Snap load increased from $45kN$ to $105kN$, an increase of 133%. On the other hand, reducing it by 50 % eliminated all snap loads due to slack umbilical.

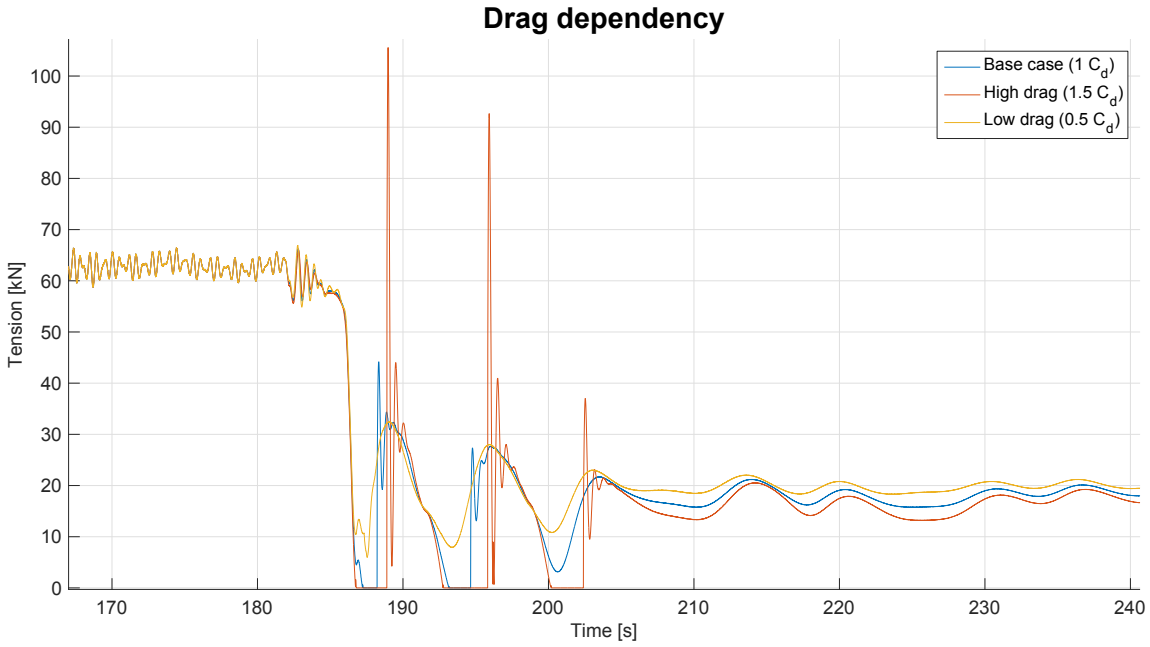

Figure 5.5: Sensitivity analysis of drag coefficient on umbilical tension.

Based on these results, both the added mass and drag coefficients seems to be important for the umbilical tension. Small changes in the added mass coefficient do not affect the umbilical tension much. However, the reduction in tension when eliminating added mass proves the importance of including it. The added mass term does not seem to influence the occurrence of slack umbilical. On the contrary, change in the quadratic drag coefficient will influence both occurrence of zero umbilical tension and the size of the following snap load. Consequently, uncertainties in quadratic drag coefficient are more critical than for the added mass coefficient. This is further discussed in Section 5.3.6.

Depth dependent coefficients

To simulate vertical variations of the hydrodynamic properties for the horizontal slender elements, depth dependency has been added to the volume and force coefficients. This is particularly important for the slamming force due to the slamming model in SIMO. In Figure

5.6, the vertical distance of active coefficients has been changed 50 %. The influence is largest for the tension spike around the first water impact and for the snap load during re-tensioning of the umbilical. However, the influence is small compared to the sensitivity analysis of the coefficient values. Thus, which of the coefficients that are responsible for the deviation is not further investigated.

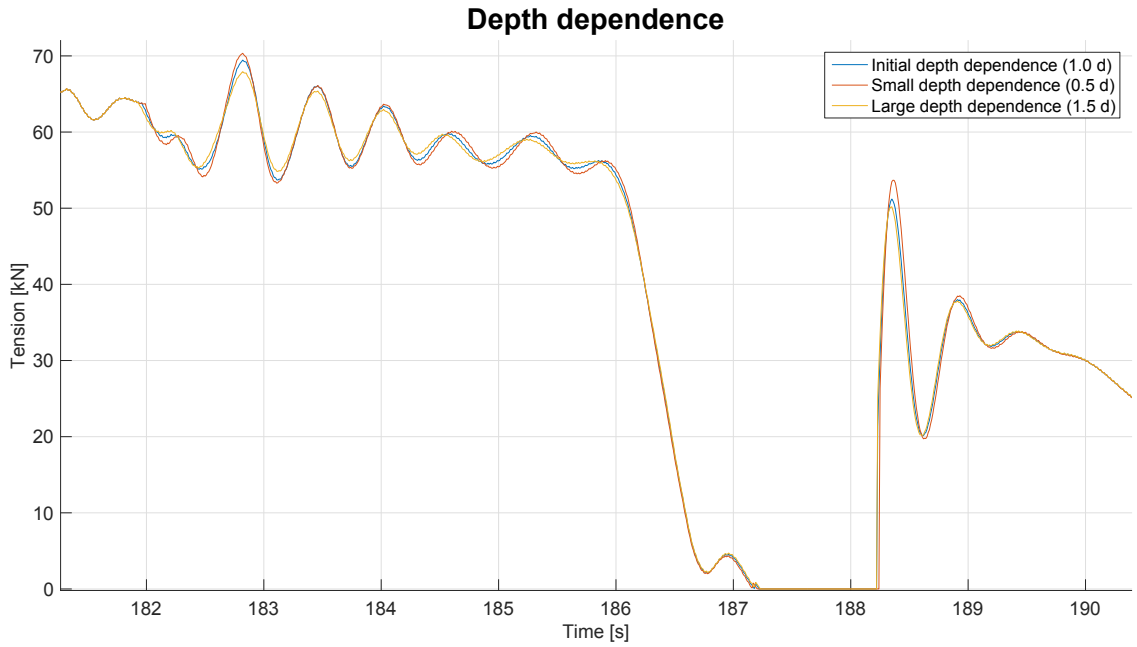

Figure 5.6: Depth dependent coefficients sensitivity for the lower element frame.

Horizontal forces

To check the importance of the horizontal hydrodynamic coefficients, a ROV model without horizontal added mass and drag was run. In Figure 5.7, the results from 30 wave seeds in $H_s = 4\ m$ and $T_p = 8\ s$ are presented. The results indicates that the vertical hydrodynamic forces only will increase the umbilical tension. Thus, the risk of zero tension is non-existing. This indicates that the ROV moves horizontally to the position where the wave forces do not work against the gravitational force. Consequently, also the horizontal hydrodynamic coefficients are important to obtain correct umbilical tension.

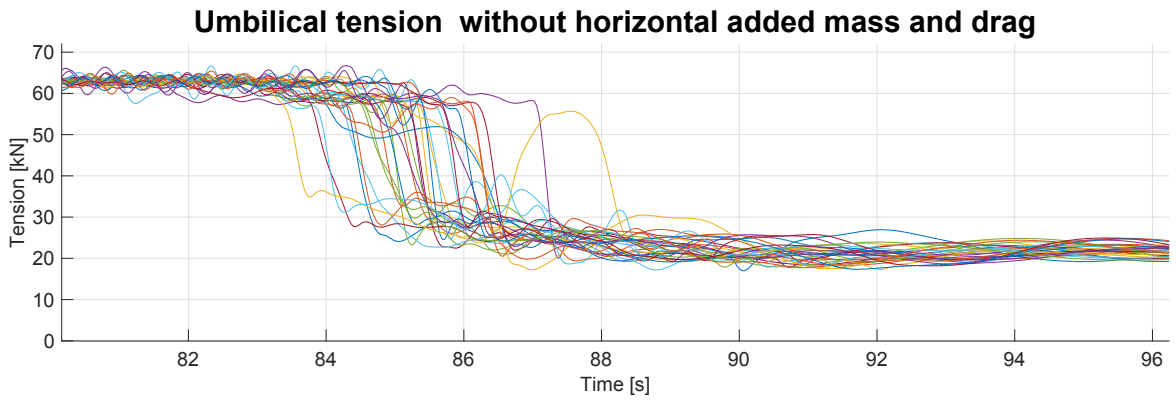

Figure 5.7: Umbilical tension in $H_s = 4\ m$ and $T_p = 8\ s$ without horizontal drag and added mass coefficients.

5.3.2 Winch speed

The winch speed is an important parameter during launch and recovery. In addition to control the time that the ROV is situated in the splash zone, also the slamming forces and the steady vertical drag forces will be influenced.

Based on the sensitivity analysis of the added mass coefficient, the slamming force is assumed to have a limited effect. Drag forces will reduce the umbilical tension when the winch speed is increased due to a larger relative velocity. Thus, the probability for slack umbilical will rise. On the contrary, the ROV will transit the wave zone faster with a higher winch speed. This way the ROV is exposed to wave forces for a shorter time span, and unfavourable wave kinetics leading to slack umbilical can be avoided

To check which effects that are most important, two winch speeds have been run with 60 wave seeds in $H_s = 4\ m$ and $T_p = 8\ s$. In addition, 30 wave seeds were run for each speed with $T_p = 7\ s$. The results are found in Table 5.5. Due to different winch speed, the ROV is subjected to different wave kinetics at the same wave seed. That is the reason for running the large number of simulations. Slack in the umbilical occurs in 10 of the 60 runs with winch speed 0.4 m/s and 15 of the 60 runs with winch speed 0.8 m/s. Also the periods of zero tension are in general longer for the highest winch speed. However, the largest umbilical tension occurs for the lowest winch speed. Several factors will influence this. A shorter period of slack combined with lower winch speed means that the ROV will travel a shorter distance. Since the wave kinematics decreases with depth, the wave forces will be higher when the snap load occurs. Further, lower winch speed will reduce the vertical drag force due to a steady velocity. A winch speed of 0.8 m/s gives a steady drag force of 3.4 kN, while 0.4 m/s reduces it to 0.85 kN.

Table 5.5: Snap load characteristics variation due to winch speed in $H_s = 4\ m$.

Spectrum peak period T_p [s]	7		8	
Winch speed $[m/s]$	0.4	0.8	0.4	0.8
No of periods with slack [-]	3	12	10	15
Mean period of slack [s]	1.53	1.28	0.74	0.97
Max tension [kN]	133.1	132.6	112.5	111.7

Based on this, it seems like the winch speed will influence the probability for slack umbilical, while other factor are more important for the maximum snap load tension. This will be further investigated in Section 5.3.6.

5.3.3 Horizontal translation

The clearance between the ROV and the platform hull can cause problems during launch and recovery. Even though the deck opening is positioned midway between the platform hull columns, the horizontal distance between the pontoon side and the sheave position is only about 6 meters (Bruset, 2014). To check the risk of impact, the horizontal ROV position relative to the sheave has been plotted in Figure 5.8. The red lines in the top plot indicates the approximate position of the pontoon wall relative to the sheave position, while the blue lines represent the ROV position for 30 wave seeds in the direction of incoming waves.

As observed in Figure 5.8, the centre of the ROV passes the 6 meter mark once in $H_s = 4\ m$ and $T_p = 7\ s$. However, the pontoon position is normally 12.5 meters below the mean water surface (Bruset, 2014). When considering where the largest translations occur, impact between the ROV and the pontoon does not occur in this case. Taking into account the ROV's horizontal extent, the latest critical position happens 195 seconds out in the time series when the ROV buoyancy element is 7.2 meters below the mean water surface.

To investigate if this represents the worst case in $H_s = 4\ m$, a longer wave period and lower winch speed have been checked. In addition, the case with $H_s = 4\ m$ and $T_p = 7\ s$ has been run using 30 additional wave seeds to check if the first runs provides a good representation. The latest critical position occurs with the buoyancy element 7.3 meters below the mean water surface, which coincides well with 7.2 meters. On the contrary, a longer wave period gives smaller translation. Setting $T_p = 8\ s$ with $H_s = 4\ m$ gives the latest critical position at 5 meters below the mean surface. Further, reducing the winch speed from 0.8 to 0.4 m/s with $T_p = 8\ s$ decreases the depth to one meter below the mean water surface. This indicates that impact is most likely with a short wave period combined with high winch speed.

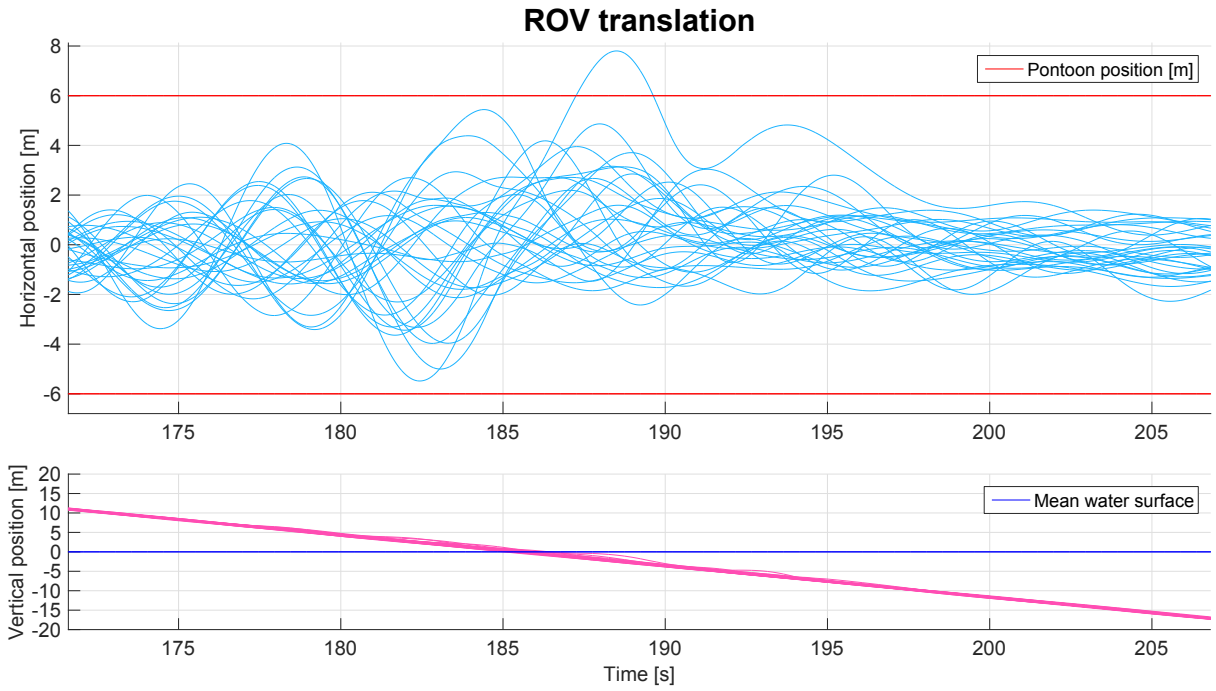

Figure 5.8: ROV horizontal and vertical position during 30 wave seeds in $H_s = 4\ m$ and $T_p = 7\ s$.

Also the motion of the pontoon has to be taken into consideration. If the ROV motion is 180 degrees out of phase with the pontoon motion, both the critical depth and horizontal translation will be reduced for the ROV. To check which motions that can be expected, the platform translations from SIMO has been transferred to a point at $z = -10\ m$ and $y = 24.5\ m$. In Figure 5.9, the pontoon position in $H_s = 5\ m$ and $T_p = 9\ s$ relative to the deck opening position is presented. The horizontal motion is limited to an amplitude of 0.7 m, while the vertical motion amplitude is maximum 0.3 m. Based on this, the motion of the pontoon will only have a limited effect on the risk of impact between the ROV and the pontoon.

Considering that the real position of the pontoon is more than 10 meters below the mean water surface, the SIMO analysis indicates that impact between the ROV and the pontoon does not occur in $H_s = 4\ m$.

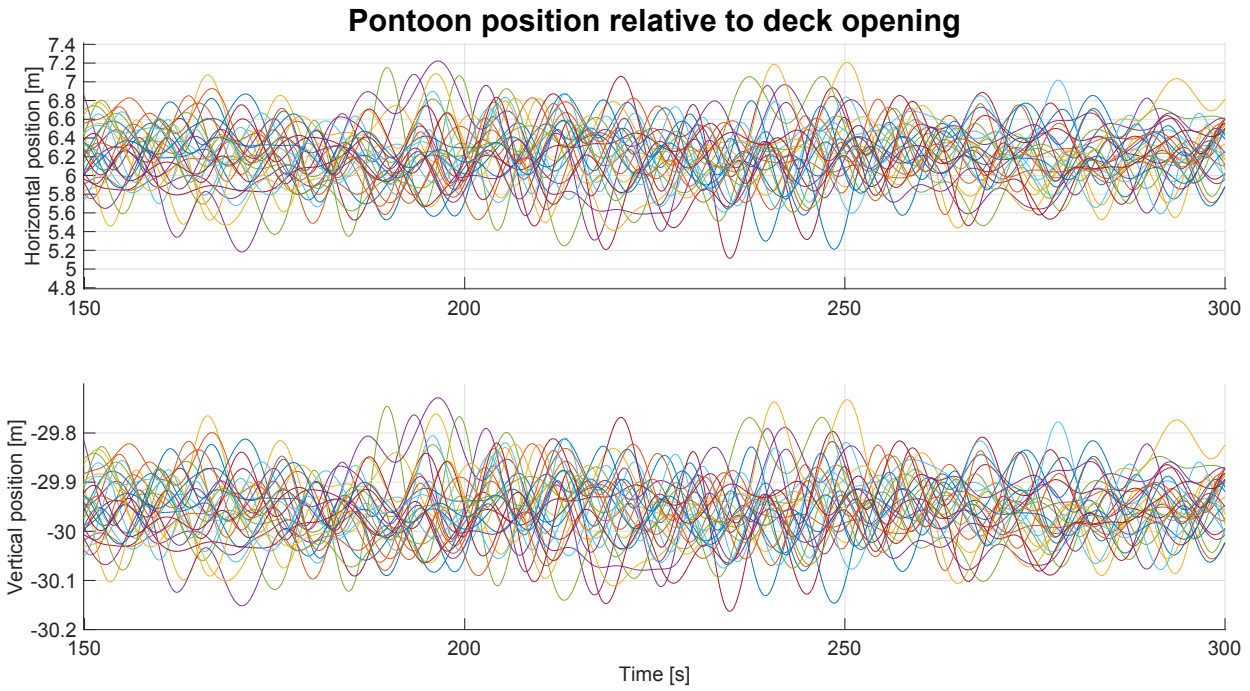

Figure 5.9: Pontoon horizontal and vertical position relative to the deck opening position during 30 wave seeds in $H_s = 5\ m$ and $T_p = 9\ s$.

5.3.4 ROV recovery phase

Most of the analysis are based on the ROV launch phase. That is assumed to be most vulnerable to slack umbilical leading to snap loads. In the recovery phase, the winch speed will increase the tension due to drag forces, and slamming on the ROV are less probable. However, the ROV is still exposed to wave forces and water exit effects. Thus, also recovery has been simulated. Higher mass due to entrapped water has not been included as the ROV system is assumed to have a high degree of perforation.

Figure 5.10 shows the umbilical tension for 30 wave seeds during recovery of the ROV. In contrast to launching the ROV in the same sea state, the umbilical tension is never near zero. The lowest tension obtained is 14.5 kN, corresponding to 23 % of the static weight in air. This indicates that the launching operation is more critical than the recovery operation in terms of slack umbilical. In addition, the tension in the umbilical does not exceed the transient tension variations in air observed during the launch simulations, despite using the maximum winch speed of 0.8 m/s.

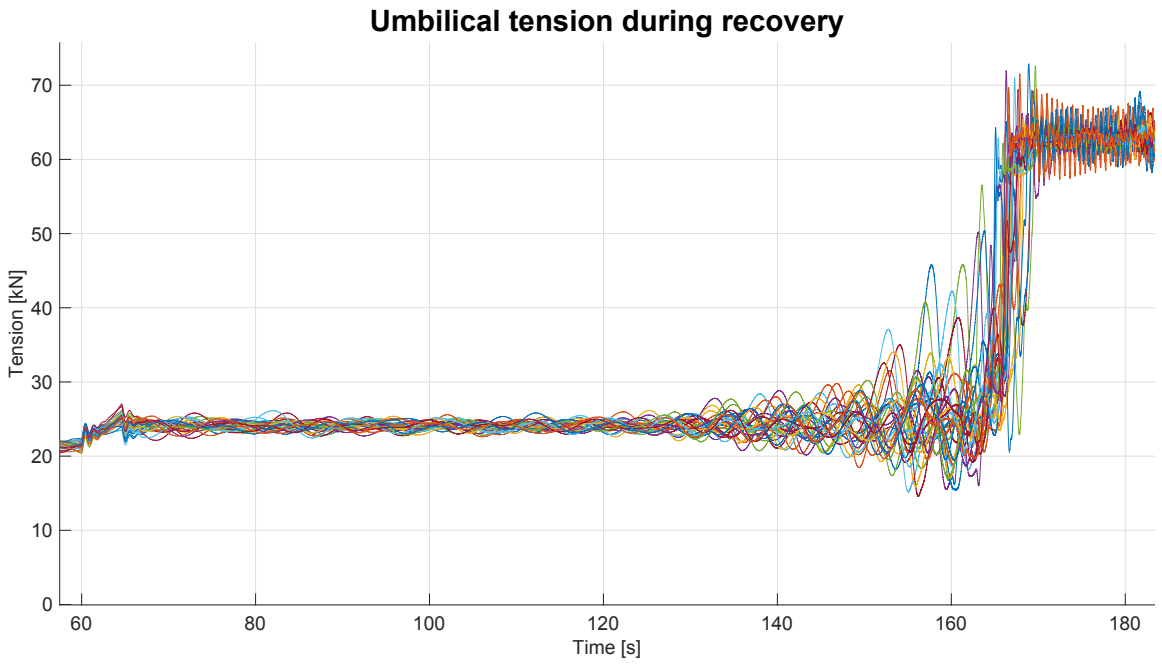

Figure 5.10: Umbilical tension during recovery for 30 wave seeds in $H_s = 4\ m$ and $T_p = 8\ s$.

5.3.5 Weather condition

To investigate how the weather condition influences the results, 30 wave seeds have been run using a JONSWAP wave spectrum for different significant wave heights and peak periods. The sea state properties are presented in Table 4.12. Umbilical tensions from each run are presented in Appendix B. Two aspects are particularly interesting, the maximum umbilical tension and if slack in the umbilical occurs. That is indicated by the maximum and minimum tension for each run in the plots.

The current weather criterion is set at a significant wave height of four meters regardless of the wave period. Therefore, four meters significant wave height has been checked with a spectrum peak period varying between 7 and 14 seconds. In addition, five meters significant wave height has been used to investigate consequences of a higher wave limit. Due to a long simulation run time, the number of conditions has been limited. Change in the direction of incoming waves has not been checked. One reason is that the platform heave transfer function changes little due to the symmetrical hull. In addition, wave shadow effects due to interaction with the columns are not modelled. That is assumed to affect the forces more than change in the platform motion. Thus, changing the wave direction by 45 degrees is considered to introduce more uncertainties in the results.

The general observation is that the maximum umbilical tension increases with lower wave period and increasing wave height. This is as expected due to larger water particle velocities and accelerations with increasing wave amplitude and frequency. Since the wave period is increased until slack umbilical is avoided, snap loads occurs for all sea states except the two longest periods. However, the snap loads are significantly higher for lower wave periods. Most of the slack umbilical incidents do not cause higher tension than the weight of the ROV system in air. This is due to the high buoyancy of the ROV and tool skid, which will increase the risk of slack umbilical and reduce the total force during snap loads when the ROV is submerged.

Impact between the ROV and the pontoon can also be critical. This was discussed in Section 5.3.3, but mainly for $H_s = 4\ m$. To check the influence from wave height, the translation at $H_s = 4\ m$ and $T_p = 7\ s$ has been compared with the result from $H_s = 5\ m$ and $T_p = 8\ s$. In both simulations, a winch speed of 0.8 m/s was used. By assuming a critical horizontal translation of 4.4 meters, the latest occurrence was found to be with a buoyancy element submergence of 6.1 meters. That is less than 7.2 meters found for $H_s = 4\ m$, and supports the theory that pontoon impact is less important for the weather criterion.

5.3.6 Snap loads in SIMO

The time domain analysis indicates that the largest umbilical tension occur due to snap loads after a period of slack umbilical. When the period without tension increases, the size of the tension spike gets larger. Thus, it is important to investigate which effects cause zero tension in the umbilical.

Wave forces

To check how the wave forces influence the largest umbilical tension, vertical wave kinematics have been plotted against the tension in Figure 5.11. Particle velocity and acceleration have been taken at the middle of the slender element simulating the buoyancy element in the length direction. Before the element is submerged, the data represents surface wave kinematics.

The umbilical tension reaches zero when the declining vertical particle acceleration crosses the increasing vertical particle velocity. Since the drag forces are dependant to the velocity component while the inertia forces are proportional to the acceleration, this indicates that the drag coefficient is most important for occurrence of slack umbilical. When the velocity reaches zero, re-tensioning in the umbilical is observed. This happens as the acceleration is at the lower extreme value, and will induce the highest downwards wave induced inertia force. Thus,

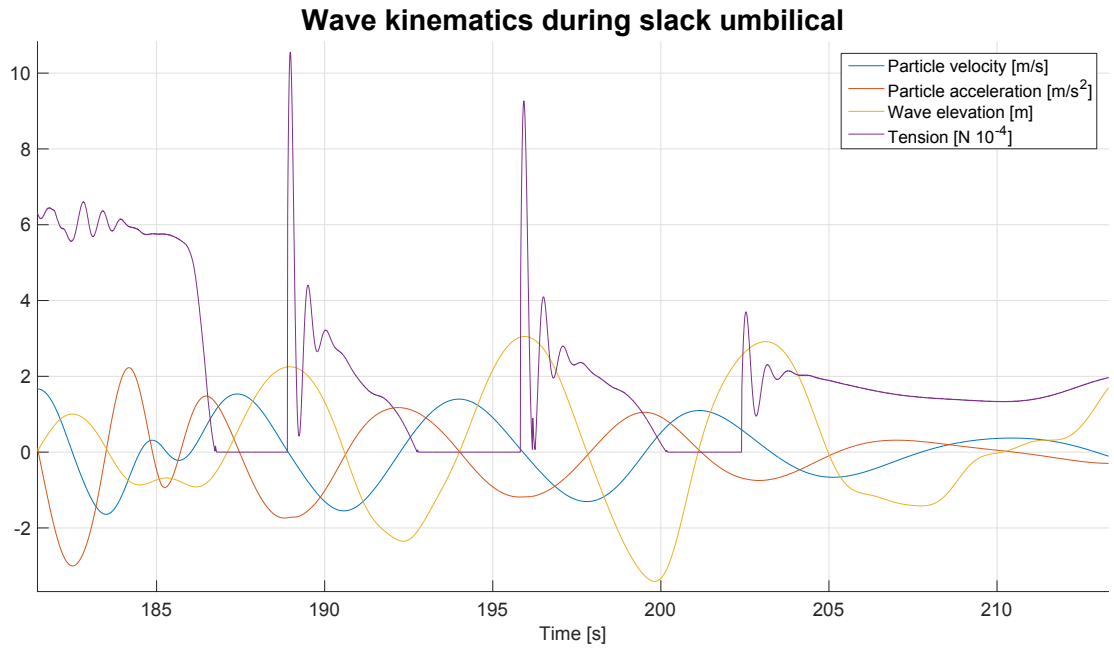

Figure 5.11: Vertical wave kinematics compared to umbilical tension.

inertia forces influence the snap load as indicated during the sensitivity analysis. Also the drag force will start acting downwards. However, the downwards velocity will be much smaller than the acceleration during the snap load.

Based on this, it seems like drag forces are most important for occurrence and length of slack umbilical. The inertia term will act maximum downwards during the re-tensioning of the umbilical. In addition, the inertia force will influence the time of slack umbilical and snap velocity. This is because of the negative vertical water particle acceleration most of the period of slack umbilical. Assuming that the tension is restored when the particle velocity reaches zero, the maximum snap load increase found in the drag coefficient sensitivity analysis will be limited by the period of positive particle velocity.

Quantifying the snap load

The simplified calculation of the snap load, F_{snap}, can be derived from conservation of energy. Kinetic energy is assumed to be transformed into potential energy as spring energy. This gives $F_{snap} = v_{snap} \cdot \sqrt{K \cdot (M + A_{33})}$, where v_{snap} is the velocity absorbed, K is the system stiffness and $M + A_{33}$ corresponds to the mass term including vertical added mass when submerged. However, this implies that other external forces do not contribute by external work during the snap load.

To check which parameters that are important for the umbilical tension, the snap load in Figure 5.12 has been evaluated. Following the same wave kinetics pattern as in Figure 5.11, a snap load occurs at maximum wave elevation. The ROV velocity plot indicates a downward vertical velocity of $1.415 m/s$ before the snap load. Since the winch speed is 0.8 m/s and the sheave velocity is 0.171 m/s, the snap velocity is taken as $v_{snap} = 1.415\ m/s - 0.800\ m/s + 0.171\ m/s = 0.786\ m/s$. Using a cable length of $L = 34.5\ m$ and a mass term of $M + A_{33} = 6400\ kg + 3000\ kg = 9400\ kg$ gives a snap force of $F_{snap} = 81.0 kN$. To obtain the total force, the weight is added in $F_{total} = (M - \rho V) \cdot g + F_{snap}$. In this case $M = 6400\ kg$ and $\rho V = 4215\ kg$, giving $F_{total} = 102.5\ kN$. The tension plot shows 111.7 kN, 8.9 % higher than calculated. This indicates that additional forces will influence the ROV during the snap load, but that the assumption can give an indication of the total force.

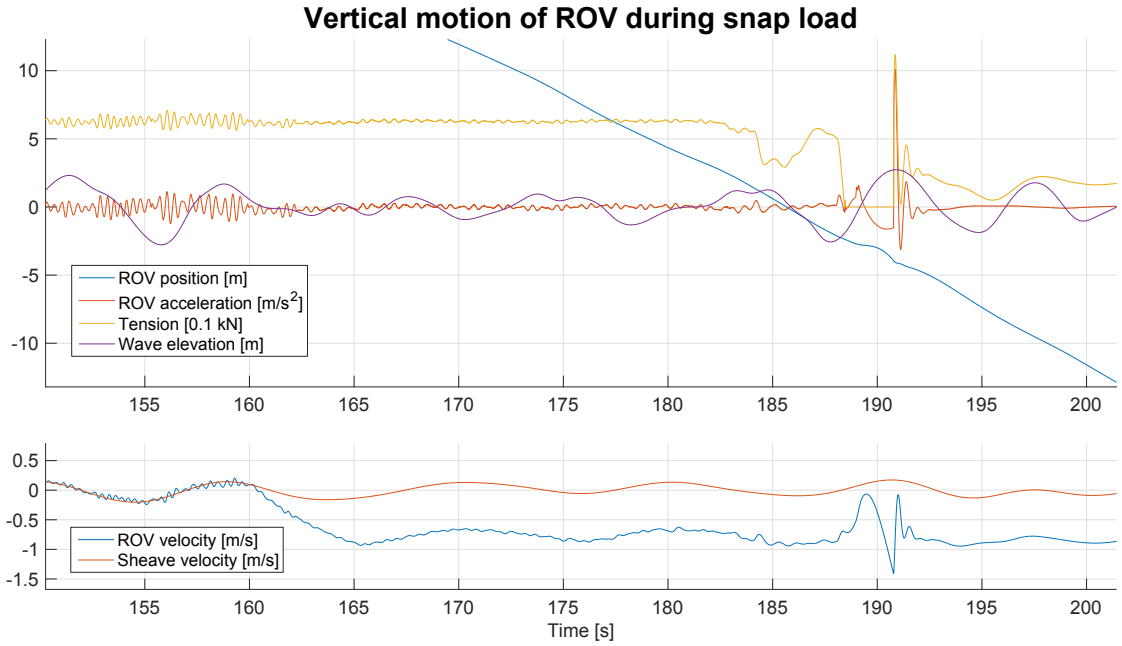

Figure 5.12: ROV vertical motion during snap load in $H_s = 4\ m$ and $T_p = 8\ s$.

The calculation gave a lower total force than what was obtained in SIMO. This indicates that other external forces contributes as work. Based on the maximum downward water particle acceleration, the wave induced inertia forces are assumed to influence on the umbilical tension during snap loads. In addition, the inertia force contribution to the snap velocity during slack umbilical is included in the calculation. This is done by taking the ROV velocity from the SIMO results. Contribution from the inertia force is confirmed by the sensitivity analysis of the added mass coefficient presented in Figure 5.4. Although, whether the contribution was due to ROV velocity change or forces acting during the force impulse was not established.

For a snap load occurring with a fully submerged ROV, the simple formula provides an indication of the total force during snap loads. However, the calculation is based on known steady drag force, added mass and stiffness of the system. These properties are easy to determine from the input values, but are subject to uncertainties in the real system. In addition, the sheave and winch speed are taken into account. Based on this, a snap velocity taken as the free fall velocity without umbilical tension, v_{ff}, corrected for crane tip velocity, v_{ct}, and winch speed, v_c seems to be a good approximation. This will require a good approximation of the free fall velocity of the ROV exposed to wave forces.

5.3.7 Stiffness and damping in the launching system

The launch and recovery system influences both the stiffness and damping in the problem. For most of the simulations, the effect from the sheave stiffness is left out of the model by assuming large stiffness. Then the stiffness and damping properties of the umbilical will be the dominating effects. To check the validity of this assumption, three different ways of modelling the stiffness and damping in the launching system have been checked. This will also give an indication of the effect by using a sheave suspension system.

In addition to assuming large sheave stiffness, both adding a tensioner at the winch and reducing the sheave stiffness for the connection flexibility in the simple wire coupling input have been checked. The input was based on assumptions around the current sheave suspension system. This represents course simplifications of the system, but will give an indication of how the snap loads are affected by reducing the stiffness in the system.

Based on the assumptions in JMC Engineering (2006b), the stiffness of the sheave suspension is set to 196 kN/m. Using the same umbilical characteristics with a length of 30 meters, the effective axial stiffness is reduced from 1299.5 kN/m to 170.3 kN/m. In Figure 5.13, the effect by including the sheave stiffness is illustrated by the yellow line compared to only model the umbilical stiffness for the blue line. The tensioner will represent a passive pneumatic hydraulic cylinder (SIMO Project Team, 2013), and the effect from using the tensioner is presented as the red line. By using the tensioner, better representation of the combined stiffness and damping properties can be obtained.

The alternative modelling do not influence the time duration of slack umbilical. In contrast, the resulting snap load is reduced to 75.7 % with the tensioner and to 62.0 % with reduced sheave stiffness compared to only including umbilical stiffness. Further, the decreased stiffness gives a longer period of oscillation following the snap load. A longer natural period will reduce

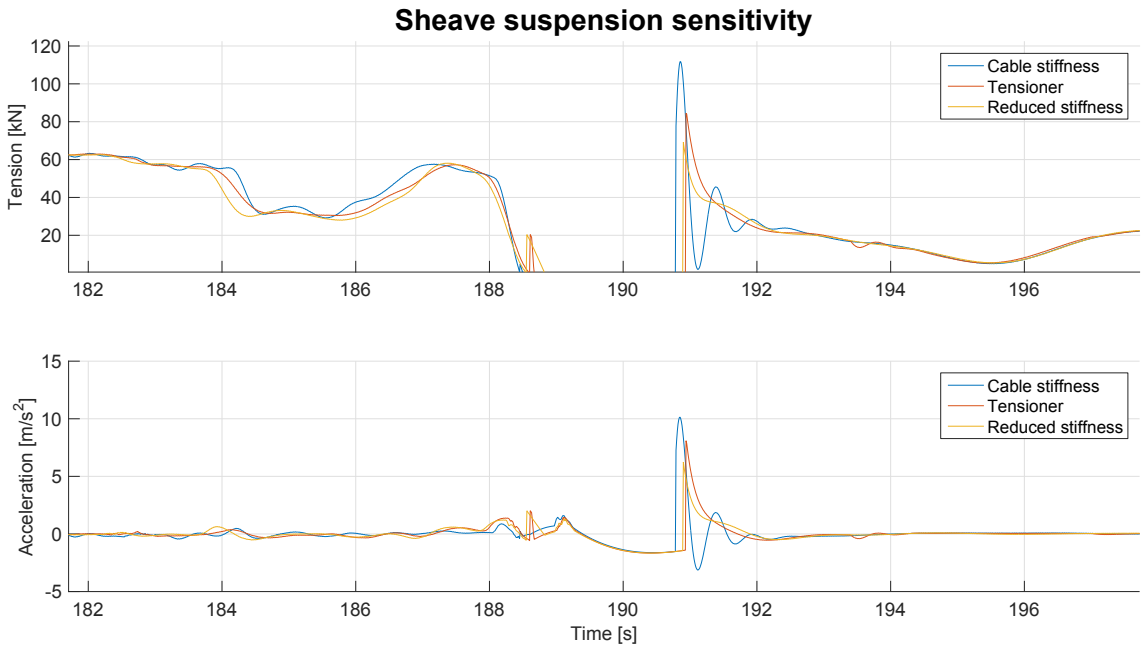

Figure 5.13: Tension and vertical acceleration variation due to change in stiffness.

the ratio between the length of the force impulse and the natural period of the system. This will decrease the dynamic amplification of the displacement for the following oscillations, as illustrated by Figure 3.5 in Larsen (2012). Assuming a triangular shaped impulse lasting 1/6 of the natural period, the dynamic amplification factor is around 0.5 for the following free oscillation. The example corresponds to an impulse duration of 0.25 seconds combined with a natural period of 1.5 seconds. In comparison, an impulse duration ratio of 1.0 will cause a dynamic amplification factor of around 1.5. Thus, lower stiffness can prevent additional snap loads caused by the first oscillation after the snap load impulse.

It is clear that decreasing the stiffness can be beneficial in terms of reducing maximum umbilical tension. However, the stiffness reduction due to the current passive suspension system will be limited by the piston stroke length. If the stiffness is set too low, the piston will hit the end stops with high velocity. This will cause large forces in the suspension system and the reduced stiffness effect disappears. The suspension stiffness has to be adjusted so that the stroke length is utilized, but the piston does not hit the end stops. The natural period must also be taken into consideration. Based on the current stiffness, the natural period is around 1.5 seconds in the wave zone and approximately 2.3 seconds at the operation depth of 350 meters. Further decreasing the stiffness may increase the natural period into the wave band, causing resonance in vertical motion at the operation depth. This can make it difficult to dock the ROV onto the TMS and cause snap loads in the umbilical at operation depth.

Due to uncertainties in the input parameters and improvement potential, the effects of different sheave stiffness and damping modelling has not been further investigated at this stage. Both the value of the suspension stiffness and the linear behaviour found from JMC Engineering (2006b) should be verified. In addition, the improvement potential of a modified system will be dependant on space limitations and the chosen solution.

5.4 Comparison of results

Results and discussions of the measurements, SIMO analysis and simplified calculations have now been presented. In this section, relevant results from each method will be compared to give an indication of the representation of the real ROV launch and recovery operation.

When comparing the results, it is important have the simplifications in the SIMO model and uncertainties in the input parameters in mind. Examples are neglected wind forces and sheave suspension stiffness in the SIMO model and only a JONSWAP wave spectrum using linear wave theory is used to model the irregular waves. The real environment and equipment will be more complex. Also the measurements includes uncertainties due to transformation, filtering and lack of references.

5.4.1 Steady accelerations

In Figure 5.1, measured accelerations in the wave zone are presented. This represents a launch in approximately $H_s = 4\ m$ and $T_z = 7\ s$, based on the obtained MIROS data Larsen (2015). The horizontal accelerations are found to be between $-3.5\ m/s^2$ and $2.5\ m/s^2$. In addition, the period indicates that the ROV enters the water more than once. To check if the SIMO model can reproduce these accelerations, four plots of the ROV acceleration in global y-direction are presented in Figure 5.14. The vertical position of the buoyancy element relative to the wave elevation is used to give an indication of the submergence of the ROV. Different wave seed have been used to obtain the data in $H_s = 4\ m$ and $T_p = 8\ s$ with winch speed $0.4\ m/s$.

The results from the current SIMO model confirms that horizontal accelerations in the order of $3\ m/s^2$ are possible. The upper right plot shows the largest positive acceleration obtained after running 30 different wave seeds. After 195 seconds, the acceleration increases from $-2\ m/s^2$ to $3.5\ m/s^2$. The sudden decrease in relative vertical position indicates impact with a wave top. Variations in vertical relative position is assumed to be mainly due to the wave elevation. Rise

in horizontal acceleration combined with a local position decrease is also seen in the other plots.

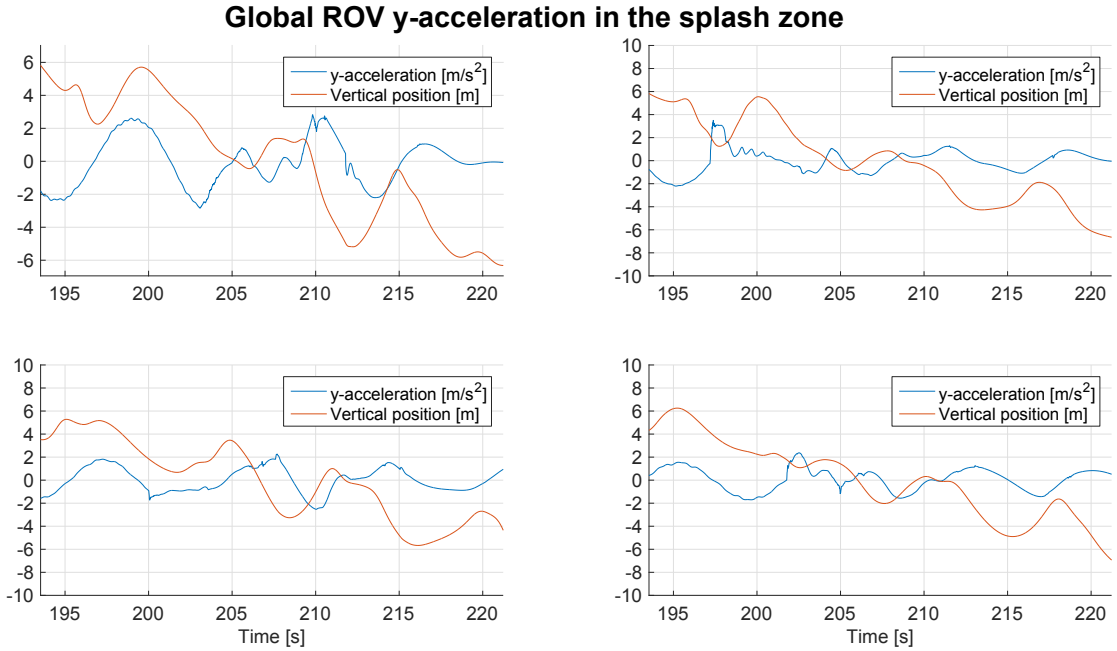

Figure 5.14: ROV acceleration in global y-direction versus position relative to wave elevation in $H_s = 4\ m$ and $T_p = 8\ s$ with winch speed 0.4 m/s.

Both the measured accelerations and the results from SIMO shows large variation in the horizontal accelerations. In addition, the SIMO results includes large transient accelerations before the winch is started, which will influence the ROV accelerations until the first water contact. This makes direct comparison difficult. However, the results have given an indication of the magnitude of the accelerations due to water impact and wave forces. The analysis results shows that horizontal accelerations up to 3.5 m/s^2 occurs with the current SIMO model in a similar sea state. The largest horizontal accelerations happens when a wave top is hit, as indicated by the upper right plot in Figure 5.14. Based on the motion measurements, the SIMO model seems to provide realistic horizontal accelerations in the wave zone.

5.4.2 Vertical acceleration spikes

Due to lack of references, it is difficult to verify theories related to the motion measurements. That is particularly critical for the suspected snap load occurrence presented in Figure 5.2. To further investigate possible causes, the acceleration measurements are compared to vertical ROV accelerations during a snap load occurrence in SIMO.

In Figure 5.15, the largest snap load occurrence during launch in $H_s = 4\ m$ and $T_p = 8\ s$ with winch speed 0.4 m/s is presented. The top plot shows global vertical velocity and acceleration of the ROV related to the umbilical tension, while the bottom plot indicates the corresponding vertical wave properties. In addition, the ROV buoyancy element vertical position is presented to indicate the degree of submergence.

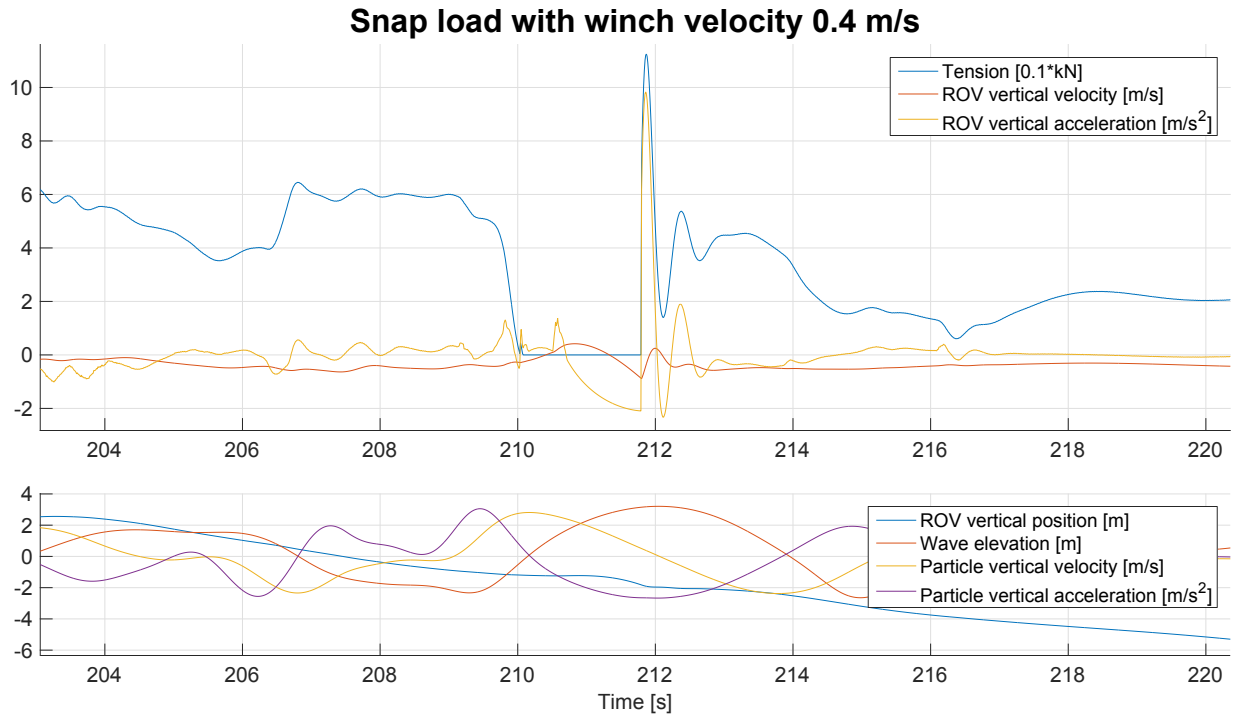

Figure 5.15: ROV motion and wave kinetics in $H_s = 4\ m$ and $T_p = 8\ s$ with winch speed 0.4 m/s.

The vertical ROV accelerations from SIMO shows a similar pattern as the measurement in Figure 5.2. First there is a negative acceleration lasting approximately 1.5 seconds. In the analysis this accelerations has a slightly shorter duration, but ends at a higher negative acceleration. Both cases ends by an acceleration spike of around 9.5 m/s^2 followed by oscillations. The lower plot in Figure 5.15 shows that slack in the umbilical starts when the ROV is partially submerged, but the snap load happens when the ROV is fully submerged under the wave top. Damping in water explains the underdamped behaviour for the following oscillations. The first three oscillations in the measured vertical acceleration indicates an undamped behaviour, suggesting that the ROV is out of the water. In addition, the vertical acceleration decreases before the spike in the measurement. Assuming slack umbilical, reduction in static weight as parts of the ROV system exits the water can be an explanation. Also decreasing downward water particle acceleration before the wave exit can be a cause. This requires the relative contribution from the inertia forces to be important.

Based on the comparison, the analysis from SIMO indicates that the measured spike can be due to re-tension in the umbilical. Also the snap velocity of 0.79 m/s found in Figure 5.12 coincides well with the approximated velocity change of 0.83 m/s during the acceleration spike in Figure 5.2. However, limited references makes it difficult to conclude. In addition, the comparison shows that the vertical position of the ROV relative to the water surface may be different during the acceleration spikes. If the measured spike is re-tensioning in the cable, the vertical position relative to the water surface will influence the snap load due to different mass term, buoyancy force and exit forces in the water surface.

5.4.3 Umbilical tension

The simplified calculations gave larger snap loads compared to the SIMO analysis. A free fall velocity of 3.07 m/s is the main reason. That was based on the drag force expression, and was not dependant on the duration of slack umbilical. Neither the SIMO analysis nor the measurements proves the occurrence of such large vertical velocities. This can indicate that the procedure for finding the snap velocity is over conservative. However, a certain safety factor is required due to uncertainties in the analysis input. Also the limited amount of measurements combined with uncertainties in the post processing must be taken into consideration. One example is that pitch motions of the ROV can influence the vertical acceleration measurements. Considering the gyroscope data will limit that uncertainty.

The largest snap loads from each set of wave seeds in SIMO seems to be a result of the same occurrence. The ROV enters the water, the vertical water particle velocity causes slack umbilical and the snap load occurs as the vertical water particle velocity reaches zero and the particle acceleration is maximum downwards below the wave top. This is not confirmed by the assumed snap load in the measurement in Figure 5.2. If the ROV is partially out of the water, exit forces and lower buoyancy forces will increase the umbilical tension as mentioned. In addition, added mass may still contribute in the mass term for determining the snap load. Consequently, verification of the snap loads occurring in the SIMO analysis is not achieved with the current data available. On the contrary, the vertical acceleration pattern during slack umbilical and the snap load in SIMO shows similarities with the measured acceleration in Figure 5.2.

5.5 Weather criterion

Measurements, time domain simulations and simplified calculations confirms the complexity and variability of lifting operations in the wave zone. This means that the weather criterion must be based on a conservative estimation of a close to real procedure.

Large variability in the forces within each sea state makes it difficult to evaluate the weather criterion. However, the acceleration measurements and the SIMO simulations gives an indication of the most critical factors. The results shows that lowering the ROV through the wave zone is the dimensioning phase. That is based on horizontal and vertical accelerations in the measurements and large umbilical tension obtained in SIMO. Lower measured accelerations and no slack umbilical occurrence in the simulations confirms the assumption that recovery is less critical. Further, parameter variations in SIMO indicates that snap loads following from slack umbilical provides the dimensioning forces for the weather criterion. In addition, pontoon impact has not occurred in the performed simulations.

The current ROV launch and recovery system is dimensioned for snap loads in the umbilical. That is based on the simplified calculations, where the dimensioning force is reduced by a sheave suspension system. The simulations in SIMO without the sheave suspension has not resulted in higher tension than the safe working load for the umbilical in $H_s = 4\ m$ and $H_s = 5\ m$. However, even if the safe load is not exceeded, other effects might cause limitations for the weather criterion. That can be damage to the inner core of electrical and optical conductors in the umbilical, which is especially relevant for tension impulses (Driscoll et al., 2000c). At Snorre B, the combination of snap loads and concentrated umbilical loads over the sheave wheels and winch spooling device can be critical. In addition, uncertainties in the SIMO input parameters requires a conservative estimate of the forces. The sensitivity analysis proved that changes in the drag coefficients are particularly critical. A 50 % increase in the quadratic drag coefficient more than doubled the umbilical tension during a snap load.

The modelling of a sheave suspension system in SIMO reduced both the snap load and the following tension oscillations. This indicates that a proper sheave suspension arrangement is the best solution to reduce umbilical tension. However, including this in the weather criterion evaluation requires detailed knowledge about the properties of the suspension system. When designing an effective snap load reduction system, information about duration and size of the impulses will also be necessary. That can be obtained using reliable measurements combined with statistics from time domain simulations.

Chapter 6

Conclusions and further Work

6.1 Conclusions

Based on the description of the launch and recovery phases and procedure, the wave zone was assumed to be the most critical when determining the weather criterion. Thus, this phase has been further investigated using simplified calculations, time domain simulations in SIMO and motion measurements of the ROV. The results confirms that large forces occurs in the wave zone. In addition, variability in the simulations and measurements indicates the complexity of the wave zone transit.

The largest umbilical tensions obtained in the time domain simulations were a consequence of slack umbilical leading to snap loads. Thus, this seems to be the most critical effect during launch. Impact between the ROV and the pontoon has not occurred in the SIMO simulations performed, and is assumed to be of less concern. By reducing the winch speed from 0.8 to 0.4 m/s, the number of slack umbilical occurrences decrease. However, the maximum umbilical tension was of the same size, with an increase of less than 1 % for two sea states. Simulations of the recovery phase did not lead to slack umbilical, which indicates that the launch phase is more critical.

Occurrence of slack umbilical coincides with the results from simplified method calculations. However, the large slamming impact force was not obtained in the time domain simulations. This indicates that a slamming coefficient of 5 is conservative. The simulations also indicates that the simplified method overestimates the snap velocity. This resulted in a dynamic amplification of 5.5 compared to maximum 2.2 from SIMO in $H_s = 4\ m$. Further, the acceleration pattern during snap loads in SIMO was compared to the motion measurements.

One occurrence with similar vertical acceleration shape was found. This was based on the velocity change during the acceleration spike and the pattern prior to the spike. The comparison can indicate that slack umbilical occurred. However, lack of references for the ROV position and umbilical tension during the measurement makes it difficult to conclude.

The SIMO analysis indicates that the drag force due to vertical water particle velocity is the dominating effect for slack umbilical to occur. This means that the drag coefficients used in SIMO is especially important for the dimensioning forces. Increasing the drag coefficients by 50 % increased one snap load by 133 %. However, the wave kinetics during slack umbilical indicates that the maximum snap load will be limited by the period of positive vertical water particle velocity. Wave induced inertia forces also contributes to the snap load, but were less sensitive to change in the force coefficient. Despite uncertainties in the input parameters, measured horizontal ROV accelerations were of similar magnitude as the accelerations obtained in SIMO. This suggests that the model provides an indication of the real ROV behaviour in the wave zone.

Based on the critical factors, reducing the launch and recovery system stiffness by implementing an effective sheave suspension is assumed to be a good measure to reduce the umbilical tension. However, the effect will depend on the characteristics. Implementing the current sheave suspension in SIMO by changing the stiffness and using a tensioner reduced a snap load to 62 % and 76 % of the original force respectively. This was compared to assuming high stiffness in the sheave. Uncertainties in the properties of the current suspension system can result in simulating lower forces than the real system loads. In addition, the measurement with the suspected slack umbilical indicates a limited effect of the current system. Thus, more detailed analysis will require verified properties of the current suspension system or of an alternative new system. This should be obtained before extending the weather window based on a sheave suspension system.

6.2 Recommendations for Further Work

In this work, the main focus has been to determine the critical factors for the weather criterion and measures that can influence these. This has been based on simulations and measurements where assumptions and uncertainties influences the results.

The interpretation of motion measurements requires position references to reduce the uncertainties. Measures like video of the behaviour during water entry or data from the other ROV sensors synchronized in time, can be used to provide the position relative to the water surface. More detailed full scale measurements can also include better environmental description. An example can be time series of the wave elevation.

Further, including motion measurements of the sheave frame can be used to investigate the sheave suspension system behaviour. Based on the measurements, the effect of the suspension on stiffness and damping can be evaluated. This may be used to investigate whether the end stops in the suspension cylinders are hit. In addition, accelerations of the ROV can be compared to the sheave motions. Based on the comparison, a better indication of the umbilical tension during acceleration spikes may be obtained. If the weather criterion should be changed based on the sheave suspension, the influence on stiffness and damping needs to be verified. Reliable measurements of the umbilical tension will provide a good basis to evaluate the weather criterion, and can be used together with motion measurements as described in Driscoll et al. (2000b).

If more reliable measurements are obtained, the model of the ROV system in SIMO can be improved. Especially the drag coefficient has proved to be important for occurrence of slack umbilical in the wave zone and the resulting forces. Thus, the force coefficients should be properly verified. Alternative methods for determining the coefficients can also be carried out. This can be model tests or numerical calculations. Further, different methods to model the ROV can be compared. The current model has been made based on assumptions about mass and buoyancy distribution, which introduces additional uncertainties.

An improved model verified by measurements can provide statistics to determine a new weather criterion. Additional parameters in the criterion can also be considered, for example the wave period or platform motion. Variation of the wave period in the SIMO simulations indicates variability within each significant wave height, as illustrated in Appendix B. Reliable data of all the criterion parameters must then be available for the decision making prior to the operation. A clear limit for the accepted loads in the umbilical and launch and recovery system will also be required when determining the criterion. In addition to the safe working load limit,

other factors like bending radius of the umbilical can affect the accept criterion. High concentrated loads will influence wear and damage to the internal components of the umbilical, which increases maintenance costs and down time of the ROV system. This is especially important if snap loads in the umbilical are accepted. Based on this, the benefits of extending the weather criterion should also be considered against higher maintenance costs.

Further work can be summarized in the following points:

- Further verify the dimensioning effects found from the SIMO simulations by using reliable measurements combined with alternative modelling and force coefficient determination for the analysis.
- Establish more accurate properties of the current sheave suspension system by tests, measurements and observations.
- Determine the potential of a modified sheave suspension system in terms of space limitations at Snorre B and forces in the launch and recovery system.
- Combine measurements and simulations to establish a new weather criterion.

Bibliography

Bruset, O. (2014). Snorre B info – ROV Operations.

COSALT Offshore Norge AS (2012). Certificate No. AHLY43GRU for test and examination of lifting equipment and appliances. Report.

Det Norske Veritas (2014a). DNV-RP-C205 Environmental Conditions and Environmental Loads.

Det Norske Veritas (2014b). DNV-RP-H103 Modelling and Analysis of Marine Operations.

Driscoll, F. R., Buckham, B., and Nahon, M. Numerical optimization of a cage-mounted passive heave compensation system. In *Oceans 2000*, volume 2, pages 1121–1127. IEEE.

Driscoll, F. R., Lueck, R. G., and Nahon, M. (2000a). The motion of a deep-sea remotely operated vehicle system part 2: Analytical model. *Ocean Engineering*, 27(1):57–76.

Driscoll, F. R., Lueck, R. G., and Nahon, M. (2000b). The motion of a deep-sea remotely operated vehicle system. Part 1: Motion observations. *Ocean Engineering*, 27(1):29–56.

Driscoll, F. R., Nahon, M., and Lueck, R. G. (2000c). A comparison of ship-mounted and cage-mounted passive heave compensation systems. *Journal of Offshore Mechanics and Arctic Engineering*, 122(3):214–221.

Faltinsen, O. M. (1990). *Sea loads on ships and offshore structures*. Cambridge University Press, Cambridge.

Irgens, F. (1999). *Formelsamling mekanikk: statikk, fasthetslære, dynamikk, fluidmekanikk*. Tapir, Trondheim. 1. utg. 1987 3. utg.

JMC Engineering (2006a). Dynamic amplification for ROV sheave. Report S6-KC-NCE-1000.

JMC Engineering (2006b). Structural calculation of the ROV-sheave suspension at Snorre-B. Report S6-KC-NCE-1001.

Larsen, C. M. (2012). *Marin dynamikk: kompendium for bruk i faget TMR 4182 Marin dynamikk ved Institutt for marin teknikk, Fakultet for ingeniørvitenskap og teknologi, NTNU*, volume UK-2012-09. Marinteknisk senter., Trondheim. Omslagstittel: TMR4182 Marin dynamikk.

Larsen, K. (2015). MIROS Data - Snorre B.

Madgwick, S. (2013). Oscillatory-Motion-Tracking-With-x-IMU. http://github.com/xioTechnologies/Oscillatory-Motion-Tracking-With-x-IMU. Online; accessed 14-April-2015.

Madgwick, S. O. H., Harrison, A. J. L., and Vaidyanathan, R. (22275550). Estimation of imu and marg orientation using a gradient descent algorithm. In *Rehab Week Zurich 2011 - 2011 IEEE International Conference on Rehabilitation Robotics, ICORR 2011*.

Morison, J. R., Johnson, J. W., and Schaaf, S. A. (1950). The force exerted by surface waves on piles. *Journal of Petroleum Technology*, 2(5):149–154.

Øritsland, O. (1989). *A summary of subsea module hydrodynamic data*, volume 511110.05. Norsk marinteknisk forskningsinstitutt, Trondheim. Arkivnr. MT51 89-0045.

Øritsland, O. and Lehn, E. (1987). *Hydrodynamic forces on subsea modules during lifting operations*, volume 511003.02. Norsk marinteknisk forskningsinstitutt, Trondheim. Arkivnr MT51 87-0194.

Saipem LTD (2012). MRV09 Load Test. Report WI-SUKL-ASST-947-E.

Sarpkaya, T. and Isaacson, M. (1981). *Mechanics of wave forces on offshore structures*. Van Nostrand Reinhold, New York.

SIMO Project Team (2013). SIMO - Theory Manual Version 4.0 rev. 3. Report 516412.00.03.

x-IO Technologies (2012). Open source IMU and AHRS algorithms. http://www.x-io.co.uk/open-source-imu-and-ahrs-algorithms/. Online; accessed 14-April-2015.

Xsens Technologies B.V. (2010). MTi and MTx User Manual and Technical Documentation. Report MT0100P.

Appendix A

Motion measurements

In this appendix, accelerations and angular velocities from the IMU data loggings are presented. To remove the gravitational acceleration, the accelerations have been transferred into a global reference system. However, neither the gyroscope nor accelerometer data have been subjected to further filtering to avoid removing relevant details in the measurements. Only the parts showing launches or recoveries are included in the plots.

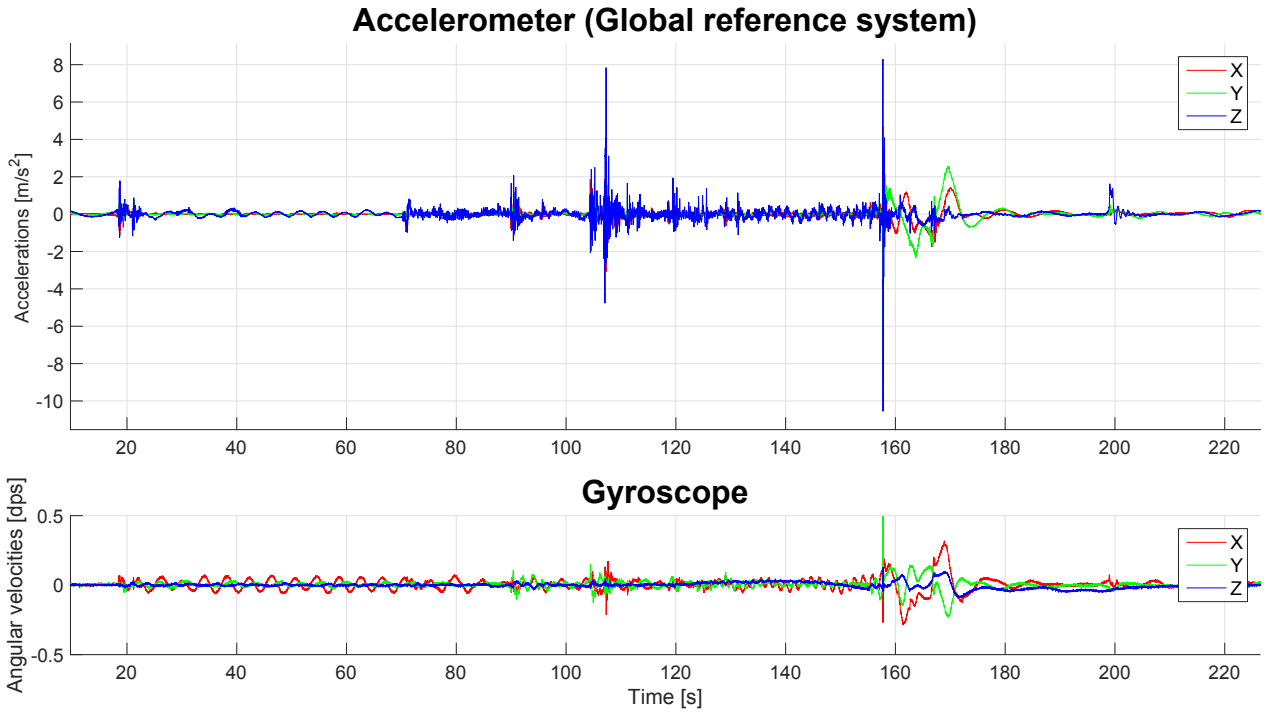

Figure A.1: Launch from 2015-04-02 at 19:58

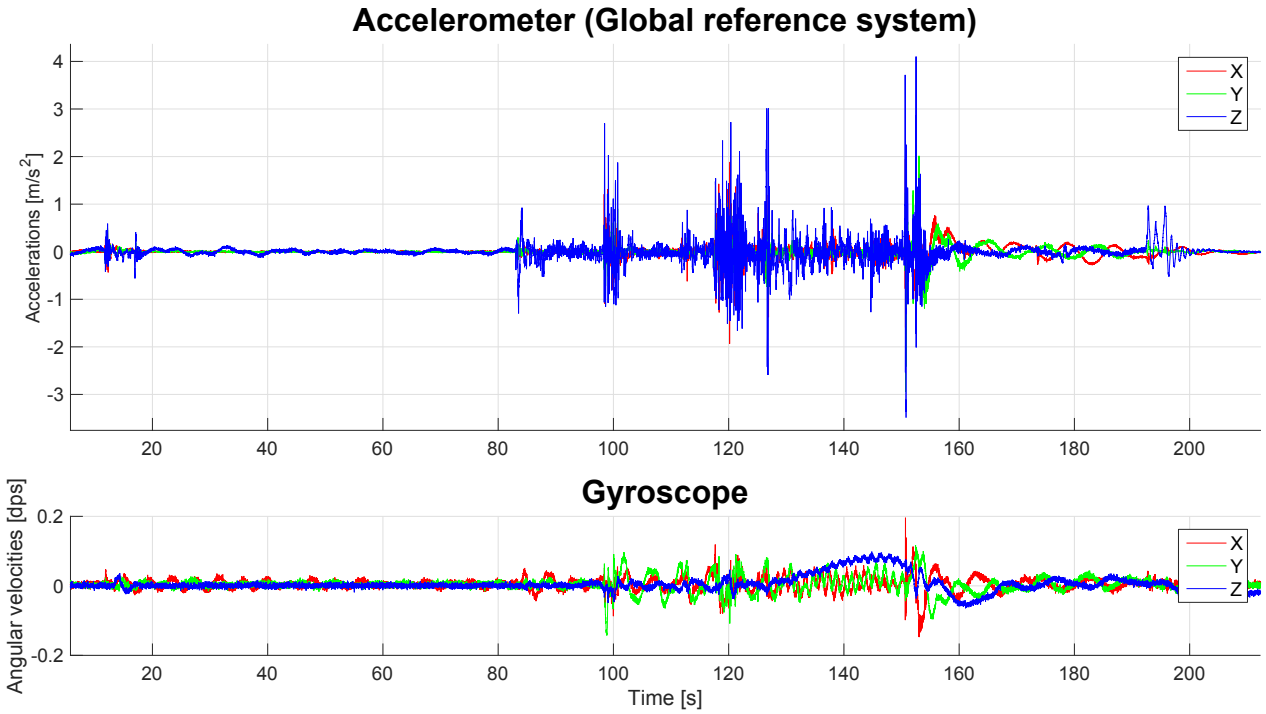

Figure A.2: Launch from 2015-04-04 at 14:19

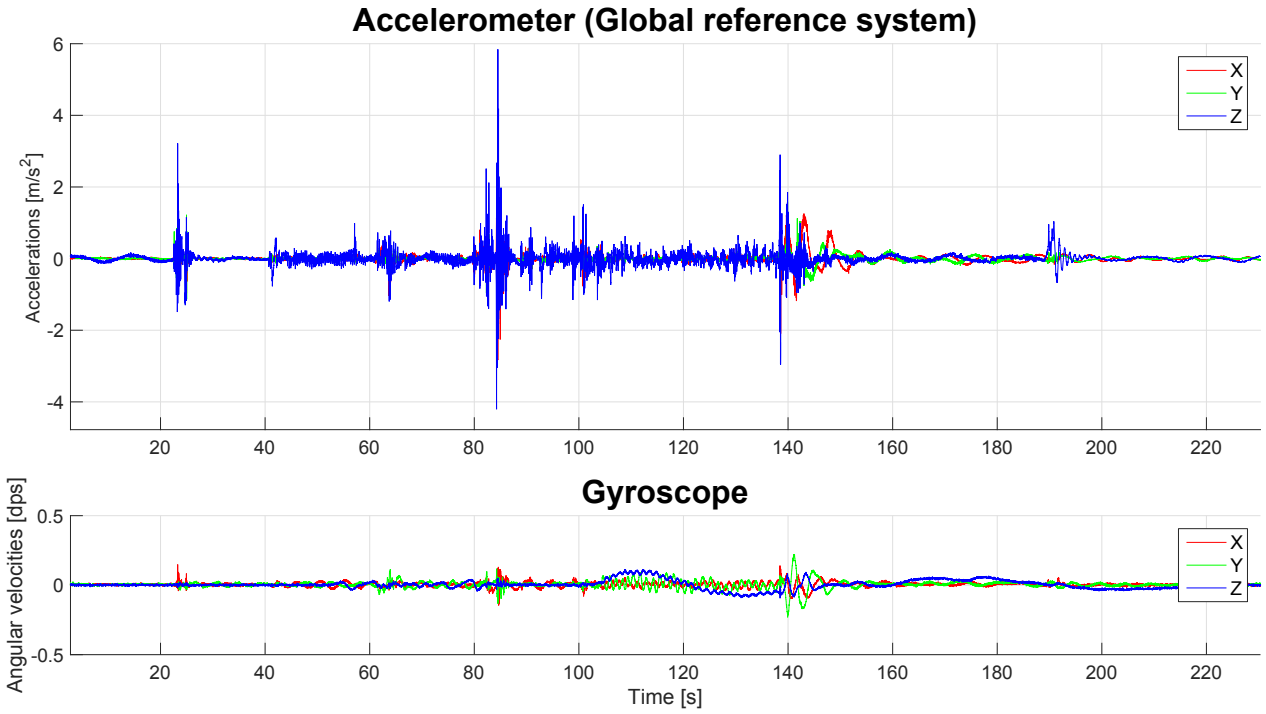

Figure A.3: Launch from 2015-04-05 at 03:47

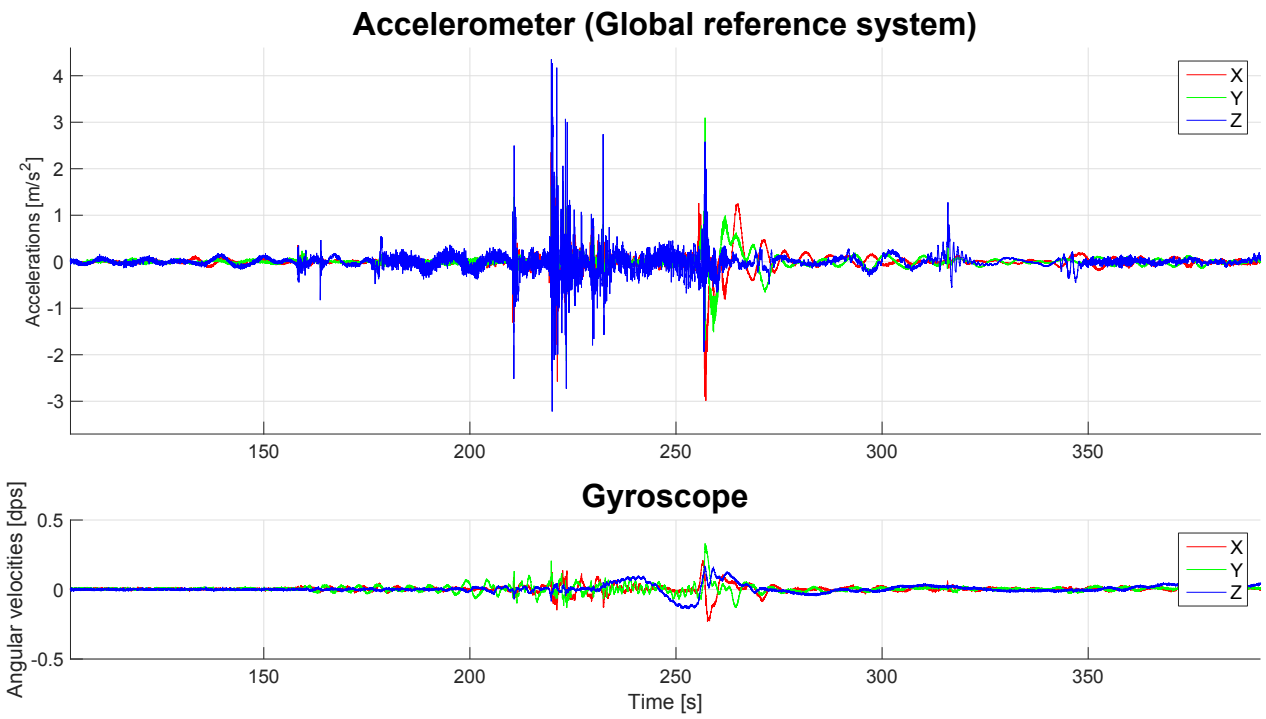

Figure A.4: Launch from 2015-04-09 at 22:36

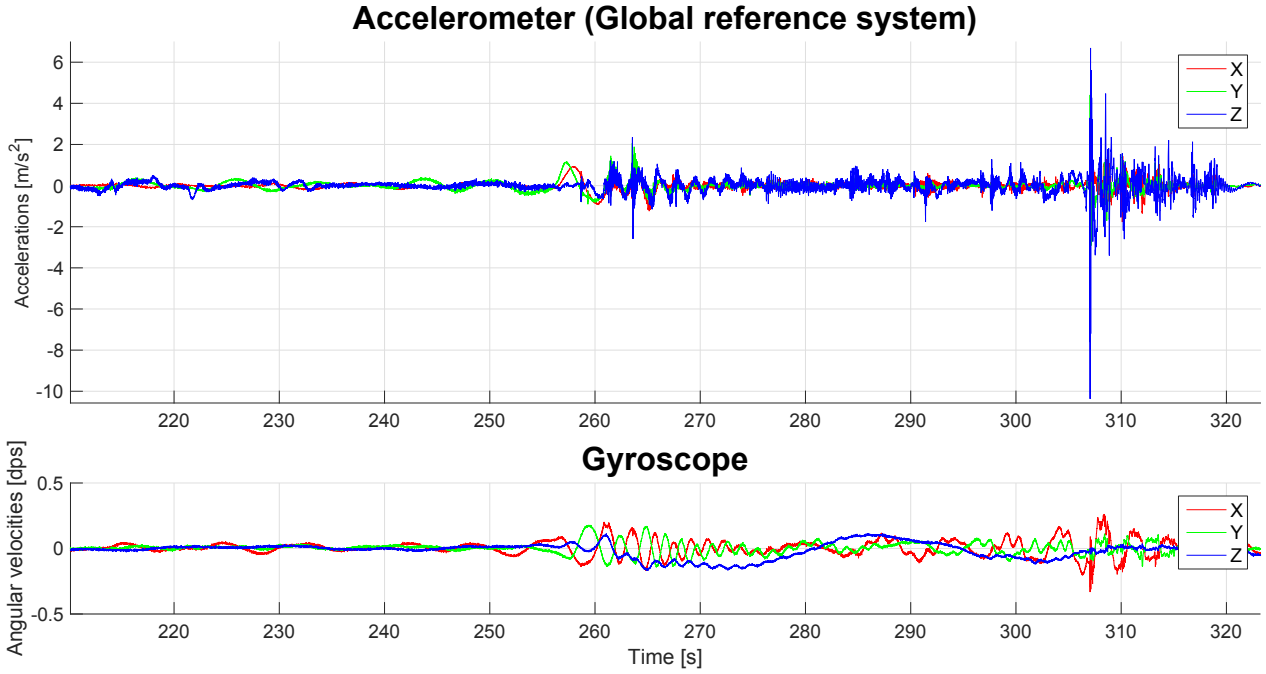

Figure A.5: Recovery from 2015-04-12 at 20:32

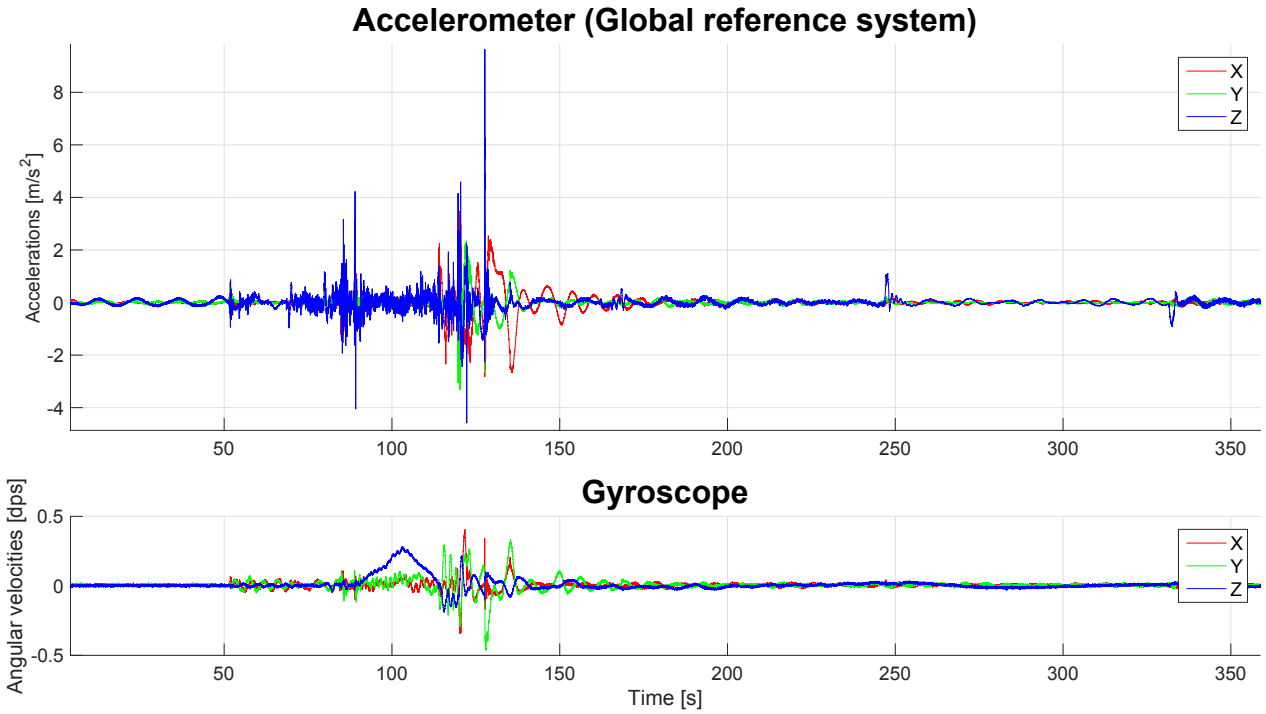

Figure A.6: Launch from 2015-04-13 at 01:47

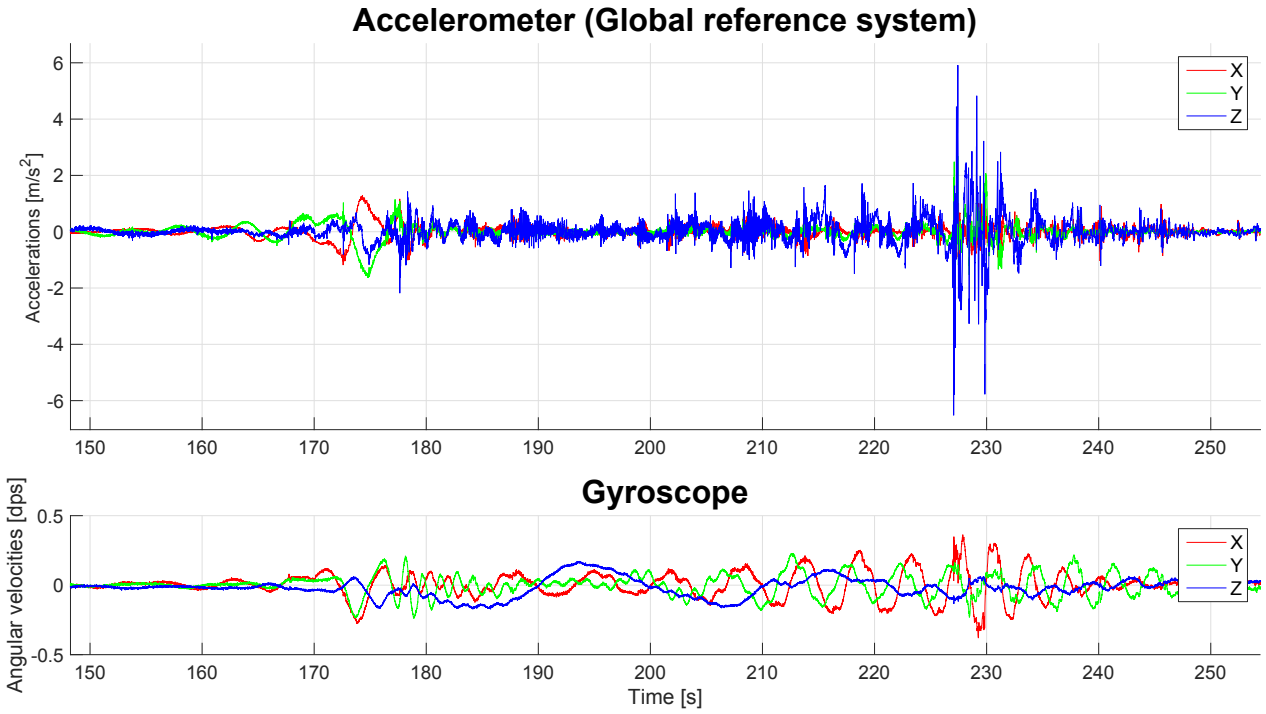

Figure A.7: Recovery from 2015-04-14 at 00:15

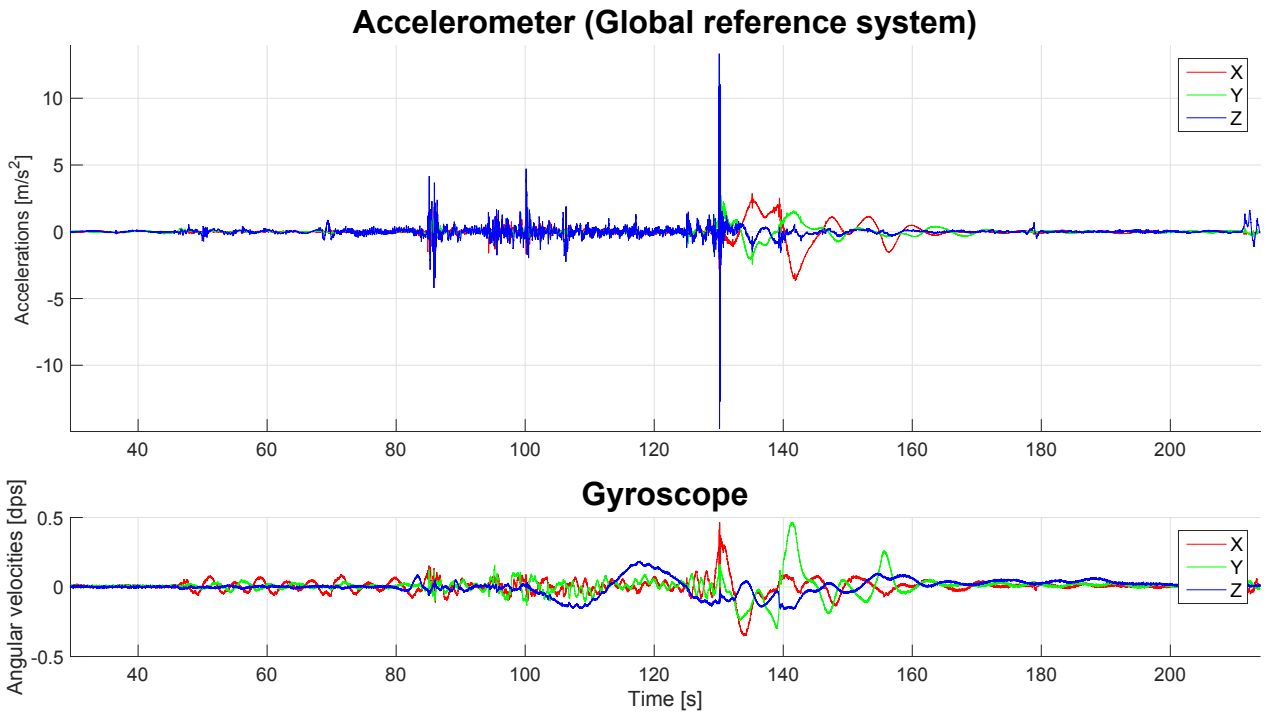

Figure A.8: Launch from 2015-04-14 02:50

Appendix B

SIMO analysis

In this appendix tension plots extracted from SIMO are presented. For each sea state, 30 different wave seeds are run. The winch is started 160 seconds after the simulation start, and the velocity is set to 0.8 m/s. All simulations presented are without the sheave suspension modelling. Total simulation time was 300 seconds, but only the most critical phase is presented. A two parameter JONSWAP spectrum was used, and γ together with the relationship between T_z and T_p are found in Table 4.12.

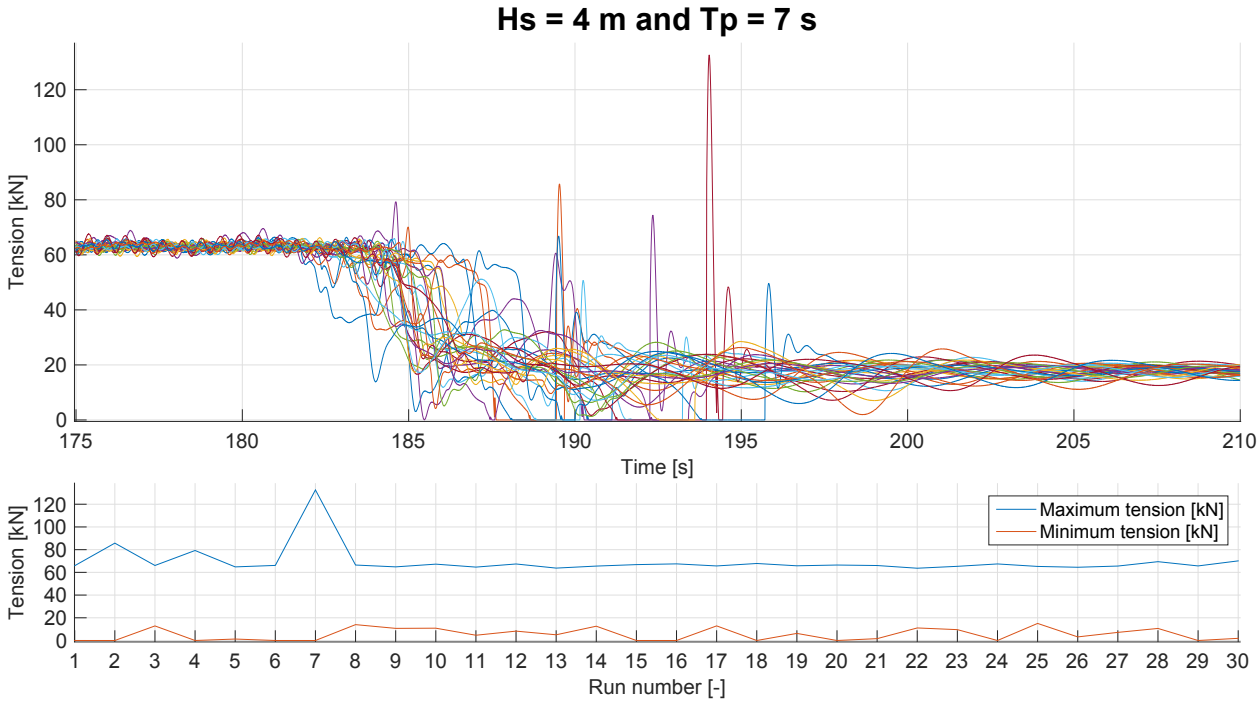

Figure B.1: Umbilical tension in $H_s = 4\ m$ and $T_p = 7\ s$.

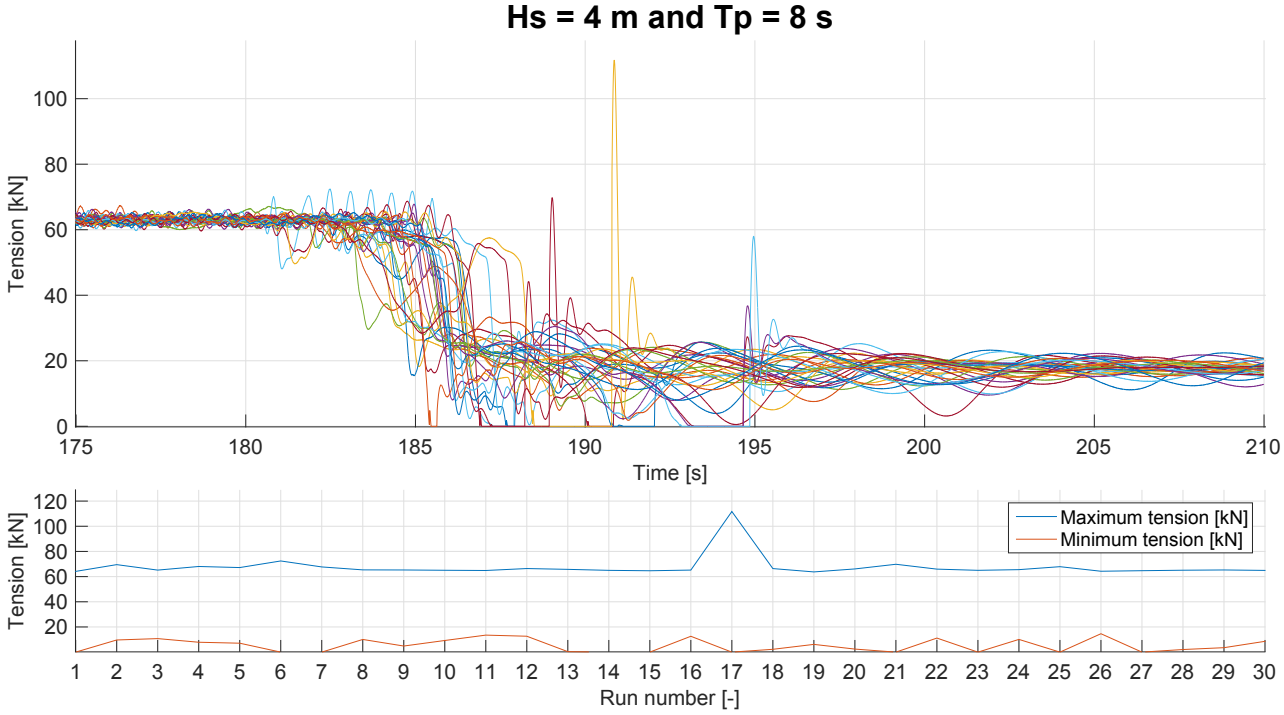

Figure B.2: Umbilical tension in $H_s = 4\ m$ and $T_p = 8\ s$.

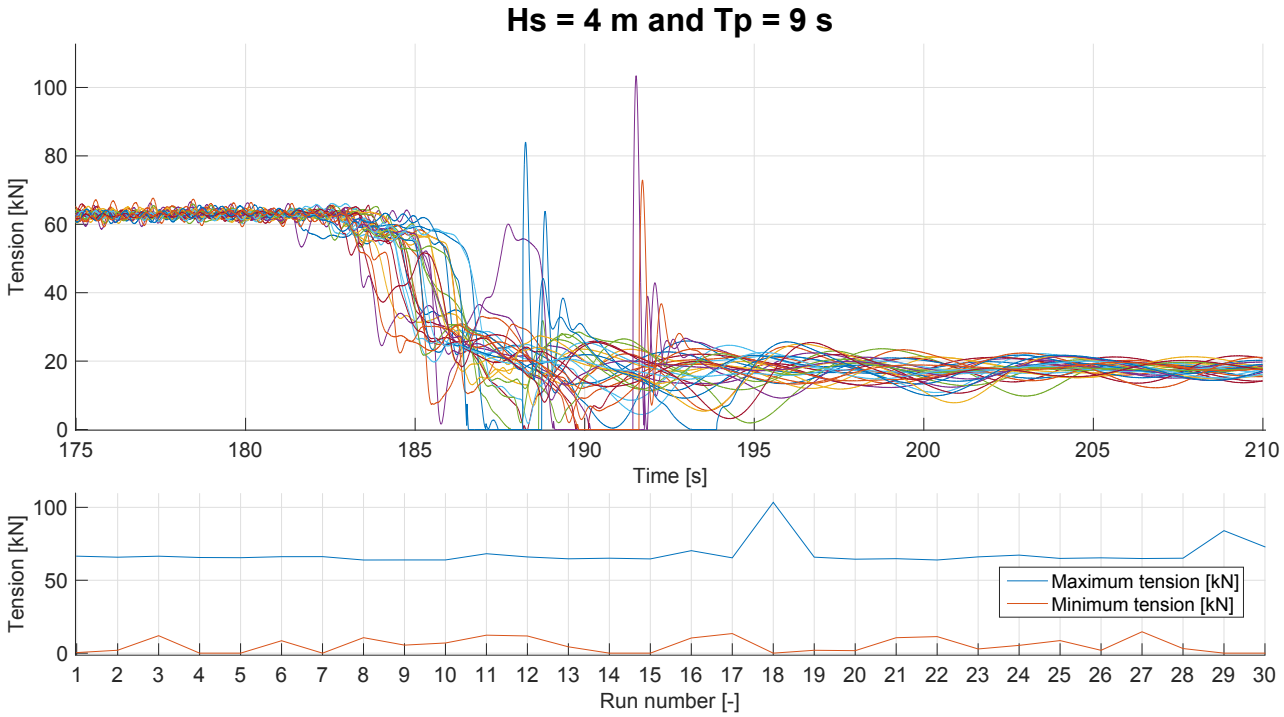

Figure B.3: Umbilical tension in $H_s = 4\ m$ and $T_p = 9\ s$.

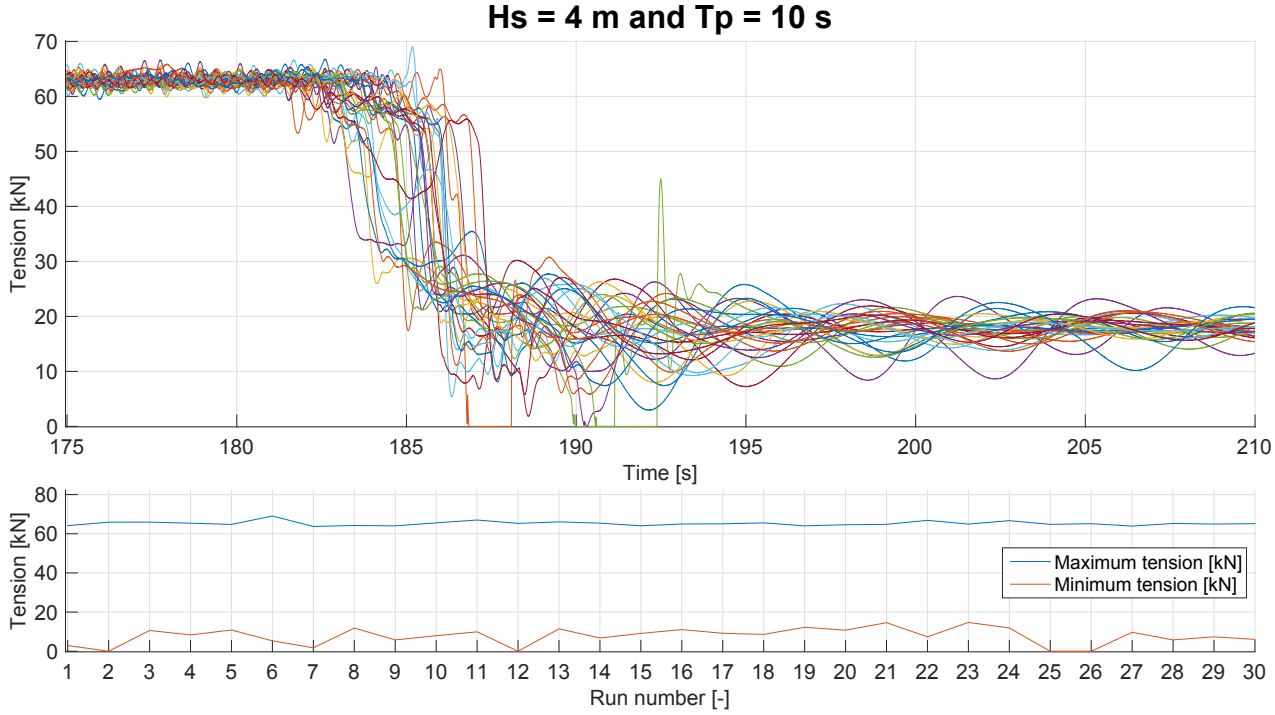

Figure B.4: Umbilical tension in $H_s = 4\ m$ and $T_p = 10\ s$.

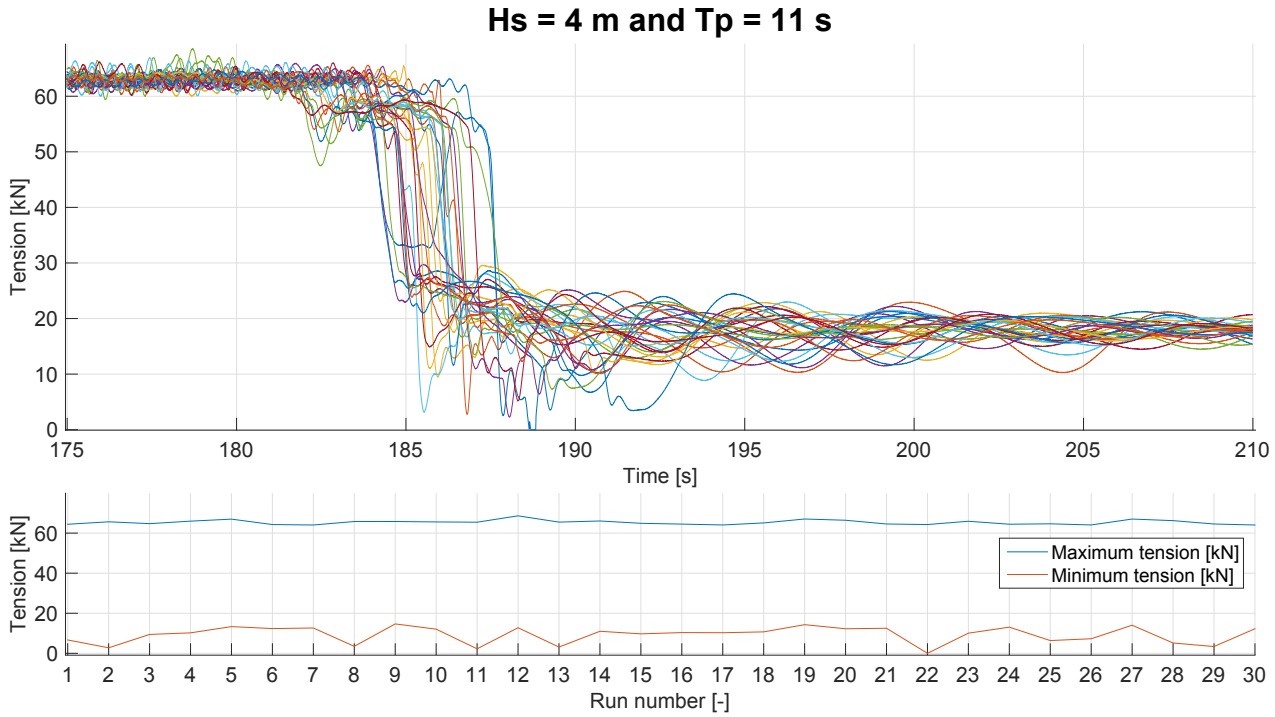

Figure B.5: Umbilical tension in $H_s = 4\ m$ and $T_p = 11\ s$.

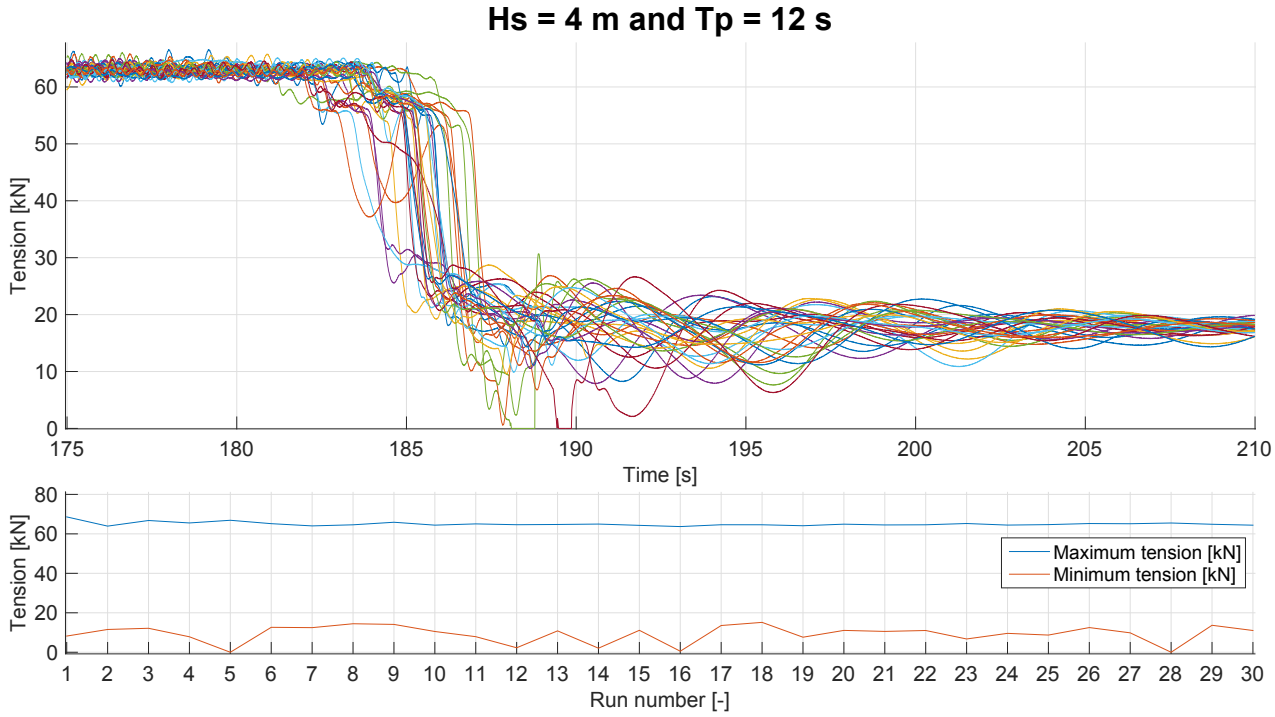

Figure B.6: Umbilical tension in $H_s = 4\ m$ and $T_p = 12\ s$.

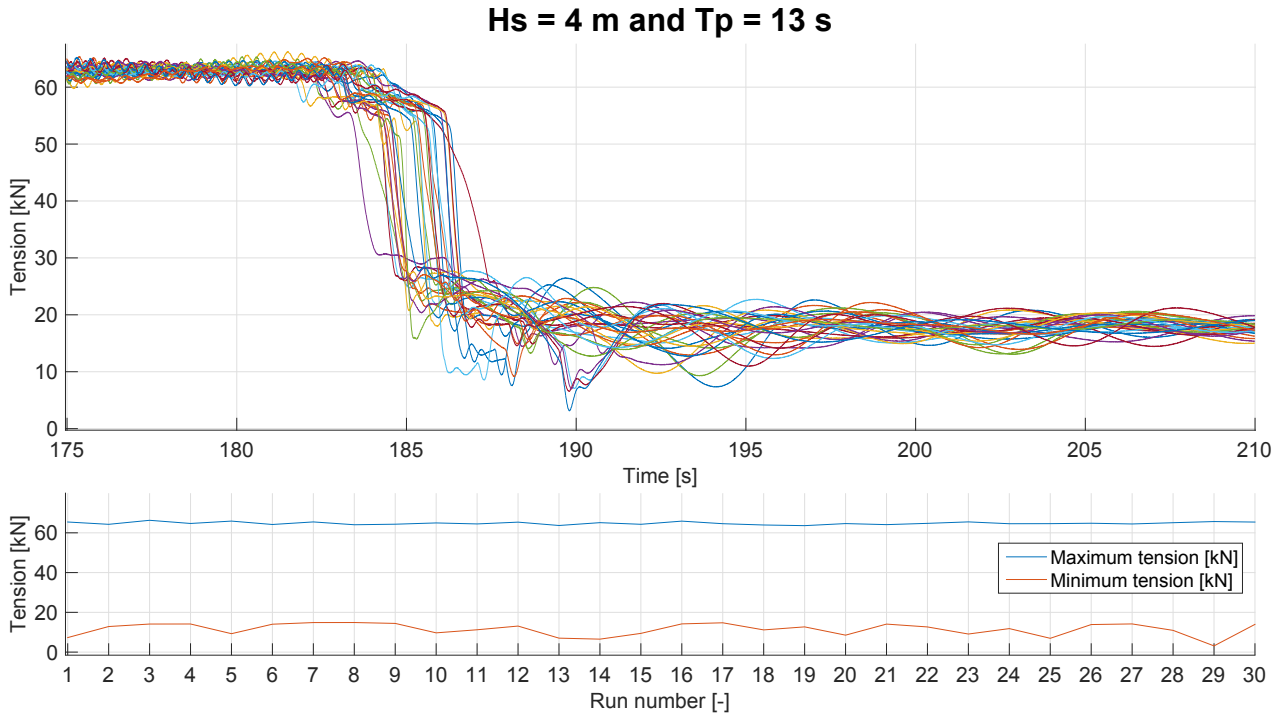

Figure B.7: Umbilical tension in $H_s = 4\ m$ and $T_p = 13\ s$.

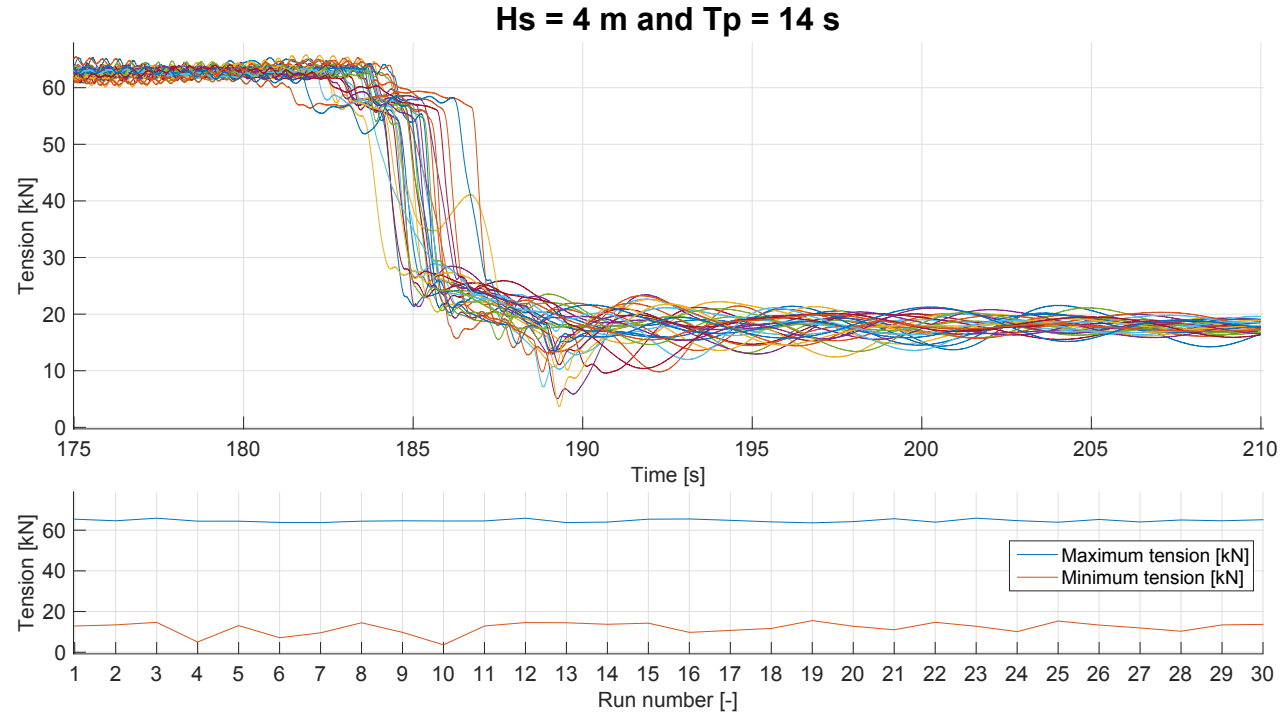

Figure B.8: Umbilical tension in $H_s = 4\ m$ and $T_p = 14\ s$.

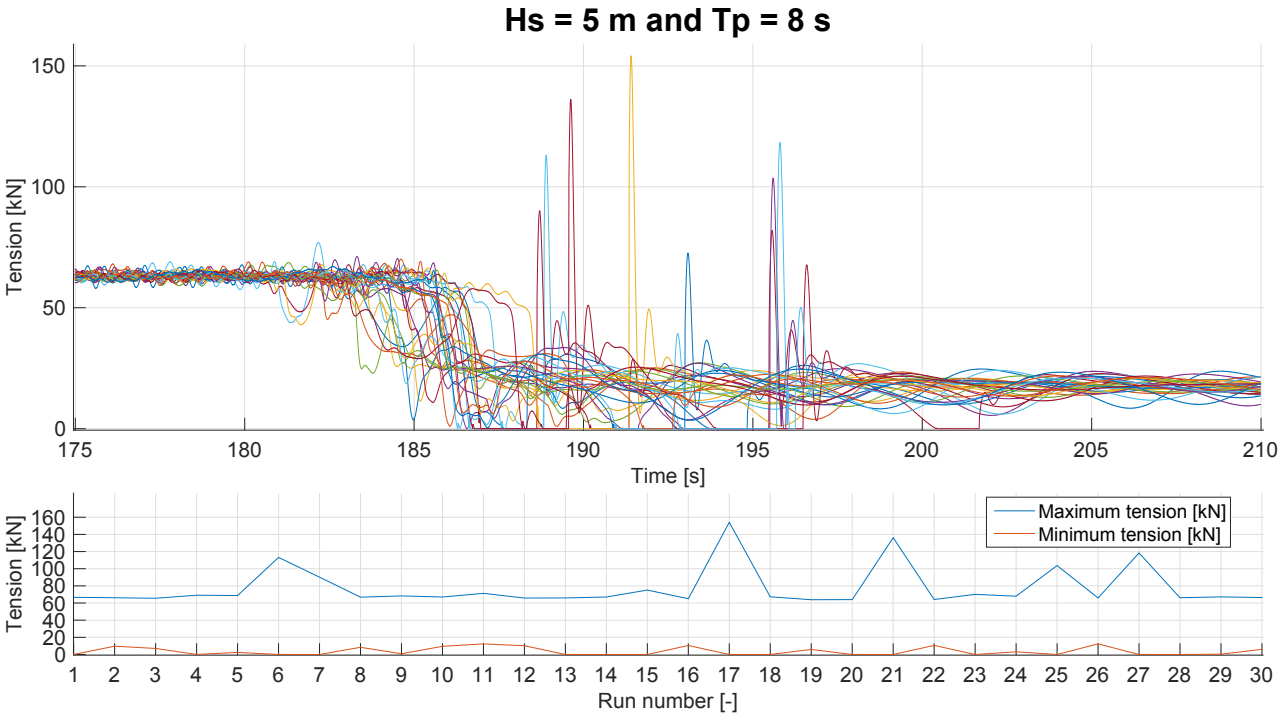

Figure B.9: Umbilical tension in $H_s = 5\ m$ and $T_p = 8\ s$.

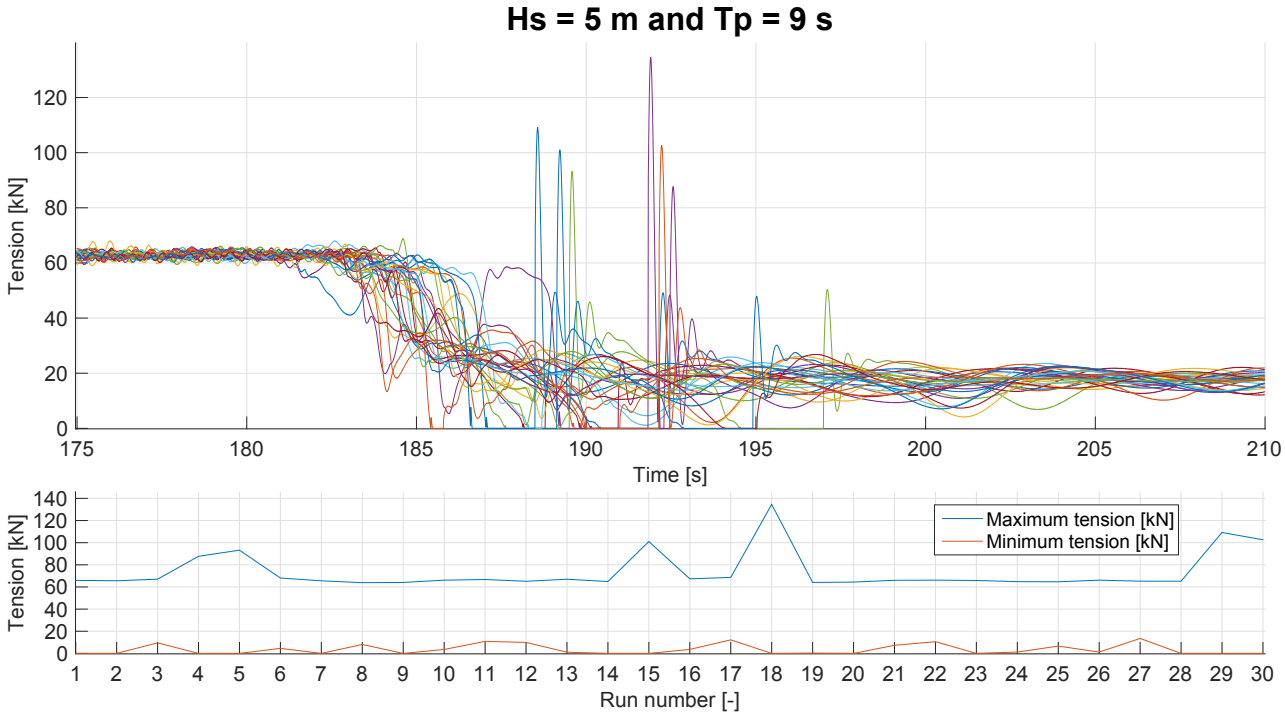

Figure B.10: Umbilical tension in $H_s = 5\ m$ and $T_p = 9\ s$.

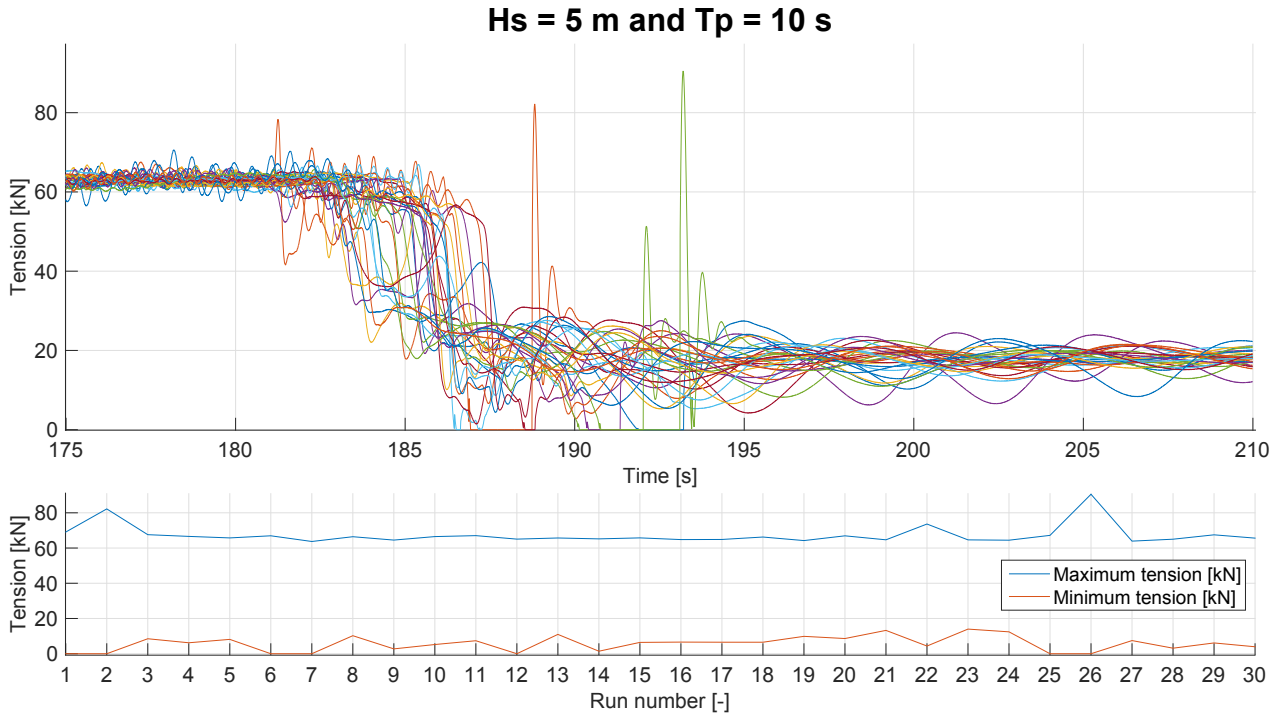

Figure B.11: Umbilical tension in $H_s = 5\ m$ and $T_p = 10\ s$.

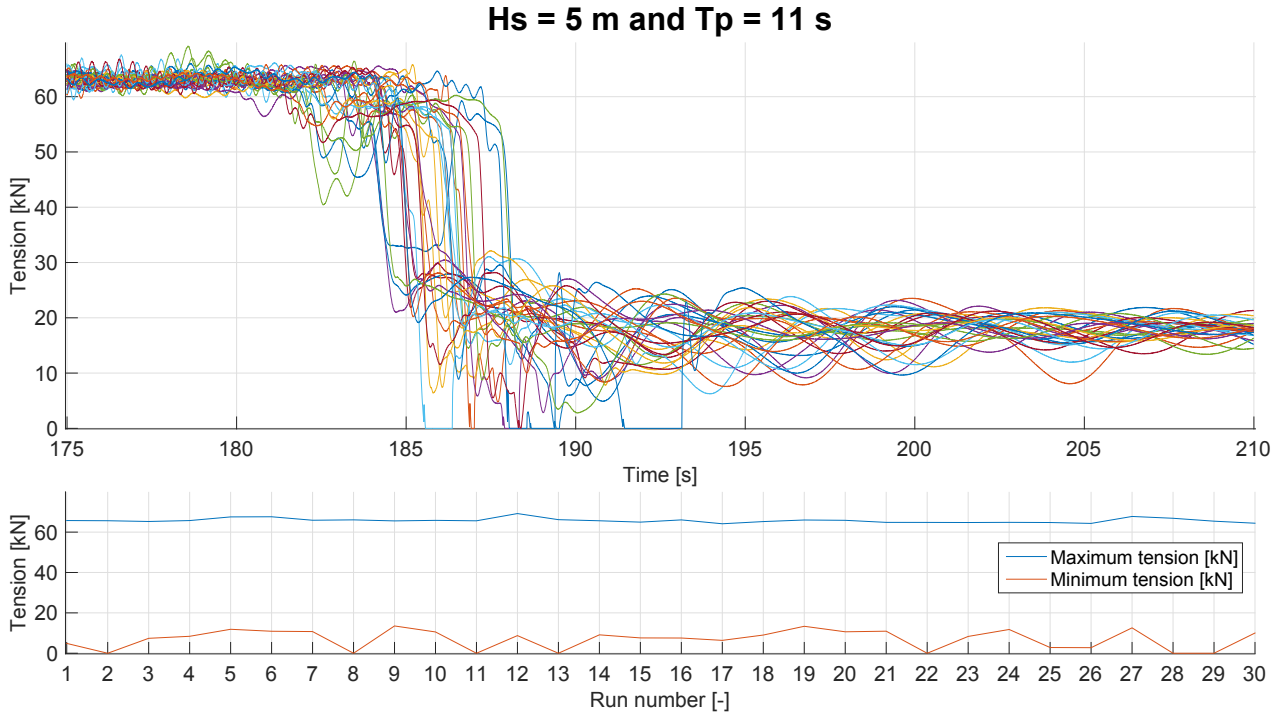

Figure B.12: Umbilical tension in $H_s = 5\ m$ and $T_p = 11\ s$.

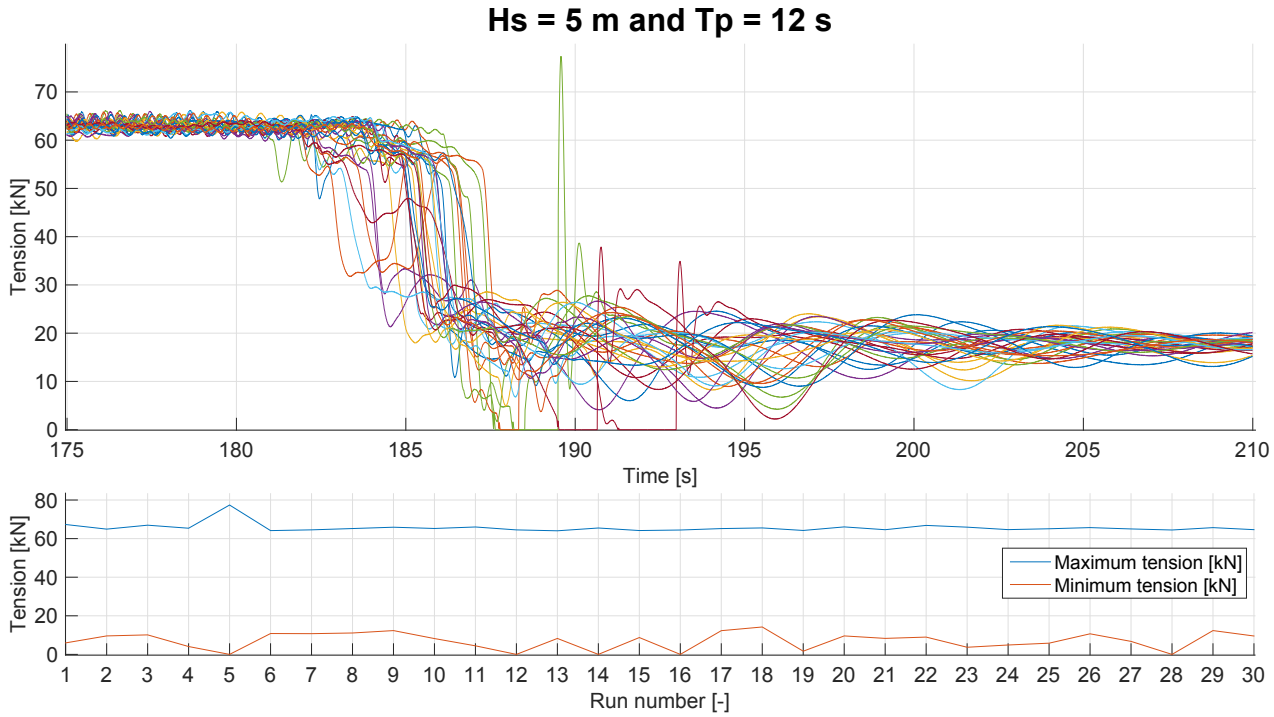

Figure B.13: Umbilical tension in $H_s = 5\ m$ and $T_p = 12\ s$.

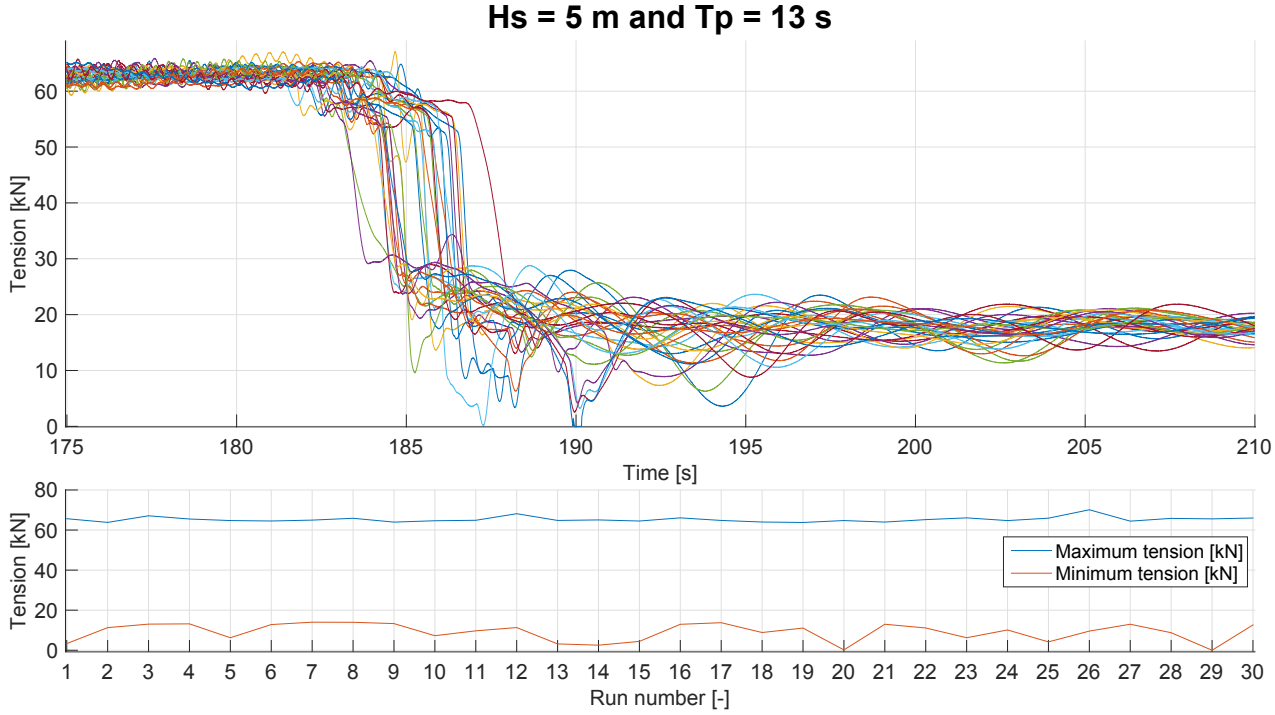

Figure B.14: Umbilical tension in $H_s = 5\ m$ and $T_p = 13\ s$.

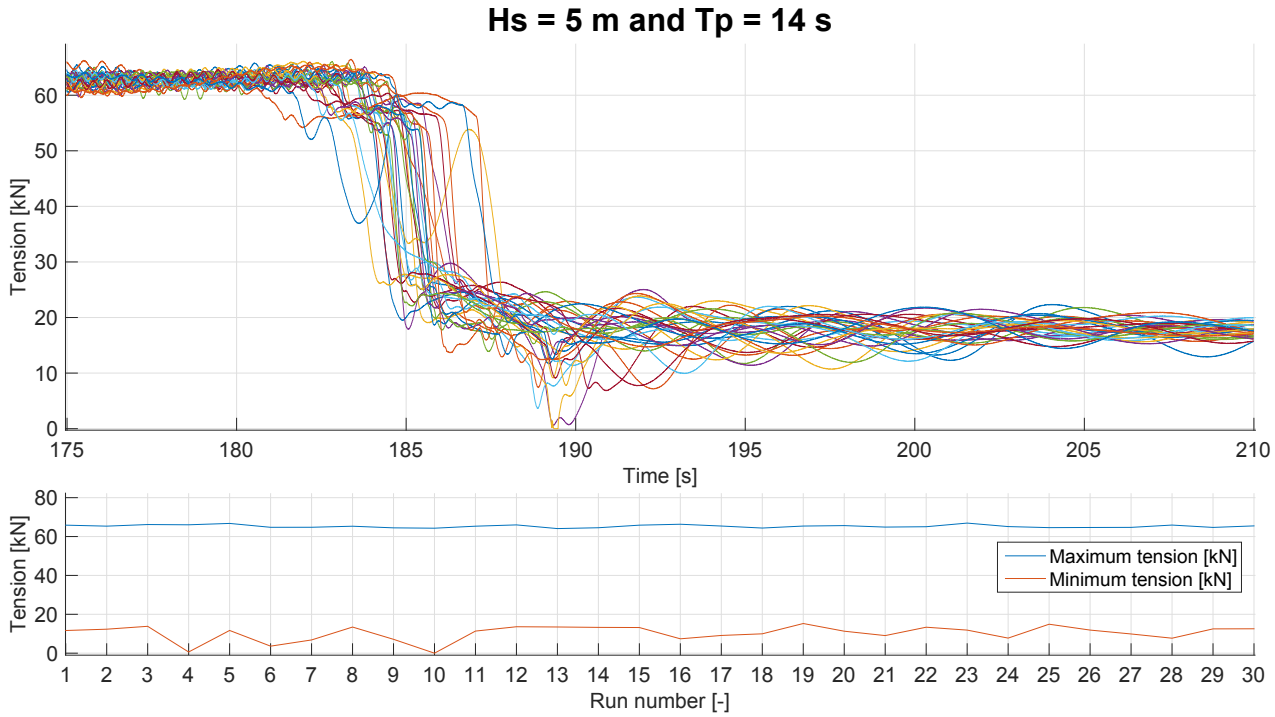

Figure B.15: Umbilical tension in $H_s = 5\ m$ and $T_p = 14\ s$.

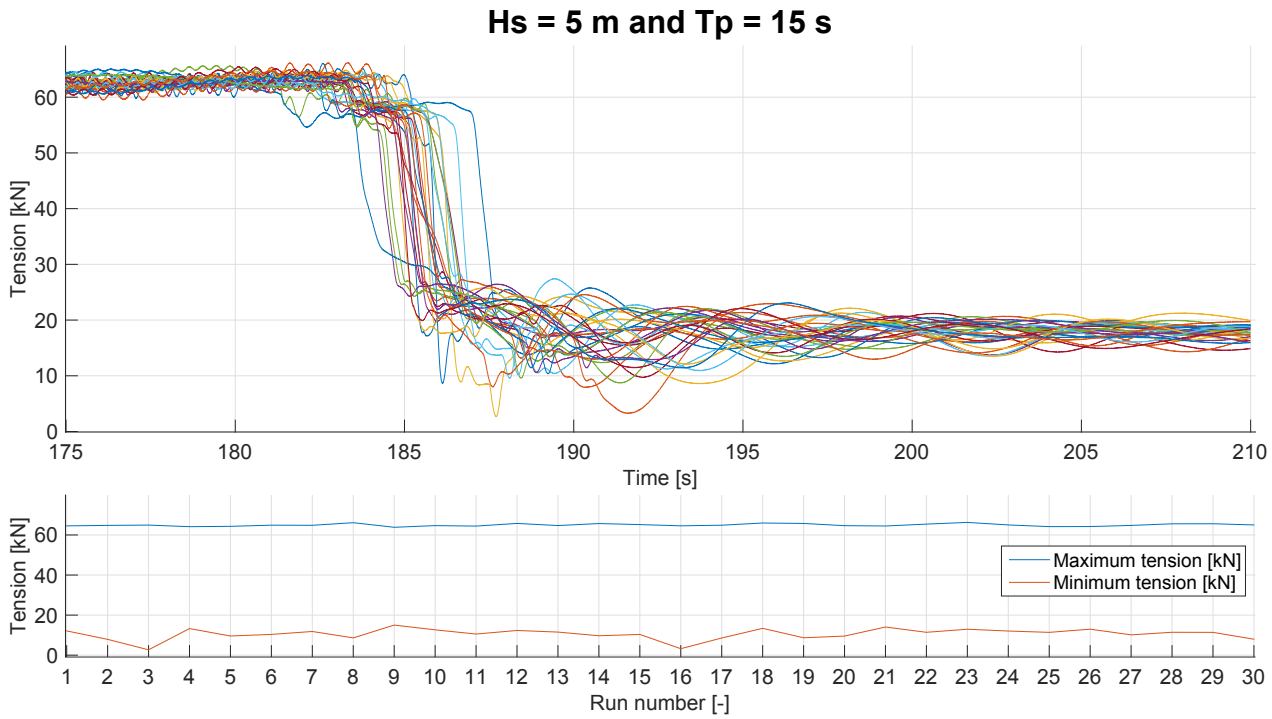

Figure B.16: Umbilical tension in $H_s = 5\ m$ and $T_p = 15\ s$.

Appendix C

Slender elements properties

The properties of the slender elements used to build the ROV model in SIMO are presented in Table C.1. Linear drag input, B_1, are set to 10 % of the quadratic drag input based on the calculated values in Table 4.10, and are not included in the table. In Figure 4.4, the coordinate system for the directions is shown. Input refers to the values used in SIMO, while total is calculated to be compared to the calculations.

Table C.1: ROV slender element properties in SIMO.

Element name	Length [m]			Radius		Displ.	CoB [m]	A_m input [kg/m]			Total A_m [kg]			B_2 input [Ns^2/m^3]			Total B_2 [Ns^2/m^2]		
	y	x	z	R [m]	A [m^2]	V [m^3]	z	y	x	z	y	x	z	y	x	z	y	x	z
buoy_ROV_1	3,2	0	0	0,37	0,430	1,376	2,064	0	0	0	0	0	0	0	0	0	0	0	0
buoy_ROV_2	3,2	0	0	0,37	0,430	1,376	2,064	0	0	0	0	0	0	0	0	0	0	0	0
lFrame_ROV_1	3,2	0	0	0,103	0,033	0,107	0,000	0	95	120	0	304	384	0	190	245	0	608	784
lFrame_ROV_2	3,2	0	0	0,103	0,033	0,107	0,000	0	95	120	0	304	384	0	190	245	0	608	784
lFrame_ROV_3	0	1,5	0	0,103	0,033	0,050	0,000	80	0	120	120	0	180	180	0	245	270	0	367,5
lFrame_ROV_4	0	1,5	0	0,103	0,033	0,050	0,000	80	0	120	120	0	180	180	0	245	270	0	367,5
tFrame_ROV_1	3,2	0	0	0,103	0,033	0,107	0,213	0	95	120	0	304	384	0	190	245	0	608	784
tFrame_ROV_2	3,2	0	0	0,103	0,033	0,107	0,213	0	95	120	0	304	384	0	190	245	0	608	784
tFrame_ROV_3	0	1,5	0	0,103	0,033	0,050	0,100	80	0	120	120	0	180	180	0	245	270	0	367,5
tFrame_ROV_4	0	1,5	0	0,103	0,033	0,050	0,100	80	0	120	120	0	180	180	0	245	270	0	367,5
mFrame_ROV_1	0	0	2	0,103	0,033	0,067	0,067	80	95	0	160	190	0	180	190	0	360	380	0
mFrame_ROV_2	0	0	2	0,103	0,033	0,067	0,067	80	95	0	160	190	0	180	190	0	360	380	0
mFrame_ROV_3	0	0	2	0,103	0,033	0,067	0,067	80	95	0	160	190	0	180	190	0	360	380	0
mFrame_ROV_4	0	0	2	0,103	0,033	0,067	0,067	80	95	0	160	190	0	180	190	0	360	380	0
mFrame_TMS_1	0	0	2	0,103	0,033	0,067	0,200	80	95	0	160	190	0	180	190	0	360	380	0
mFrame_TMS_2	0	0	2	0,103	0,033	0,067	0,200	80	95	0	160	190	0	180	190	0	360	380	0
mFrame_TMS_3	0	0	2	0,103	0,033	0,067	0,200	80	95	0	160	190	0	180	190	0	360	380	0
mFrame_TMS_4	0	0	2	0,103	0,033	0,067	0,200	80	95	0	160	190	0	180	190	0	360	380	0
tFrame_TMS_1	1,5	0	0	0,103	0,033	0,050	0,200	0	95	120	0	142,5	180	0	190	245	0	285	367,5
tFrame_TMS_2	1,5	0	0	0,103	0,033	0,050	0,200	0	95	120	0	142,5	180	0	190	245	0	285	367,5
tFrame_TMS_3	0	1,5	0	0,103	0,033	0,050	0,200	80	0	120	120	0	180	180	0	245	270	0	367,5
tFrame_TMS_4	0	1,5	0	0,103	0,033	0,050	0,200	80	0	120	120	0	180	180	0	245	270	0	367,5
Total						4,112	1.61				2000	3021	2976				4500	6042	6076

Appendix D

IMU Calibration certificate

Motion Tracker Test & Calibration Certificate

Type name:	MTi
Product ID:	MTi-28A53G35
Device ID:	01301955
Tested on:	29-Nov-2011
Calibrated on:	29-Nov-2011

Test Engineer Signature

IMU Specifications	**Accelerometer**		**Rate Gyro**		**Magnetometer**	
Full Scale:	50	[m/s2]	300	[deg/s]	5	[a.u.]
Bandwidth [Hz]:	30		40		10	
Default Sample Frequency [Hz]:	100					
Default Baudrate [bps]:	115200					

Basic test results	**Accelerometer**		**Rate Gyro**		**Magnetometer**	
Noise:	0.010	[m/s2]	0.004	[rad/s]	0.001	[a.u.]
Static accuracy residual:	0.348	[deg]	Temperature residual:		0.191	[deg]

Calibration Data
Please refer to Technical Documentation for interpretation of values!

Accelerometer

Gains

413	412	415

Alignment Matrix

1.00	0.01	0.01
-0.01	1.00	0.01
-0.02	-0.02	1.00

Offsets

33168	33290	32459

Temperature Parameters

a	b
0.030	0.003

Rate Gyro

Gains

4456	4607	4612

Alignment Matrix

1.00	-0.01	0.04
0.01	1.00	0.00
0.00	0.00	1.00

Offsets

32681	32471	32899

Temperature Parameters

a	b
n/a	0.143

Magnetometer

Gains

7561	7033	7678

Alignment Matrix

1.00	0.00	0.01
0.00	1.00	-0.02
0.00	0.00	1.00

Offsets

32143	32507	32131

Temperature Parameters

a	b
0.352	0.000

Xsens Technologies B.V.

Pantheon 6a
P.O. Box 559
7500 AN Enschede
The Netherlands

phone +31-(0)88-9736700
fax +31-(0)88-9736701
internet www.xsens.com
support www.xsens.com/support